Commande robuste pour une gestion énergétique fonction de l'état de santé de la batterie au sein des véhicules hybrides

Tinghong Wang

UNIVERSITÉ DE GRENOBLE

THÈSE

Pour obtenir le grade de

DOCTEUR DE L'UNIVERSITÉ DE GRENOBLE

Spécialité: Automatique

Arrêté: 7 août 2006

Présentée par

Tinghong WANG

Thèse dirigée par **Olivier SENAME** et

codirigée par **John-Jairo MARTINEZ-MOLINA**

préparée au sein du

GIPSA-lab

dans L'**École Doctorale: Electronique, Electrotechnique, Automatique & Traitement du Signal**

Commande robuste pour une gestion énergétique fonction de l'état de santé de la batterie au sein des véhicules hybrides

Thèse soutenue publiquement le **23 Octobre 2013**,

devant le jury composé de:

M. Jimmy LAUBER

MCF, Université de Valenciennes et du Hainaut-Cambrésis, Rapporteur

M. Argyrios ZOLOTAS

Senior Lecturer, University of Sussex, Rapporteur

M. Alireza KARIMI

Professeur, Ecole Polytechnique Fédérale de Lausanne, Examinateur

M. Mazen ALAMIR

Directeur de recherche CNRS, Grenoble, Examinateur, Président

M. Olivier SENAME

Professeur, INP Grenoble, Directeur de thèse

M. John-Jairo MARTINEZ-MOLINA

MCF, INP Grenoble, Co-directeur de thèse

Abstract

Title: Robust control approach to battery health accommodation of EMS in HEV

In recent years, growing public concern has been given both on the energy problem and on the environment problem resulted from dramatically increased vehicles equipped with Internal Combustion Engine (ICE). Subsequently, intensive contributions have been made by the automotive industries and research institutes on vehicles that depend less on the fossil fuels, and introduce less pollutant emissions. This has led to the emergence of environment-friendly and energy-saving vehicles such as the Hybrid Electric Vehicle (HEV) that is usually equipped with one or more additional electric motors and the associated power battery compared with the Conventional vehicles (CVs) propelled solely by the ICE.

The key point of an HEV is to design a proper Energy Management Strategy (EMS) that decides how to split the demanded power between the engine and the motor (battery). As the most important and expensive part of an HEV, it is important to take into account battery states, such as battery State of Charge (SOC) and battery ageing, aiming at maintain the optimality of the achieved EMS, as well as prolonging the battery life.

In this dissertation, an HEV of parallel structure, which is equipped with a Lithium-ion battery is considered. This dissertation is focused on accounting for battery related items, i.e. battery SOC and SOH indicated by battery parameters, in the EMS developments leading to a kind of fault tolerant EMS.

Keywords: Hybrid Electric Vehicle (HEV), Energy Management Strategy (EMS), battery State of Charge (SOC), battery ageing, robust H_∞ control, Linear Parameter Varying (LPV).

Résumé

Au cours des dernières années, la préoccupation croissante du public a focalisé à la fois sur le problème de l'énergie associé à la pénurie aggravante des combustibles fossiles qui sont non renouvelables, et sur le problème de l'environnement associé à l'augmentation progressive de l'émission des polluantes. Par la suite, les contributions intensives ont été déployées par de nombreux secteurs de l'industrie automobile et des instituts de recherche sur la production et l'utilisation de carburants alternatifs qui sont renouvelables, ainsi que sur les véhicules qui dépendent moins sur les carburants. Cela a conduit à l'émergence de véhicules respectueux de l'environnement et économes en énergie, comme les véhicules électriques (EV), les véhicules électriques hybrides (HEV) et les véhicules électriques à pile à combustible (FCEV), qui possèdent des mérites significatifs en termes de consommation d'énergie et d'émission d'effluents gazeux par rapport aux véhicules classiques (CV) équipés d'un moteur diesel ou d'un moteur à allumage par étincelle (SI).

La source d'alimentation (énergie) d'un EV est stockée dans la batterie rechargeable et/ou l'ultra-condensateur. En comparaison avec le CV, l'énergie stockée est transformée en force mécanique pour la propulsion du véhicule, par un moteur électrique au lieu d'un moteur à combustion interne (ICE).

Contrairement à l'EV qui est propulsé uniquement par le moteur électrique, la propulsion d'un HEV est la combinaison du moteur électrique et de l'ICE. Les différentes manières dont l'hybridation peut se produire entraînent principalement à l'hybride en série et à l'hybride parallèle.

Le FCEV peut être considéré comme une filiale d'HEV où l'ICE est remplacé par une pile à combustible, qui convertit l'énergie chimique d'un combustible (le plus souvent de l'hydrogène) en électricité par l'intermédiaire d'une réaction chimique avec l'oxygène ou un autre agent d'oxydation, pour produire de l'électricité qui est soit utilisée pour alimenter le moteur électrique de bord soit stockée dans un dispositif de stockage, tel

qu'une batterie ou d'un ultra- condensateur.

Cependant, les FCEVs ne sont pas encore bien prêts pour la production de masse à court terme en raison de l'indisponibilité de l'infrastructure suffisante pour la production et la distribution d'hydrogène, la technologie relativement immature, le prix plus élevé, ainsi que le cycle de vie inacceptable des piles à combustible.

Les EVs semblent une solution idéale pour faire face à la crise d'énergie et au problème de réchauffement climatique. Cependant, des facteurs tels que le coût initial élevé, la distance de déplacement courte et la longue durée de charge d'une batterie limitent la croissance des EVs. Aujourd'hui, les EVs sont utilisés principalement pour les courtes distances ou les applications spéciales, comme le tourisme ou le sport de golf.

Ainsi, les HEVs ont attiré beaucoup d'attention et ont été considérés comme l'alternative la plus prometteuse aux CVs, d'un point de vue à court terme.

Parmi les éléments clés, les batteries sont les éléments les plus importants pour tous les XEVs (EVs, HEVs et FCEVs). Historiquement, de différentes batteries d'alimentation, telles que la batterie plomb-acide, la batterie nickel-cadmium (NiCd), la batterie à l'hydrure métallique de nickel (NiMH) et la batterie Lithium-ion (Li-ion), ont été proposées pour les applications dans les véhicules de nouvelle génération, et le marché de la batterie a constamment évolué en ce qui concerne l'amélioration de la performance de la batterie, l'amélioration de la sécurité et la réduction de coût.

La batterie Li-ion est supérieure parmi toutes les sortes de de batteries proposées au niveau de la densité d'énergie qui détermine le rayon de déplacement et la taille de la batterie, la puissance spécifique qui détermine la capacité d'alimentation et le poids de la batterie, et la sécurité, qui sont cruciales pour les XEVs. Les batteries Li-ion sont plus légères que d'autres types de batterie. La haute tension de la cellule entraîne à l'augmentation de la quantité de puissance et au courant plus faible. En outre, ce type de batterie est respectueux de l'environnement car il n'y a pas d'éléments toxiques existants. Ainsi, la batterie Li-ion est considérée comme l'option la plus prometteuse pour son application dans le véhicule, même si elle n'a pas encore trouvé un marché important dans les applications réelles due aux problèmes concernant le coût, le cycle de vie et la performance à basse température. Toutefois, l'amélioration rapide de la technologie de batterie Li-ion réduira sans doute ses coûts et de prolongera sa durée de vie.

Quel que soit le type de batterie et la manière d'hybridation avec le moteur et les autres composants de powertrain, le point clé d'un XEV (notamment les HEVs) est de concevoir une propre stratégie de contrôle de surveillance, qui gère la manière de répartir la puissance demandée parmi les sources d'énergie.

La stratégie de gestion de l'énergie (EMS) est une sorte de contrôleur de surveillance, qui gère les points de fonctionnement des composants (moteur, moteur électrique et boîte de vitesses) d'un HEV afin que le véhicule fonctionne de la manière la plus efficace et optimale.

Dans la pratique, quelle que soit la qualité de la batterie, le système va vieillir au fil du temps. Par conséquent, il est important de tenir compte du vieillissement et des autres états de la batterie, comme l'état de charge (SOC), qui vise à maintenir l'optimalité de l'EMS sur place. Puisque, comme une partie des signaux d'entrée, les états de la batterie auront sans doute une influence sur la qualité de l'EMS. De plus, un EMS défectueux basé sur les mauvaises informations de la batterie peut donner les objectifs inadaptés de charge ou décharge de la batterie qui va sans doute entraîner des défaillances graves, voire une panne de l'ensemble du système, ainsi qu'une perte financière importante.

Basé sur toutes les questions présentées ci-dessus, cette thèse examinera un HEV de structure parallèle, qui est propulsé par la combinaison d'un moteur SI avec son réservoir de carburant associé et d'un moteur électrique associé à une batterie Li-ion pour stocker l'énergie électrique, en tant que le problématique de recherche. Ainsi, le HEV et la batterie utilisés dans ce travail seront respectivement le HEV parallèle et la batterie Li-ion à moins que d'autres déclarations spécifiques soient données. L'objectif principal ici est de tenir en compte les éléments connexes de la batterie, tels que le SOC et l'état de santé (SOH) de la batterie indiqué par les paramètres comme les résistances internes et la capacité de la batterie, dans le développement de l'EMS conduisant à une sorte d'EMS tolérant aux fautes. Dans le détail, d'une part, le SOC de la batterie est toujours considéré comme une des entrées du système visant à maintenir les usages corrects de la batterie (ni surcharge ni sur-décharge) et à garantir la qualité de l'EMS en fonction. D'autre part, basé sur l'estimation des paramètres connexes de la batterie qui peuvent indiquer son vieillissement (SOH), le système est modélisé sous la forme de transformation linéaire fractionnaire (LFT) avec les différents paramètres de la batterie (comme la capacité de la batterie) représentés par un bloc d'incertitude, puis le contrôleur EMS programmé par les paramètres variantes de la batterie est synthétisé pour déterminer le rapport de division de la puissance entre le moteur et la batterie, ce qui maintient le SOC de la batterie dans une plage raisonnable pour éviter le dysfonctionnement indésirable la batterie en présence d'un défaut de la batterie. Les méthodes principales adoptées pour un tel travail sont le contrôle H_∞ robuste et le contrôle variable de paramètre linéaire (LPV).

Modèle de système

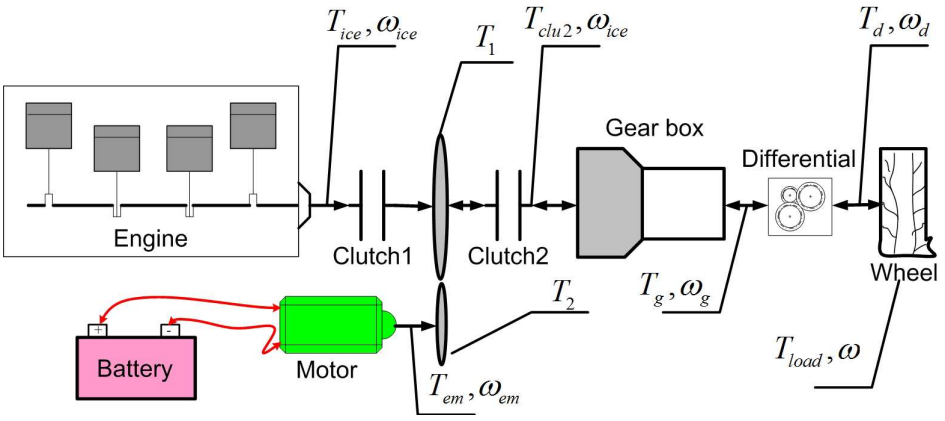

L'architecture du HEV considérée dans cette thèse possède le driveline de type pré-transmission constitué par le moteur, la batterie, le moteur électrique et les composants de transmission tels que les embrayages, la boîte de vitesses et le différentiel final.

En ce qui concerne le modèle de véhicule, les hypothèses fondamentales suivantes sont faites :

- Seulement la dynamique longitudinale du véhicule est prise en compte, et tous les effets de couplage indirects dus aux mouvements verticaux et latéraux sont négligés.
- Les pertes de puissance du driveline sont représentées par les efficacités regroupées appliquées aux composants relatifs.
- Seulement les inerties remarquables, telle que l'inertie du moteur, du moteur électrique, des embrayages et des pneus, sont prises en compte, l'inertie des composants plus petits (par exemple, les essieux) qui ont moins d'effet sur la dynamique du système est ignorée pour la raison de simplicité.
- Les effets d'amortissement et de ressort sur les composants de transmission sont également négligés.

Ensuite, les quatre composants principaux du HEV sont modélisés : le moteur, le moteur électrique, le driveline et la batterie. Pour le moteur et le moteur électrique, la méthode Willans est adoptée pour tenir compte de l'efficacité de conversion d'énergie correspondante. Le modèle du driveline réalisé capture la dynamique d'inertie et les relations torque-vitesse des composants de powertrain concernés. Il est aussi capable de représenter le mouvement longitudinal et la charge de route du HEV. En outre, la

dynamique de la batterie est incorporée dans la description du système visant à prendre en compte l'influence des éléments de la batterie sur l'évolution de l'EMS.

Un modèle de batterie avec la précision et la complexité suffisantes est nécessaire à la fois pour l'estimation de la batterie et pour le développement de l'EMS. Il est aussi important de noter que le modèle présenté dans ce travail n'est pas une nouvelle contribution dans le domaine de la modélisation de la batterie.

Les termes suivants au sujet de la batterie sont la base d'une compréhension suffisante sur la batterie Li-ion et sa modélisation.

- **La capacité de la batterie**

  La capacité de la batterie est une mesure de la charge stockée dans une batterie. La capacité nominale de la batterie représente la quantité de charge qui peut être retirée à partir d'une batterie sous certaines conditions. Cependant, la capacité réelle de la batterie varie considérablement de la valeur nominale, puisqu'elle dépend fortement de l'historique d'utilisation et les conditions d'opération, par exemple, les courants de décharge/charge et la température interne de la batterie. En règle générale, la capacité d'une batterie est calculée en ampère-heure (Ah).

- **C-rate**

  Le C-rate est une mesure du niveau du courant auquel une batterie est déchargée / chargée. Un courant de taux 1C signifie que la batterie est idéalement chargée ou déchargée en une heure, C/2 en deux heures et 2C en une demi-heure. Cela signifie que le courant de 1C pour une batterie d'une capacité nominale de 160Ah est 160A.

- **Résistance interne**

  La résistance interne d'une batterie est définie comme la résistance à la circulation du courant dans une batterie. La résistance interne d'une batterie dépend de nombreux facteurs tels que le C-rate de décharge/charge, la température de la batterie, l'état de charge de la batterie et l'état de santé de la batterie qui sera défini plus tard. L'augmentation de la résistance interne entraîne à une baisse de l'efficacité de la batterie puisque plus d'énergie de la batterie est convertie en chaleur.

- **L'état de charge (SOC)**

  Le SOC est une expression de la capacité actuelle de la batterie comme un pourcentage de la capacité nominale de la batterie, par exemple 100% signifie que la batterie est complètement chargée, et 0% indique que la batterie est épuisée. En

général, le SOC est calculé sur la base de l'intégration du courant au cours du temps de la charge/décharge.

- **Profondeur de décharge (DOD)**

  Le DOD est le contraire du SOC. Il s'agit d'un pourcentage de la capacité de la batterie qui a été déchargée. Un COS de 20% signifie que le DOD est de 80%.

- **État de santé (SOH)**

  Le SOH, qui peut également être décrite comme l'âge d'une batterie, représente l'état de santé d'une batterie. En d'autres termes, le SOH indique à quel niveau la batterie est endommagée. Dans l'application des XEVs, le SOH décrit principalement la capacité d'une batterie pour assurer une fonction particulière de décharge/charge à un moment instantané. La gamme du SOH est définie de 0% à 100%, dans laquelle 100% signifie que la batterie est totalement neuve, et 0% signifie que la batterie ne peut plus satisfaire à la demande du fonctionnement du véhicule.

  En particulier, le SOH est souvent quantifié en estimant la diminution de puissance et/ou la diminution de capacité d'une batterie. La diminution de puissance correspond au phénomène de l'augmentation de la résistance interne de la batterie due à son vieillissement. Cette augmentation de la résistance entraîne une chute de la puissance qui peut être alimentée/absorbée par la batterie. La diminution de capacité correspond au phénomène de diminution de capacité de la batterie pendant que la batterie vieillit.

- **Energie spécifique**

  L'énergie spécifique est définie comme la capacité de batterie par unité de masse. L'énergie spécifique d'une batterie/une cellule de batterie s'exprime en Wh/kg. Une énergie spécifique élevée signifie une charge légère du véhicule associée au poids de la batterie pour le rayon de déplacement requis, et garantit que le véhicule consomme moins d'énergie.

- **Puissance spécifique**

  La puissance spécifique est la puissance disponible par unité de masse d'une batterie/une cellule de batterie s'exprimant en W/kg. Il détermine le poids de la batterie par rapport à l'exigence de performance d'un véhicule. Une batterie peut avoir une énergie spécifique faible mais une puissance spécifique plus élevée, et vice versa.

- **Cycle de vie**

  Le cycle de vie de la batterie est définie par le nombre de cycles de charge/décharge qu'une batterie peut subir avant qu'il ne parvient plus à satisfaire à une exigence spécifique de performance. La définition du cycle de vie de la batterie doit être liée à un certain scénario puisque le cycle de vie réel d'une batterie est affecté par les impacts environnementaux et les paramètres de fonctionnement tels que la température, le C-rate, le DOD, etc.

Plusieurs modèles de batterie avec de divers degrés de complexité et de précision sont proposés dans la littérature. Chaque type se focalise sur les comportements spécifiques de batterie pour les fins spécifiques : de la conception de la batterie et l'estimation des performances à la simulation du circuit.

Fondamentalement, les modèles de batterie peuvent être classés dans les catégories suivantes :

- Modèles de boîte noire
- Modèles électrochimiques
- Modèles de batterie équivalents au circuit électrique (EEC)

Les modèles de boîte noire utilisent les fonctions de transfert pour décrire le comportement des batteries sans avoir à reconstruire les processus physico-chimiques sous-jacents.

La plupart des modèles de boîte noire ne conviennent que pour des applications spécifiques. Surtout, il ne s'applique pas aux batteries Li-ion dont la capacité dépend étroitement de la température de la batterie, les conditions environnementales et le courant de décharge.

Les modèles électrochimiques représentent les processus physico-chimiques complets au moyen d'une série d'équations aux dérivées partielles.

Le modèle électrochimique, d'une part, est une tâche temporellement lourde car elle nécessite beaucoup d'équations électrochimiques complexes pour obtenir une description complète du système, et, d'autre part, est principalement utilisé pour optimiser les aspects physiques de la conception des batteries, caractériser les mécanismes fondamentaux de la production d'énergie et de relier les paramètres de conception des batteries.

Les modèles EEC de la batterie sont généralement décrits par les circuits constitués de composants passifs tels que les résistances, les inductances et les capacités, qui sont configurés pour correspondre à la réponse en fréquence de l'impédance de la batterie.

Les modèles EEC sont couramment utilisés pour la conception du contrôle, et sont particulièrement adaptés pour le co-design et la co-simulation avec d'autres systèmes ou les circuits électriques. En outre, pour les applications électriques, ce genre de modèle est plus intuitif, utile et facile à manipuler. Par conséquent, le modèle EEC qui tient un bon compromis entre le temps de calcul et la précision de la simulation est adopté dans ce travail.

Le modèle de la batterie présenté dans ce travail est un de base qui ne prend pas en compte les influences de la température de batterie et d'autres facteurs, tels que l'effet d'hystérésis, la direction du courant et le C- rate.

Estimation de batterie

Une connaissance précise de la batterie, basée sur l'estimation de l'état de charge (SOC) et l'état de santé (SOH) de la batterie, est d'une part l'une des exigences liées au développement optimal d'EMS, et, d'autre part, est au cœur de l'utilisation correcte de la batterie qui assure le cycle de vie et la sécurité acceptable de la batterie.

Presque aussi longtemps que les batteries rechargeables ont existé, les systèmes capables de donner une indication de la quantité de charge disponible dans une batterie (le SOC de la batterie) ont été utilisés.

Les solutions effectivement mises en œuvre par rapport à l'estimation du SOC de la batterie peuvent être classées comme suit :

- **Comptage de Coulomb (Ampère heure (Ah) comptage)**

  Le comptage Ah est la technique la plus couramment utilisée, exigeant une mesure dynamique du courant circulant à l'intérieur et à l'extérieur de la batterie, dont l'intégrale du temps fournit une indication directe du SOC.

- **Tension de circuit ouvert (OCV)**

  L'OCV est généralement lié au SOC des batteries. Le SOC peut être évalué en laissant la batterie au repos pendant suffisamment de temps, durant lequel toutes les dynamiques de relaxation à l'intérieur de la batterie sont complétées.

- **Spectroscopie d'impédance et la résistance interne**

  La spectroscopie d'impédance est aussi appelée la spectroscopie électrochimique d'impédance (EIS). Elle est réalisée en mettant la batterie au courant alternatif (AC), et en enregistrant simultanément la réponse en tension de la batterie. Le rapport tension- courant (appelé aussi l'impédance) sur la fréquence est lié au

SOC et aux autres caractéristiques de la batterie, par exemple, le vieillissement de la batterie et le SOH.

- **Méthodes de boîte noire**

  Les méthodes de boîte noire, concernées par l'application de l'estimation du SOC, comprennent la logique floue et le réseau artificiel de neurones.

- **Filtre de Kalman (KF) et filtre de Kalman étendu (EKF)**

  Les KFs sont conçus pour estimer les états inconnus des systèmes à l'aide des mesures de certaines entrées et sorties. Le KF optimal peut être utilisé pour déterminer le SOC des batteries à base d'une description numérique du modèle de batterie dont le SOC est pris pour un de ses états. Puis, sur la base de la mesure du courant, de la température et des autres entrées, la valeur mesurée de la tension de la batterie est utilisée en tant que comparateur de correction avec la tension de sortie estimée du modèle de batterie. Une telle approche peut aussi être utilisée pour la prévision des paramètres de la batterie. Les KFs ne peuvent être conçus que pour les systèmes linéaires, tandis que les modèles réels de batterie contiennent souvent les non-linéarités de différents niveaux, dans ce cas les EKFs peuvent être utilisés à la place.

Cependant, toutes les méthodes évoquées ci-dessus ne s'appliquent pas aux applications des XEVs.

La spectroscopie d'impédance and **la résistance interne** sont les tests hors-ligne, ce qui signifie que les batteries doivent être déconnectées du véhicule pour effectuer certains tests. Ce n'est évidemment pas possible pour les XEVs, où la batterie doit toujours être disponible pour stocker ou fournir de l'énergie électrique.

La tension de circuit ouvert (OCV) est largement utilisée dans les applications électroniques de faible puissance, grâce aux conditions prévisibles de travail et à l'environnement contrôlé. En outre, en raison de la longue période caractéristique associée à la relaxation de la batterie, l'estimation du SOC à base de l'OCV n'est pas disponible pour les applications automobiles.

Le comptage de Coulomb, autrement dit l'intégration de courant, offre la méthode la plus simple pour détecter les variations du SOC, car elle est une bonne source d'information pour le SOC. Cependant, il est affecté par l'imprécision de la condition initiale du SOC, la dégradation accumulée de la capacité de batterie au cours du vieillissement de la batterie.

Le réseau de neurones and **la logique floue** produisent souvent de bonnes performances d'estimation en ligne, et ils ne nécessitent pas de déconnecter les batteries. Cependant, le processus d'apprentissage des **méthodes de boîte noire** est lourd en calcul, même s'ils peuvent atteindre une haute précision d'estimation.

De même, le **filtre Kalman (KF)** a de bonnes performances pour les estimations SOC en ligne. De plus, il peut fournir une estimation robuste au cas des mesures bruitées, initialisations inexactes et incertitudes du modèle.

La méthode envisagée pour l'estimation du SOC de la batterie dans ce travail est le KF. En modélisant le système de batterie avec le SOC comme un de ses états, l'estimation du SOC peut alors être réalisée en utilisant le filtre Kalman.

La façon la plus simple et directe pour l'estimation du SOH est d'estimer les caractéristiques électriques de la batterie qui peuvent être modélisées par un EEC qui est principalement composé d'une série de résistances et condensateurs. Cela signifie que l'estimation des paramètres du modèle EEC peut faciliter l'estimation du SOH.

D'ailleurs, il est largement prouvé que la résistance et la capacité de la batterie sont les deux caractéristiques électriques principales de la batterie qui sont liées au SOH d'une batterie. Donc, dans la pratique, l'estimation du SOH se résume souvent au problème d'estimation des paramètres en termes de la capacité et/ou la résistance de la batterie. De plus, la plupart des algorithmes utilisés pour l'estimation des paramètres de la batterie sont basés sur le KF qui réalise les estimations robustes en dépit des mesures bruitées et des incertitudes du modèle, en modélisant le système de batterie pour inclure les paramètres recherchés de la batterie dans la description de son état.

Comme, dans ce mémoire, la capacité de la batterie est le seul paramètre de la batterie qui est utilisé pour programmer le contrôleur EMS (une des contributions principales de ce travail), toutes les estimations des paramètres discutées sera l'estimation de la capacité. Par conséquent, il faut noter que la capacité n'est pas le seul paramètre qui pourrait être utilisé pour indiquer le SOH de la batterie.

Dans ce travail, l'algorithme Least Mean Squares (LMS), qui est plus simple et plus directe que le KF, est adopté pour l'estimation de la capacité de la batterie. De plus, de différentes périodes de cycle sont affectées pour l'estimation du SOC et de la capacité de batterie. En détail, le SOC est toujours estimé afin de suivre la dynamique rapide de la batterie, alors que la capacité de la batterie est occasionnellement estimée pour assurer l'optimisation de l'estimation du SOC, et fournir l'indication du SOH de la batterie.

Pour estimer la capacité de la batterie en utilisant le LMS, le modèle simple suivant, qui est une reformulation de l'équation d'état SOC, est adopté :

$$-I_{k-1}Ts = Cb_{k-1}(SOC_k - SOC_{k-1} + n_w) + n_v$$

où Ts est la période d'échantillonnage, k est le point d'échantillonnage, I est le courant de la batterie qui est mesurable, Cb est la capacité de la batterie à estimer, les SOCs héritent les valeurs estimées en utilisant le KF, n_w est utilisé pour compter l'erreur de l'estimation du SOC, et n_v représente l'entrée de bruit du capteur.

Estimation du défaut de batterie basée sur l'observateur H_∞

Dans la pratique, toutes les batteries vieillissent. Par conséquent, il est important de détecter la dégradation éventuelle de la batterie, d'une part pour prévoir dans combien de temps la batterie va dysfonctionner ou va atteindre l'état qui ne peut plus garantir les performances satisfaisantes, et d'une autre part pour éviter les défaillances graves ou la panne complète à l'ensemble du système, car, en tant que le composant principal, la batterie a un impact décisif sur la performance des XEVs.

Pour la détection du défaut de batterie, l'approche bien connue et largement utilisée est la méthode d'identification des paramètres de la batterie basée sur le KF. Bien que les informations de défaut d'une batterie déduites de l'estimation de batterie soient précieuses, les résultats expérimentaux ont montré des variations importantes des paramètres de la batterie dans les différents environnements, en particulier sous les différentes températures ambiantes.

Des expérimentations pratiques ont montré que les paramètres de la batterie sont sensibles à la variation des situations environnementales telles que la température, le SOC, le vieillissement de la batterie, etc.

Dans ce travail, l'influence de la température, qui a un impact significatif sur les paramètres de la batterie, ainsi que celle du vieillissement de la batterie, sont mises en évidence.

En général, la résistance interne de la batterie diminue lorsque la température augmente. En effet, à côté de la résistance interne, la résistance au transfert de charge et la résistance à la diffusion diminuent en parallèle avec l'augmentation de la température.

En plus de la dépendance de la résistance de batterie sur la température, la capacité de la batterie varie également en fonction des températures. Dans ce cas la capacité de la batterie monte à haute température et chute à basse température. Le SOH de la batterie, qui peut également être décrit comme l'âge d'une batterie, représente l'état de santé d'une batterie. En d'autres termes, le SOH indique le niveau auquel la batterie est

endommagée.

Au cours du processus de vieillissement, la résistance au transfert de charge et la résistance à la diffusion de la batterie varient légèrement, tandis que la résistance interne augmente de manière significative. De plus, il est dit que la résistance augmente jusqu'à 160% de sa valeur initiale dans les mêmes conditions (même température et même SOC) lorsque la batterie arrive en fin de vie, ce qui signifie que la puissance maximale d'une batterie diminue à 60% de sa valeur initiale à l'état neuf (même température et même SOC).

La capacité d'une batterie à plat (avec le SOH de 0%) diminue à 80% de sa capacité maximale initiale dans les mêmes conditions (même température et même SOC), ce qui signifie que la capacité de la batterie diminue lorsque le SOH baisse.

Ici, les influences du changement de la température et le vieillissement de la batterie sur la résistance et la capacité de la batterie sont considérées et modélisées comme les variations additives aux valeurs nominales des paramètres de la batterie, basé sur un modèle EEC de la batterie à 2^{nd} ordre.

En outre, la variation de la température est traitée comme une perturbation du système, tandis que le vieillissement de la batterie est traité comme un défaut du système.

Ensuite, le problème d'observation de défaut est considéré comme un problème standard H_∞, et l'objectif est de trouver un observateur de stabilisation qui minimise l'influence des perturbations sur la détection de défauts.

Les simulations dans le domaine temporel prouvent que :

- L'observateur de défaut réalisé permet non seulement de détecter l'occurrence du défaut de la batterie, mais aussi de suivre la tendance d'évolution de défauts en présence des autres influences, telles que le courant d'entrée et la variation de la température.

- L'observateur réalisé peut suivre le processus de vieillissement de la batterie, qu'il soit lent ou brusque.

Comme l'observateur de défaut réalisé ici est basé sur la linéarisation de la description du système, la performance d'estimation est limitée en ce qui concerne le système réel non-linéaire. Ainsi, il sera intéressant de viser le futur travail à concevoir un observateur LPV qui est plus adapté aux systèmes de batterie réels.

La conception d'EMS à base de H_∞

Le principal avantage d'une architecture hybride électrique est la présence des sources d'énergie supplémentaires (souvent la batterie d'alimentation et son moteur électrique associé) en plus du réservoir de carburant, qui peuvent être utilisées pour réduire la consommation de carburant et/ou les émissions du véhicule, tout en conservant les performances requises du véhicule. Ensuite, pour chaque instant de temps, la puissance demandée par le véhicule peut être fournie par une ou une combinaison de ces sources.

Le point clé à développer le plein potentiel de l'hybridation est de concevoir une propre stratégie de contrôle, qui gère la manière de répartir la puissance demandée parmi les sources d'énergie de façon efficace et optimale. Ainsi, l'EMS est adopté pour jouer un tel rôle dans les HEVs.

L'EMS est aussi appelé le contrôleur de supervision, contrairement aux contrôleurs de bas niveau ou au niveau du composant, qui sont utilisés pour gérer les composants associés afin qu'ils se comportent comme dicté par le contrôleur de supervision. Dans un CV, il n'y a pas besoin d'un contrôleur de supervision, parce que le moteur est la seule source de puissance. La puissance demandée par le conducteur est directement traduite en action du contrôleur du moteur (contrôleur de bas niveau) qui détermine l'opération du moteur. Dans le HEV, la puissance requise est d'abord transmise au contrôleur EMS (contrôleur de supervision), qui détermine la division de puissance entre le moteur et le moteur électrique, et envoie les signaux de demande de puissance au contrôleur du moteur et au contrôleur du moteur électrique. Ensuite, le moteur et le moteur électrique fonctionne selon l'indication donnée par leur propre contrôleur au niveau du composant. Les décisions de l'EMS devraient également tenter de minimiser la consommation de carburant, l'émission des polluants, mais aussi de maintenir les performances du véhicule, ou d'assurer un compromis entre tous ces objectifs.

De nombreux algorithmes de gestion d'alimentation ou des stratégies de contrôle et de supervision pour les HEVs ont été proposés dans la littérature. L'EMS peut être généralement divisé en deux groupes principaux : les stratégies à base de règles et les stratégies à base d'optimisation. Les stratégies à base de règles sont ensuite classées par les méthodes à base de règles floues et celles à base de règles déterministes. Les stratégies à base d'optimisation sont ensuite classées par les méthodes d'optimisation globale et celles d'optimisation en temps réel.

L'aspect principal impliqué dans les approches à base de règles est leur efficacité dans le contrôle de supervision en temps réel du flux de puissance dans un driveline hybride. Les règles sont principalement basées sur les heuristiques, l'intuition et l'exper-

tise humaine, et sont généralement indépendantes de la connaissance a priori d'un cycle de conduite prédéfini. L'idée principale des stratégies à base de règles est généralement basée sur le concept de load-leveling. Pour chaque vitesse du moteur, la stratégie de load-leveling décale le couple moteur le plus près possible du point de fonctionnement optimal en tenant compte du rendement, de la consommation de carburant et des émissions. L'écart entre la puissance demandée par le conducteur et la puissance générée par le moteur est compensé par le moteur électrique.

Les règles déterministes sont basées sur les cartographies de rendement et d'émissions du moteur, ainsi que sur l'expérience de conduite. Ce type de règles sont généralement mises en œuvre par l'intermédiaire des cartes statiques, afin de partager la puissance requise entre le moteur et le moteur électrique. Au lieu d'utiliser les règles déterministes, les connaissances des experts peuvent être utilisées pour former une logique floue, et une stratégie de gestion de l'énergie en temps réel peut être réalisée en utilisant la capacité de prise de décision de la logique floue.

Compte tenu de la rigidité inhérente d'une approche à base de règles, les designers ont tourné leur attention vers les stratégies à base d'optimisation qui sont utilisées pour calculer les couples de référence optimales du moteur, les couples de référence du moteur électrique et le braquet des HEVs en minimisant une fonction de coût qui représente généralement la consommation de carburant ou les émissions de polluants. Si cette optimisation est effectuée pour les cycles de conduite spécifiques à l'aide des informations du passé et du futur (anticipées), une solution d'optimisation globale peut être réalisée. De toute évidence, cette approche ne peut pas être utilisée directement pour la gestion pratique d'énergie, même si les résultats obtenus peuvent être considérés comme des repères utiles pour analyser, évaluer et déduire les stratégies de contrôle en temps réel. D'autre part, une stratégie d'optimisation en temps réel peut être trouvée par la définition d'une fonction de coût instantanée qui ne dépend que des variables du système à l'heure actuelle. Bien sûr, la solution d'un tel problème n'est pas globalement optimale, mais elle peut être utilisée directement pour l'implémentation en temps réel.

On peut conclure que : les stratégies à base de règles sont plus faciles à mettre en œuvre dans les applications réelles, parmi lesquelles les stratégies de contrôle à base de règles floues sont supérieures à celles à base de règles déterministes, les stratégies à base d'optimisation ont les meilleures performances que celles à base de règles, mais les méthodes d'optimisation globale ne sont typiquement pas faisable dans une application en ligne en raison de leur complicité de calcul, ainsi que les besoins de connaissance a priori sur la future demande de puissance du véhicule (profil de la route) ; d'un point de vue de l'implémentation en ligne, les méthodes optimales en temps réel et à base de

règles floues sont bien adaptées en raison des caractéristiques adaptatives et robustes.

Comme mentionné précédemment, l'utilisation des informations de la batterie est nécessaire pour améliorer les performances du système et prolonger la vie de la batterie. Ainsi, une étude préliminaire sur l'influence du défaut de la batterie sur la stratégie de contrôle est effectuée ici.

Le HEV considéré adopte l'architecture décrite précédemment. Concernant la batterie, un modèle simplifié, qui considère la batterie comme la combinaison d'une source de tension et une résistance, est adopté.

Ici, le défaut de la batterie est souvent dû au vieillissement de la batterie, et est formulé en le considérant comme une chute de tension à un certain degré par rapport à la tension normale de la batterie.

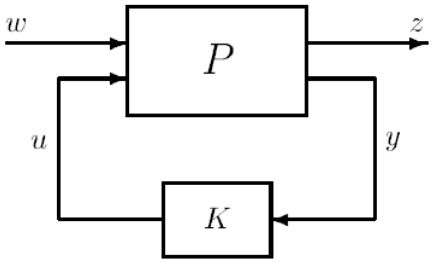

Le problème de contrôle H_∞ standard est assimilé à la recherche d'un contrôleur K tel que :

$$\|F_l(P,K)\|_\infty < \gamma$$

où γ est un certain niveau de performance prescrit.

Basé sur le modèle du système, le développement du contrôleur EMS, qui tient en compte l'influence du vieillissement de la batterie, est considéré dans un problème de contrôle H_∞ standard, et peut être résolu en utilisant la solution basée sur l'inégalité matricielle linéaire (LMI).

Etant donné que le modèle du système est fonction de la vitesse du véhicule et le couple nécessaire, alors que le contrôle H_∞ peut seulement être utilisé pour un système linéaire avec les matrices du système constantes. Par conséquent, de différents contrôleurs EMS devraient être conçus pour satisfaire à l'exigence spécifique de la vitesse et du couple du véhicule.

D'ailleurs, le contrôleur réalisé est seulement adapté au traitement de défaut. L'objectif de minimisation de la consommation de carburant nécessitera d'autres modifications sur la structure de contrôle du système.

Ainsi, la combinaison de la méthode LPV et le contrôle H_∞ est adoptée pour traiter

les paramètres variables, ainsi que le problème de minimisation de la consommation de carburant.

La conception d'EMS à base de LPV/H_∞

L'approche H_∞ est adoptée pour le développement de l'EMS dans un HEV en tenant compte de l'influence du vieillissement de la batterie, et un contrôleur de rétroaction de sortie qui minimise certaines fonctions de coût est précédemment dérivé. Malheureusement, les matrices d'état du modèle de système sont fixées sous certaines conditions de fonctionnement. Cette approche est souvent trop prudente lorsque les paramètres physiques subissent de fortes variations pendant le fonctionnement du système. Une façon de réduire le conservatisme est de concevoir les contrôleurs robustes autour de chaque point de fonctionnement et de basculer entre les contrôleurs selon certaine politique d'interpolation, mais la stabilité et les performances ne peuvent pas être garanties.

Récemment, les méthodes LPV ont été largement utilisées pour donner une approximation aux systèmes non-linéaires et aux systèmes linéaires variables dans le temps, et deux approches principales sont souvent adoptées pour la conception du contrôleur LPV : l'approche polytopique et l'approche de la transformation linéaire fractionnaire (LFT). Le principal inconvénient de la méthode polytopique est le grand nombre d'inégalités matricielles linéaires (LMI) à résoudre si le nombre de paramètre augmente, mais ce n'est pas le cas pour l'approche LFT. En outre, cette dernière permet de considérer, dans la même formulation, les divers paramètres et incertitudes (l'adaptation aux paramètres et la robustesse par rapport aux incertitudes).

Cette partie présente deux applications de l'approche LPV/H_∞ sur le développement et l'amélioration de l'EMS. La première application est une touche de l'approche LPV pour la modélisation et le contrôle du HEV. L'objectif est de tester l'efficacité d'une telle approche en tenant compte de l'influence des paramètres changeants du système sur la stratégie de contrôle. Par conséquent, un contrôleur EMS à gain réglementé est réalisé en visant à minimiser la consommation de carburant d'un PHEV, où le système est modélisé sous forme de LFT avec les paramètres variables du système (vitesse du véhicule et la capacité de la batterie) représentés comme un bloc d'incertitude, et le contrôleur est programmé en fonction des paramètres variables.

Basé sur le fait prouvé ci-dessus que le LPV est une méthode capable à l'égard de la modélisation et du contrôle du HEV, l'autre (la deuxième) application de l'approche LPV/H_∞ est concerné avec la conception d'un régulateur EMS. En supposant qu'un EMS optimal existe déjà, l'objectif est de déterminer la quantité de régulation du courant de

la batterie et le ratio de division de la puissance entre le moteur et la batterie par rapport aux valeurs optimales de ces variables obtenues par le SME existant, selon la variation du cycle de conduite et la dégradation de la capacité de batterie. De même avec la première application, le modèle du système est également sous la forme LFT et l'EMS du LPV est synthétisé en utilisant l'approche proposée par Apkarian & Gahinet (1995).

Comme indiqué plus haut, ces deux contrôleurs sont pour différents objectifs de contrôle. En outre, comme sera indiqué plus tard, les différentes structures de contrôle sont adoptées avec différentes entrées et sorties de contrôle pour chaque application. Fait plus important encore, le couple exigé est d'une valeur fixe pour le premier contrôleur, ce qui n'est pas réaliste pour le véhicule réel. De plus, la vitesse de rotation de la roue n'est pas contrôlée. La performance du premier contrôleur EMS est aussi limitée par la régularité de la cible SOC prédéfinie. Au contraire, le second contrôleur est plus raisonnable, le couple exigé est adapté aux différentes conditions routières et la maniabilité du véhicule est satisfaite (au moyen du contrôle de vitesse du véhicule).

Approche LPV/H_∞ pour minimiser la consommation de carburant et prolonger la vie de la batterie

Quelle que soit la topologie, les stratégies de gestion de l'énergie dans les HEVs sont généralement destinées à atteindre plusieurs objectifs simultanés. L'objectif principal est souvent la minimisation de la consommation de carburant du véhicule, tout en essayant de minimiser les émissions, ainsi que le maintien ou l'amélioration de la maniabilité du véhicule. En outre, les objectifs de contrôle sont souvent soumis à des contraintes intégrées, telles que le maintien nominal du SOC de la batterie dans les hybrides de maintien de charge.

Si la minimisation de la consommation de carburant est le seul objectif, le problème de la gestion de l'énergie peut être formulé ainsi : trouver le ratio instantané de division de la puissance entre le moteur et la batterie, afin que :

$$\int_0^{t_f} \dot{m}_f dt$$

est minimisé, et au niveau des contraintes

$$0 \prec SOC_{min} \leq SOC \leq SOC_{max}$$

est satisfait, où $\dot{m}_f$ est la consommation instantanée (débit massique) de carburant, le SOC_{min} et le SOC_{max} sont respectivement la limite autorisée inférieure et supérieure du

SOC.

Dans la pratique, la batterie vieillit au fil du temps, et le taux de vieillissement de la batterie est affecté par les profils de fonctionnement tels que le C-rate, la température et la profondeur de décharge, qui sont directement influencés par la stratégie de contrôle. Par conséquent, il est significatif que le vieillissement de la batterie est pris en compte dans l'élaboration des contrôleurs EMS à gain réglementé visant, d'une part, à prolonger la vie de la batterie, et d'autre part à garantir les performances du système en dépit du vieillissement de la batterie.

En règle générale, le vieillissement de la batterie peut être décrit comme la diminution de capacité (la capacité de la batterie diminue) ou/et la diminution de puissance (la résistance interne de la batterie augmente). Ici, seul le premier cas de diminution de capacité est pris en compte

Dans cette application, un contrôleur LPV/H_∞ qui optimise la consommation de carburant et prolonge la vie de la batterie est présenté. Notez que le contrôle du moteur n'est pas considéré ici, même si la stratégie de contrôle réalisée peut avoir un impact fort sur la consommation de carburant.

En termes de description du système, deux éléments principaux sont inclus : le driveline et la batterie. Le modèle obtenu du système est non-linéaire par rapport à la vitesse de rotation de la roue. En outre, les paramètres du modèle, tels que la résistance et la capacité de la batterie, varient en fonction du changement d'environnement et de l'évolution du vieillissement de la batterie.

Basé sur le fait que la méthode LPV pourrait être utilisée pour faire une approximation aux systèmes non-linéaires et aux systèmes linéaires variables dans le temps, nous donnons quelques définitions. Puis, sur la base de ces définitions, une représentation LFT peut être utilisée pour réécrire le modèle du HEV, qui inclut l'interconnexion du système comme représentée ci-dessous.

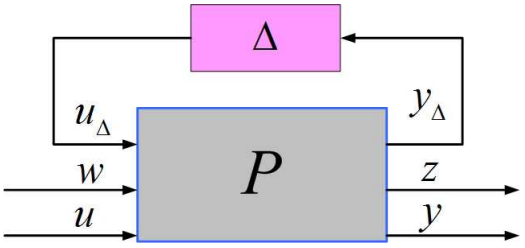

Rappelons-nous le schéma de contrôle LPV/LFT comme illustré ci-dessus, où l'opé-

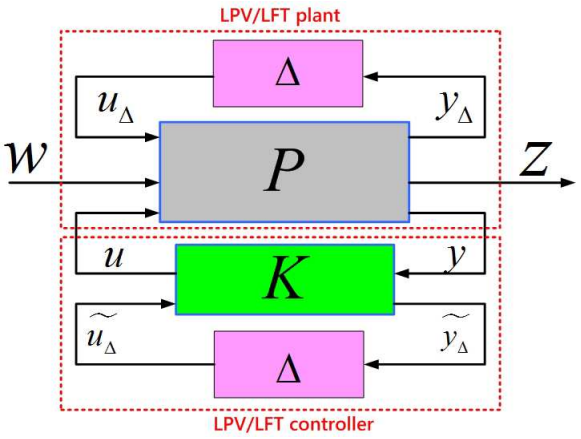

rateur en boucle fermée de w à z est :

$$T_{zw} = F_l(F_u(P, \Delta), F_l(K, \Delta))$$

L'objectif d'un contrôleur LPV/H_∞ est de garantir la performance en boucle fermée $\gamma > 0$ de w à z pour tous les paramètres Δ admissibles. Supposons que Δ est limité, le contrôle LPV/H_∞ d'un système LPV/LFT se résume à trouver une structure de contrôle K telle que les conditions suivantes sont satisfaites :

- Le système en boucle fermée est stable à l'intérieur pour tous les paramètres Δ possibles
- et $\|T_{zw}\|_\infty < \gamma$

Ensuite, le développement du contrôleur EMS est considéré comme un problème de contrôle LPV/LFT qui peut être résolu en utilisant la solution à base de LMI.

Les simulations montrent que :

- la consommation minimisée de carburant peut toujours être réalisée.
- moins d'énergie de la batterie est consommée lorsque le vieillissement de batterie empêche la dégradation continuelle de la batterie.

Régulateur EMS du LPV avec la prolongation de la vie de la batterie

De nombreuses stratégies optimales de gestion de l'énergie ont été proposées dans la littérature. En fait, l'optimalité du contrôleur EMS réalisé est aussi influencée par d'autres facteurs, qui changent au fil du temps, tels que l'état de santé de la batterie. Par conséquent, certaines corrections critiques, qui garantissent l'optimalité acquise au contrôleur EMS optimal réalisé sont nécessaires.

Le régulateur EMS développé ici est utilisé pour déterminer la quantité de régulation de courant de la batterie, qui influence implicitement le rapport de division de puissance entre le moteur et la batterie, par rapport au courant actuel de la batterie indiqué par le contrôleur EMS optimal existant, en fonction de la variation du cycle de conduite et de la dégradation de la capacité de batterie. Un tel régulateur d'un côté prolonge la vie de la batterie, et d'un autre côté garantit la performance du système et l'optimalité acquise en dépit des comportements variables du système.

En détail, d'une part, avec l'évolution du vieillissement de la batterie, moins de courant sera tiré de la batterie, ce qui conduit à la diminution du couple moteur réel par rapport à une tension de batterie spécifique, et d'autre part, si la vitesse du véhicule augmente, ce qui signifie que plus de couple est nécessaire, le courant de la batterie augmentera en conséquence pour satisfaire à l'exigence du cycle de conduite.

Le développement du régulateur EMS comprend alors les étapes suivantes : (1) la construction du modèle de système en tenant compte à la fois de la dynamique du véhicule et des comportements de la batterie, (2) l'approximation linéaire du modèle non-linéaire de système basée sur la méthode LPV/LFT, (3) la transformation du modèle en forme LFT avec les différents paramètres représentés par un bloc d'incertitude, (4) le développement du régulateur SME avec gain réglementé avec la vie de la batterie prolongée en cas de la dégradation de la capacité de batterie (vieillissement de la batterie).

Dans ce travail, l'approche LPV/H_∞ est utilisée pour : (1) le développement d'un contrôleur EMS avec gain réglementé dans un PHEV avec une consommation minimale de carburant et la vie de la batterie prolongée en cas de la dégradation de la capacité de batterie (vieillissement de la batterie), et (2) un régulateur EMS qui est utilisé pour déterminer la quantité de régulation du courant de la batterie, qui influence implicitement le rapport de division de puissance entre le moteur et la batterie, par rapport au courant actuel de la batterie indiqué par le contrôleur EMS optimal existant, en fonction de la variation du cycle de conduite et de la dégradation de la capacité de batterie.

La première application présente un test au sujet de l'efficacité de l'approche LPV sur la modélisation et le contrôle du VHE en tenant compte de l'influence des paramètres variables du système. La deuxième application peut être utilisée pour garantir l'optimalité acquise par un contrôleur EMS optimal existant en dépit de l'évolution des facteurs environnementaux et les paramètres variables du système.

Dans les deux cas, le véhicule est modélisé en LPV/LFT forme, où les paramètres variables sont représentées par un bloc d'incertitude, et le problème du développement de contrôleur/régulateur est résolu en utilisant la solution basée sur LMI. Plus important

encore, le contrôleur et le régulateur ont la fonction de prolonger la vie de la batterie.

Conclusion et perspectives

Conclusion générale

Cette thèse porte sur le développement de stratégies de contrôle robuste dans le HEV. L'objectif principal est de rendre compte du SOC et du SOH de la batterie indiqués par la capacité de la batterie, dans le développement d'EMS menant à la vie prolongée de la batterie. L'ensemble du contenu est organisé dans neuf chapitres.

- Le premier chapitre présente une introduction générale sur le HEV et sa propre classification et structure. La structure de cette thèse est aussi présentée dans ce chapitre.

- Dans le deuxième chapitre, certaines notions clés liées au contrôle robuste sont données dans le niveau relativement basique, la formulation du problème et les solutions à base de LMI de la synthèse de contrôleurs H_∞et de la synthèse de contrôleur H_∞/LPV sont présentés en détail.

- Le chapitre trois vise à faire les descriptions mathématiques par rapport aux comportements de la batterie Lithium-ion. Dans ce chapitre, le principe de fonctionnement et le classement de la batterie Lithium-ion sont donnés avec quelques notions de base de la batterie. Le modèle de la batterie EEC est construit dans lequel tous les paramètres concernés de la batterie sont inclus.

- Le chapitre quatre contribue à l'estimation du SOC de la batterie et ses paramètres. La méthode utilisée pour l'estimation du SOC de la batterie est le filtre Kalman. Ce chapitre propose aussi une nouvelle méthode d'estimation de la capacité de batterie, qui est basée sur l'algorithme LMS qui est plus simple que le KF.

- Le chapitre cinq est consacré à l'élaboration d'une nouvelle méthode d'estimation du vieillissement de la batterie basée sur l'observateur H_∞ qui tient compte des variations de l'environnement. Dans ce chapitre, l'influence de la variation de température et le vieillissement de la batterie sur sa résistance et sa capacité est considérée et modélisée comme les variations additives sur les valeurs nominales des paramètres de la batterie. La méthode d'estimation de défaut proposée permet de détecter en continu l'évolution du vieillissement, tout en minimisant l'influence des autres facteurs, tels que la température et le courant de la batterie.

- Le chapitre six est consacré au développement du modèle d'un PHEV qui est capable d'identifier les comportements dynamiques longitudinaux du véhicule affectant la consommation de carburant et la performance du véhicule. En outre, la dynamique de la batterie est incorporée de manière innovante dans la description du système afin d'inclure l'âge de la batterie dans le développement d'EMS.

- L'objectif principal du chapitre sept est de faire une étude préliminaire sur l'influence du défaut de la batterie sur l'EMS, où l'approche H_∞ est utilisée pour déterminer le rapport de division de la puissance entre le moteur et la batterie, qui maintient l'état d'énergie de la batterie à l'intérieur d'une zone raisonnable pour éviter la panne indésirable de la batterie. Ce chapitre présente aussi un aperçu de l'EMS, y compris la motivation et la structure générale du contrôleur EMS avec tous les signaux d'entrée et les signaux de contrôle en sortie.

- Dans le chapitre huit, l'approche H_∞/LPV est utilisée pour : (1) le développement d'un contrôleur EMS avec gain réglementé qui minimise la consommation de carburant et prolonge la vie de la batterie en dépit de son vieillissement, et (2) le développement d'un régulateur SME qui est utilisé pour déterminer la quantité de régulation du courant de la batterie, qui a une influence implicite sur le rapport de division de puissance par rapport au courant actuel de la batterie indiqué par un contrôleur EMS déjà existant, selon la variation du cycle de conduite et de la dégradation de la capacité de batterie.

Les contributions principales de cette thèse concernent principalement :

- La conception de l'estimation de la capacité de batterie sur la base de l'algorithme LMS qui est plus simple et moins coûteux en temps que l'approche KF en termes d'estimation des paramètres.

- Le développement de l'observateur H_∞ du défaut de la batterie, où le modèle élargi de la batterie est utilisé qui traite la variation de la température comme une perturbation et le vieillissement de la batterie comme un défaut, ce qui minimise l'influence de la température et du courant de la batterie sur la précision de l'estimation.

- Le développement de l'EMS en tenant compte à la fois de la dynamique du véhicule et des comportements de la batterie.

- Le développement des modèles de systèmes avec ceux de LPV sous la forme LFT

représentant la vitesse variable et la capacité de la batterie comme un bloc d'incertitude.

- La conception d'un contrôleur EMS avec gain réglementé visant à minimiser la consommation de carburant et prolonger la vie de la batterie en dépit de son vieillissement.

- Le développement d'un régulateur EMS du LPV qui détermine la quantité de régulation du courant de la batterie et le ratio de division de la puissance entre le moteur et la batterie à l'égard des valeurs optimales obtenues par l'EMS existant, en fonction de la variation du cycle de conduite et de la dégradation de la capacité de batterie.

Perspectives

Dans la perspective de la méthode adoptée, ainsi que les principaux résultats obtenus dans ce travail, les idées suivantes semblent d'un grand intérêt à moyen terme :

- Le développement d'un modèle de batterie plus complexe qui prend en compte les influences de la température de la batterie et d'autres facteurs, tels que l'effet d'hystérésis, la direction du courant et le C-rate, qui peuvent modéliser les comportements réels de la batterie et l'environnement d'opération avec plus de précision.

- Le développement d'un modèle du HEV qui contient des descriptions plus dynamiques en matière de composants de driveline, tels que la boîte de vitesses et le différentiel final, ce qui conduira à la description du système plus précise et une meilleure stratégie de contrôle d'énergie.

- La détermination des paramètres du modèle, ainsi que la validation du modèle de la batterie et du modèle du véhicule HEV proposé dans ce travail, basées sur des tests intensifs avec le système réel.

- Le développement de la stratégie de contrôle de freinage par récupération qui assure un système complet de gestion de l'énergie.

Et les points suivants à long terme :

- La conception d'un observateur LPV de défaut de la batterie qui s'adapte mieux aux systèmes réels non-linéaires de la batterie.

- **Stratégie de contrôle de l'énergie** : La combinaison de l'observateur de défaut proposé avec le système de contrôle classique d'un HEV, qui assure l'adaptation de la stratégie de contrôle de l'énergie à l'évolution du vieillissement de la batterie, (2) le test des stratégies de contrôle proposées H_∞ et H_∞/LPV sur un véhicule réel.

Contents

List of Figures

List of Tables

Chapter 1

Introduction and Dissertation structure

General introduction and motivations

Conventional vehicles (CVs) equipped with Internal Combustion Engine (ICE) have been in existence for more than a century. With the increase of the world population, the demand for vehicles as transportation has increased dramatically in the past decades, which induces a significantly increased demand for oil. Another problem associated with the increasing use of vehicles is the pollutant emissions. The green house effect, also known as global warming mainly resulted from the auto exhausts, is a serious issue that we have to face to, see Chan (2007).

In the recent years, growing public concern has been given both on the energy problem associated with more and more serious lack of the fossil fuels which are non-renewable, and on the environment problem associated the progressively increased pollutant emissions. Subsequently, intensive contributions have been made by many automotive industries and research institutes on the production and use of alternative fuels that are renewable (see Momoh & Omoigui (2009) for more information on the available type of alternative fuels), as well as on vehicles that depend less on the fuels. This has led to the emergence of environment-friendly and energy-saving vehicles such as Electric Vehicles (EVs), e.g. the Renault Twizy and Renault Kangoo Z.E. in France, Hybrid Electric Vehicles (HEVs), e.g. the famous Toyota Prius, and Fuel Cell Electric Vehicles (FCEVs), e.g. the Toyota FCHV-BUS, which own considerable merit in terms of energy consuming and off-gas emission compared with conventional vehicles equipped with a Diesel engine or a Spark-Ignited (SI) engine.

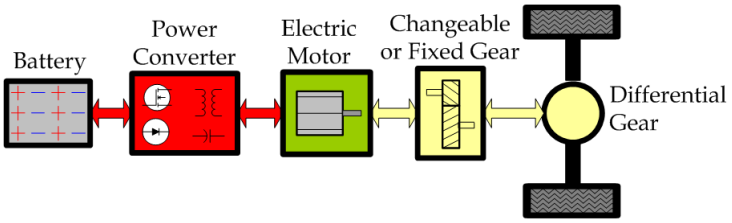

Figure 1.1: Architecture of electric vehicles, de Lucena (2013)

The power source (energy) of an electric vehicle (as depicted in Fig. 1.1) is stored in the rechargeable battery or/and the ultra-capacitor (not illustrated in Fig. 1.1). Compared with the CV, the stored energy of an EV is transformed into mechanical power for vehicle propulsion, from an electric motor instead of the ICE.

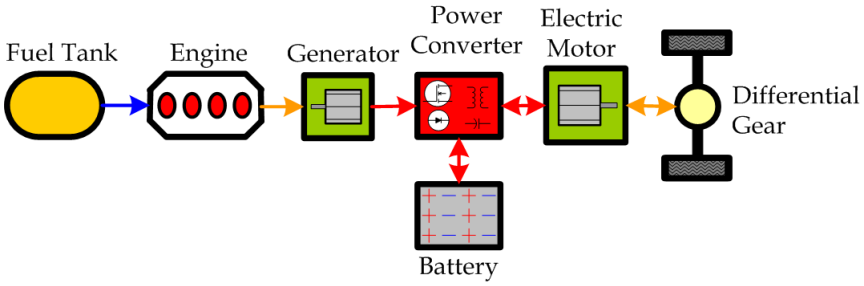

Figure 1.2: Architecture of series hybrid electric vehicles, de Lucena (2013)

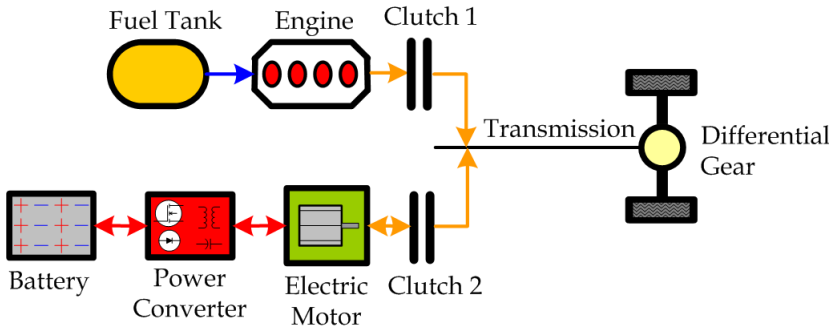

Figure 1.3: Architecture of parallel hybrid electric vehicles, de Lucena (2013)

Unlike the electric vehicle that is propelled solely by the electric motor, propulsion of a hybrid electric vehicle is the combination of electric motor and ICE. The different manners in which the hybridization can occur mainly give rise to series hybrid (with the architecture depicted in Fig. 1.2) and parallel hybrid (with the architecture depicted in Fig. 1.3). See de Lucena (2013), Chan et al. (2010), Chan (2007), Lo (2009) and Penina et al. (2010) for detailed description on each HEV type.

The fuel cell electric vehicle can be treated as a series HEV where the ICE is replaced by a fuel cell, which converts the chemical energy of a fuel (most commonly the hydrogen) into electricity via a chemical reaction with oxygen or another oxidizing agent, to produce electricity which is either used to power the on-board electric motor or stored in an storage device, such as a battery pack or ultra-capacitor pack.

However, FCEVs are still not well ready for mass production within short term due to the unavailability of sufficient infrastructure for hydrogen production and distribution, relatively immature technology, higher price and unacceptable life cycle of the fuel cells as well.

EVs seem to be an ideal solution to deal with the energy crisis and global warming problem. However, factors such as high initial cost, short driving range, and long battery charging time limit the growth of EVs. Today, EVs are mainly used for short distance or special applications, e.g. for tourism or golf sport.

While, HEVs have been attracting a great deal of attention and been treated as the most promising alternatives to CVs from the short-term point of view on account of:

- the reduced fuel consumption and exhaust emission compared to CVs
- the relatively lower initial cost for battery
- the longer driving range and independence of battery charging infrastructures compared to EVs
- the relative mature technology compared to FCEVs

Among all key components as shown in Fig. 1.1, Fig. 1.2 and Fig. 1.3, batteries are the most important elements for all XEVs (EVs, HEVs and FCEVs). Historically, various power batteries, such as lead-acid battery, Nickel Cadmium (NiCd) battery, Nickel Metal Hydride (NiMH) battery and Lithium-ion (Li-ion) battery, have been proposed for the applications in vehicles of new generation, and the battery market has evolved continuously with respect to battery performance improvement, safety improvement and cost reduce.

The Li-ion battery is superior among all kinds of suggested battery types in terms of the energy density that decides the driving range and battery size, the specific power that decides the power ability and battery weight, the safety, which are crucial for the XEVs, see Codecà (2008) and Van den Bossche et al. (2006). Li-ion batteries are much lighter than other kinds of battery. The high cell voltage means increased amount of power at a lower current. Moreover, such kind of batteries are environmentally safe

since there is no existence of toxic components. So, the Li-ion battery is treated as the most promising option for vehicle utility, even if it has not yet found a significant market in real applications due to problems with respect to cost, cycle life, and low temperature performance, see Spotnitz (2005). However, the rapid improvement of Li-ion battery technology will undoubtedly reduce its cost and prolong its life continuously.

Regardless of the battery type and its hybridization manner with the engine and other powertrain components, the key point of a XEV (especially the HEVs) is to design a proper supervisory control strategy, which manages how to split the demanded power between energy sources.

Energy Management Strategy (EMS) is such a kind of supervisory controller which manages the operating points of the components (engine, electrical motor and gear box) of an HEV such that the vehicle runs in the most efficient and optimal way. As seen later this has concerned lots of studies on HEVs.

In practice, no mater how good the battery will be, the system will age over time. Therefore, it is important to take into account of the battery ageing and other battery states such as battery State of Charge (SOC) aiming at maintain the optimality of the achieved EMS. Since, as parts of the input signals, battery states will undoubtedly influence the quality of the EMS. Meanwhile, improper EMS based on bad battery information may give unsuitable battery charge or discharge current targets which will undoubtedly result in severe failures or even breakdown of the whole system, as well as serious financial loss.

Based on the general introduction presented above, this dissertation will consider a HEV of parallel structure, which is propelled by the combination of an SI engine with its associated fuel tank and an electric motor associated with a Li-ion battery to store the electrical energy, as the research target. So, the HEV and battery used in this work will be parallel HEV and Li-ion battery respectively unless other specific statements are given. The main objective here is then to account for battery related items, i.e. battery SOC and battery State of Health (SOH) indicated by battery parameters, such as battery internal resistances and battery capacity, in the EMS developments leading to a kind of Fault Tolerant EMS. In detail, on one hand, battery SOC is always treated as one of the system inputs aiming at maintain proper battery usages (none overcharge nor over-discharge) and guarantee the quality of achieved EMS. On the other hand, based on the estimation of related battery parameters that can reflect battery ageing (SOH), the system is modeled under the Linear Fractional Transformation form with varying battery parameters (e.g. battery capacity) represented as an uncertainty block, then the EMS controller scheduled by varying battery parameters is synthesized to determine

the power split ratio between the engine and the battery, which maintains the battery SOC within a reasonable range to prevent the battery from undesirable breakdown in the presence of battery fault. The main methods adopted for such a work will be H_∞ robust control and Linear Parameter Varying (LPV) control.

Structure of the dissertation

This dissertation begins with some brief theory background on the control methods and realization approaches involved in this work, followed by two big parts: the first part is focused on battery modeling and estimation, while the second part is concerned by the vehicle modeling and few kinds of EMS development methods based on the achieved powertrian model and battery model previously taking into account battery states (i.e. the SOC and SOH inferred from the estimated battery parameters).

Chapter 2 states briefly the place of H_∞ robust control and the growing importance of Linear Matrix Inequalities (LMIs) in control; some key notions associated with the robust control (system definitions, signal and system norms, uncertainties and robustness) are given in relatively basic level; problem formulation and LMI-based solutions of H_∞ controller synthesis and H_∞/LPV controller synthesis, which are widely considered in this dissertation, are presented in details. Note that no contribution on control theory is expected in this chapter and other parts of this dissertation.

Part I: Battery modeling and estimation

Since battery model is the precondition of any battery related problems such as battery estimation and EMS design, **chapter 3** contributes to the mathematical formulations with respect to the behaviors of the lithium-ion battery. Configuration and principle of operation of a lithium-ion cell is given first, then the classification of lithium-ion battery is given followed by some basic battery notions. Then, a brief overview of battery modeling is presented, and the equivalent electric circuit battery model is recalled. Finally modeling assumption and parameters are also given. It is important to notice that the model structure used to identify the battery in this work is not new but has been already presented in literature, and the parameters are inferred from the experiment results presented in Codecà (2008).

The aim of **chapter 4** is to design the estimation algorithms of battery SOC and parameters estimation based on the Electric Equivalent Circuit (EEC) battery model achieved in chapter 3. The considered methods for battery SOC estimation is the Kalman Filter (KF). Besides, a novel method, based on the Least Mean Squares (LMS) algorithms,

for battery capacity estimation is also proposed in this chapter. Definitions and the state of the art of both SOC estimation and SOH estimation indicated by parameter estimations, as well as the introductions of KF and Extended Kalman Filter (EKF) are also included in this chapter.

Chapter 5 presents a novel observer-based fault estimation method for the lithium-ion battery, where the battery ageing is treated as a fault. First, the extended battery model is presented combining the effects of temperature and battery ageing into the EEC model achieved in chapter 3. Then the principle of fault estimation is stated, the fault observer with the general H_∞ configuration is depicted, some weighting functions, which specify the performance requirements, are given. Finally, the observer is derived and simulation results both in frequency domain and time domain are given.

Part II: Powertrain modeling and energy management strategy

Chapter 6 is exclusively concerned by mathematical descriptions of the main comments contained in a specific parallel HEV. The whole system model is then available by combining these separated component description. It is worth noting that the selected parallel structure can be seen frequently in practice.

The following two chapters contain the main contributions of this dissertation. **Chapter 7** is concerned with the H_∞ based energy management strategy design, while **chapter 8** is concerned with the design of LPV/H_∞ based energy management strategies.

Chapter 7 presents a robust fault-tolerant H_∞ approach for the EMS development of a Parallel Hybrid Electric Vehicle (PHEV) with specific structure. The objective of such a EMS is to determine the power split ratio between the engine and the battery that maintains the State of Energy (SOE) of the battery within a reasonable range to prevent the battery from undesirable breakdown in the appearance of battery fault. The system description is given first based on the achieved battery model in chapter 3 and powertrain model in 6. Then the control system structure with weighting functions, taking into account the battery fault and the control signal limit, is given. Finally, the controller is derived and some simulations are implemented. The main aim of this chapter is to do some preliminary research on the influence of battery fault on the control strategy for a PHEV, but not to design a new kind of EMS.

An overview of the energy management strategy is also included in **Chapter 7**. The problem description with respect to EMS design is presented, where the motivation for EMS developments, as well as the general structure of an EMS controller including all necessary input signals and control outputs are given. Meanwhile, the classification and

comparison of available energy management strategies proposed in literature are given.

Chapter 8 presents two applications of the LPV/H_∞ approach on EMS developments and improvement. The first application intends to give some preliminary results on the influence of varying system parameters on the control strategy, and is concerned with a gain-scheduled approach for the EMS development of a PHEV aiming at minimizing the vehicle fuel consumption. First, the system is modeled under the Linear Fractional Transformation (LFT) form with varying parameters (velocity and battery capacity) represented as an uncertainty block. Then a LPV controller scheduled by the varying parameters is synthesized using the approach proposed in Apkarian & Gahinet (1995). Finally, the performances of the LPV controller are analyzed based on simulations in the frequency and time domains.

The second application is concerned with the design of a LPV regulator for a PHEV based on an already exist optimal EMS. The aim is to determine the regulating quantity of battery current and the power split ratio between engine and battery with respect to the achieved optimal ones by the existing EMS, according to the driving cycle variation and battery capacity degradation. The system is modeled using the similar method as adopted for the first application. The synthesis of the LPV regulator, that is scheduled by the varying parameters, is based the approach proposed in Apkarian & Gahinet (1995) too. The required information on battery states (SOC and SOH) are provided using the methods proposed in chapter 4.

The dissertation is ended with the conclusion part in **chapter 9**.

Main contributions

The main contributions of this dissertation can be summarized as follows:

Part I

- A novel method, based on the Least Mean Squares (LMS) algorithm that is more simple and less time-consuming than the KF/EKF based approach in terms of parameter estimation, for battery capacity estimation is proposed in chapter 4.

- An H_∞ battery fault observer is presented in chapter 5, where an extended battery model, considering the temperature change, which have influences on battery parameters, as a disturbance and the battery ageing as a fault, is adopted for the fault estimator development, minimizing the influence of the temperature effect and the battery input current on the estimation accuracy.

Part II

- Not only vehicle dynamics but also battery behaviors are taken into account for EMS developments in chapter 7 and chapter 8.
- Systems considered in chapter 8 are modeled as LPV ones of LFT form, accounting for variant velocity and battery capacity, where varying parameters are represented as an uncertainty block.
- A gain-scheduled EMS controller is proposed in section 8.1 aiming at minimizing the fuel consumption and prolonging the battery life in the presence of battery capacity degradation (battery ageing).
- A LPV regulator is achieved in section 8.2 for a parallel hybrid electric vehicle where an optimal EMS has already existed, which determine the regulating quantity of battery current and the power split ratio between engine and battery with respect to the so-called optimal ones by the existing EMS, according to the driving cycle variation and battery capacity degradation.

Publications

- *H_∞ based supervisory control strategy for a parallel HEV with battery fault accommodation* (T.-H. Wang, O. Sename and J.J. Martinez-Molina), in 8th International Federation of Automatic Control (IFAC) Symposium SAFEPROCESS-2012: Fault Detection, Supervision and Safety for Technical Processes.
- *H_∞ observer-based battery fault estimation for HEV application* (T.-H. Wang, J.J. Martinez-Molina and O. Sename), in 2012 IFAC Workshop on Engine and Powertrain Control, Simulation and Modeling (E-COSM'12).
- *A LPV EMS regulator for the parallel HEV with battery life prolongation* (Tinghong Wang, Olivier Sename and John-jairo Martinez-molina), in 21st Mediterranean Conference on Control and Automation (MED'13).
- *A LPV/H_∞ approach for fuel consumption minimization of the PHEV with battery life prolongation* (T.-H. Wang, O. Sename and J.J. Martinez-Molina), in 7th IFAC International Symposium on Advances in Automotive Control (IFAC-AAC 2013)

Chapter 2

Background on Robust Control and LMI Techniques

2.1 Introduction

Most control designs are based on a plant model which is used to describe characteristics of the system under consideration. In fact, it is unavoidable that there will be differences between models and real systems, which are often referred to as uncertainties. Besides, the real system is disturbed by various disturbances and noises. A well designed control system is then expected to maintain a certain degree of stability and performance level in spite of these uncertainties, disturbances and noises, which is referred to as the robustness of a control system.

During 1960's and 1970's, the emphasis was only laid on achieving good performances, but not on robustness, with MIMO (Multiple-Input Multiple-Output) control methods, mainly based on linear quadratic performance criteria and Gaussian disturbances. However, such Linear Quadratic Gaussian (LQG) methods exhibit poor robustness properties, refer to Gu et al. (2005), Poussot-Vassal (2008) and Sánchez (2003) for more details.

In the early 1980's, the pioneering works by Zames (1981) and Zames & Francis (1983) contributed to the emergence of robustness principle and H_∞ optimal control theory which led to present robust control theory.

Firstly, the solution to the H_∞ control problem is based on the use of Algebraic Riccati Equations (AREs), Doyle et al. (1989) and Zhou et al. (1996). More recently, the Linear Matrix Inequality (LMI) approach has been proved to be a powerful tool for many control problems, such as the H_∞ and H_2 ones, refer to Scherer (1996), Chilali et al. (1999)

and Guerra & Vermeiren (2004). In Gahinet & Apkarian (1994), LMI-based solution of the H_∞ control problem is given.

In this dissertation, we will be interested in the design of robust controllers in the framework of H_∞ approach, and, furthermore, to the synthesis of Linear Parameter Varying (LPV) controller to account for some parameter variations and model non-linearities.

This chapter presents briefly the theoretical notions, that have been used in this work, in section 2.2; the LMI techniques in section 2.2.7; LMI-based H_∞ control synthesis and H_∞/LPV synthesis in section 2.3 and 2.4 respectively. For more details, the interested reader may refer to Doyle et al. (1992), Skogestad & Postlethwaite (2007), Zhou et al. (1996), Scherer & Weiland (2000) and Sename et al. (2013).

2.2 Basic definitions

2.2.1 Control system

A control system is a combination of components that makes the output of a plant behave in a desired way by manipulating the plant inputs.

Generally, control systems are divided in to two categories: open-loop systems and closed-loop systems. For open-loop system, the output has no effect on the input. In contrast, in feedback control, the actual output is measured by sensors and is used to adjust the input, aiming at achieving the desired performances for the closed-loop control system. Note that only feedback configurations are able to achieve the robustness of a control system, see Gu et al. (2005), Doyle et al. (1992) and Skogestad & Postlethwaite (2007).

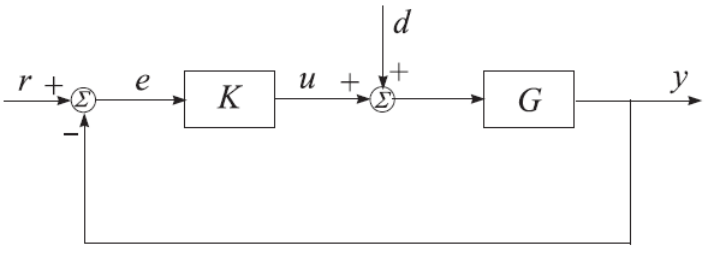

Figure 2.1: One degree-of-freedom feedback system

Fig. 2.1 depicts a feedback system of one degree-of-freedom, where G is the plant to be controlled, K is the system controller, r is the reference or target value, e is the tracking error, u is the controller output, d is the plant disturbance, y is the plant output.

In order to analyze and design a control system, the real system (plant), which is to be controlled, is usually modeled based on a series of Ordinary Differential Equations (ODEs).

2.2.1.1 Nonlinear systems

A nonlinear system is not directly proportional to its inputs, and can be described by nonlinear ODEs.

Given functions f and g, a nonlinear system can be described as:

$$\begin{cases} \dot{x}(t) = f(x(t), u(t)) \\ y(t) = g(x(t), u(t)) \end{cases} \tag{2.1}$$

where $x(t) \in \mathbb{R}^n$ is the state vector of state variables, $u(t) \in \mathbb{R}^m$ is the input vector, $y(t) \in \mathbb{R}^p$ is the plant output vector (system measurement).

2.2.1.2 Linear Time Invariant systems

In the case of Linear Time Invariant (LTI) system, the plant can be described by linear ODEs.

Given matrices A, B, C and D, a LTI system can be described as:

$$\begin{cases} \dot{x}(t) = Ax(t) + Bu(t) \\ y(t) = Cx(t) + Du(t) \end{cases} \tag{2.2}$$

where $x(t) \in \mathbb{R}^n$ is the state vector of state variables, $u(t) \in \mathbb{R}^m$ is the input vector, $y(t) \in \mathbb{R}^p$ is the system measurement.

2.2.1.3 Linear Parameter Varying Systems

A Linear Parameter Varying (LPV) system has a representation similar to the LTI system (namely, it is linear in the state variables), but the matrices A, B, C and D are dependent on some varying parameters (possibly in a non-linear way), refer to Mohammadpour & Scherer (2012), Sename et al. (2013), Tóth (2010), Poussot-Vassal (2008) and Bruzelius (2004) for more details.

A LPV system is usually described as:

$$\begin{cases} \dot{x}(t) = A(\rho)x(t) + B(\rho)u(t) \\ y(t) = C(\rho)x(t) + D(\rho)u(t) \end{cases} \tag{2.3}$$

where $x(t) \in \mathbb{R}^n$ is the state vector of state variables, $u(t) \in \mathbb{R}^m$ is the input vector, $y(t) \in \mathbb{R}^p$ is the system measurement, $\rho \in \mathbb{R}^l$ is the vector of varying parameters.

Usually, it is assumed that:

$$\rho_i \in \left[\underline{\rho_i} \quad \overline{\rho_i}\right] \qquad \forall i = 1, \cdots, l \tag{2.4}$$

where l is the number of varying parameters.

The parameter dependence in an LPV system can have several forms. The most common one, which is referred to as the affine parameter dependence (LPV-A), is defined as:

$$A(\rho) = A_0 + \sum_{i=1}^{l} A_i \rho_i \tag{2.5}$$

and similarly for $B(\rho)$, $C(\rho)$ and $D(\rho)$, where A_i are real matrices.

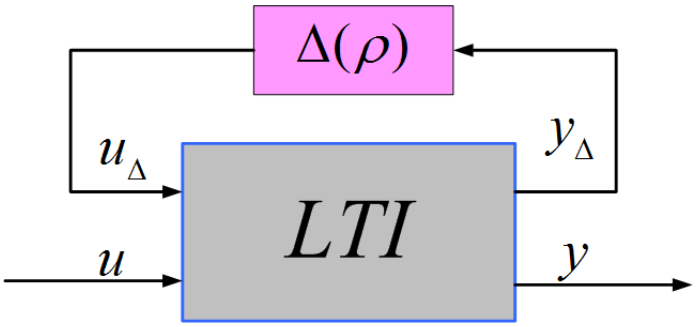

Figure 2.2: LPV system in LFT form

Another important form is the Linear Fractional Transformation (LFT) parameter dependence (LPV-LFT), see Fig. 2.2, where the LPV system is split into two part: (1) the known LTI plant independent of the varying parameters, and (2) the uncertain part $\Delta(\rho)$ specifying how the varying parameters enters the plant dynamics, see Apkarian & Gahinet (1995) and Roche (2011).

The associated mathematical formulation of such kind of dependency is written as:

$$\begin{bmatrix} \dot{x} \\ y_\Delta \\ y \end{bmatrix} = \begin{bmatrix} A & B_\Delta & B_1 \\ C_\Delta & D_{\Delta\Delta} & D_\Delta \\ C_1 & D_1 & D_2 \end{bmatrix} \begin{bmatrix} x \\ u_\Delta \\ u \end{bmatrix} \tag{2.6}$$

with

$$u_\Delta = \Delta y_\Delta, \qquad \Delta = diag(\rho_1 I_{r_1} \cdots \rho_l I_{r_l}) \tag{2.7}$$

where $u_\Delta, y_\Delta \in \mathbb{R}^r$, $r = r_1 + \cdots + r_l$, all matrices A, B_Δ, B_1, C_Δ, $D_{\Delta\Delta}$, D_Δ, C_1, D_1 and D_2 are time-invariant.

2.2.2 Signal and system norm

In order to describe the performance of a control system, signal norms are used to describe the "size" of signals of interest. Based on the signal norms, system norms can be induced to measure the "gain" of the operator which represents the control system.

2.2.2.1 Signal norms

All following signal norms are given based on a complex signal $x(t) \in \mathbb{C}^n$, with $x^*(t)$ denoting the conjugate of $x(t)$.

- L_2 **norm** The L_2 norm of a signal $x(t)$ is defined by:

$$\|x\|_2 := \left(\int_{-\infty}^{\infty} x^*(t)x(t)dt\right)^{\frac{1}{2}}$$

  The square of the L_2 norm, $\|x\|_2^2$, is often called the energy of the signal $x(t)$.

- L_∞ **norm** The L_∞ norm of a signal $x(t)$ is defined by:

$$\|x\|_\infty := \sup_{t\in\mathbb{R}} |x(t)|$$

  The L_∞ norm is the amplitude or peak value of the signal $x(t)$.

- **Power signal** The average power of $x(t)$ is:

$$\lim_{T\to\infty} \frac{1}{2T} \int_{-T}^{T} x^*(t)x(t)dt$$

  The signal $x(t)$ will be called a power signal if the above limit exists.

2.2.2.2 System norms

Suppose that G is a strictly proper LTI system which maps the input signal $u(t)$ into the output signal $y(t)$, and $G(s)$ is the transfer function of G.

- H_2 **norm** The H_2 norm of $G(s)$ that belongs to $\mathcal{RH}_2$ is given by:

$$\|G(s)\|_2 := \left(\frac{1}{2\pi} \int_{-\infty}^{\infty} Trace\left[G^*(j\omega)G(j\omega)\right] d\omega\right)^{\frac{1}{2}}$$

- H_∞ **norm** The H_∞ norm of $G(s)$ that belongs to $\mathcal{RH}_\infty$ is given by:

$$\|G(s)\|_\infty := \sup_\omega \bar{\sigma}(G(j\omega))$$

where $\bar{\sigma}(G(j\omega))$ denotes the largest singular value of G.

Note that the H_∞ norm is indeed the L_2-induced norm, and

$$\|G(s)\|_\infty = \sup_\omega \frac{\|y\|_2}{\|u\|_2}$$

In particular, for LPV systems, the L_2-induced norm will be referred to as the H_∞ norm by abuse of langage.

2.2.3 System stability

An essential issue in control system design is stability. Any unstable controlled system is meaningless from the practical point of view.

A controlled system is internally stable if all outputs of the system are bounded for any input that is bounded. Taking the system given in Fig. 2.1 for example, there exists two inputs r (reference) and d (disturbance), as well as two outputs y (plant output) and u (controller output). Transfer matrices with respect to all inputs to all outputs, respectively, are:

$$T_{yr} = GK(I_p + GK)^{-1}$$

$$T_{yd} = G(I_p + GK)^{-1}$$

$$T_{ur} = (I_m + KG)^{-1}K = K(I_p + GK)^{-1}$$

$$T_{ud} = -KG(I_m + KG)^{-1}$$

where subscripts p and m are dimensions of y and u respectively.

Hence, the control system as shown in Fig. 2.1 is internally stable if and only if all the transfer functions shown above are Bounded-Input-Bounded-Output (BIBO) stable.

Note that, for linear systems, BIBO stability is equivalent to stability and asymptotic stability.

2.2.4 System performance

Although stability is an important issue, the main objective of a control system is to improve the system performances, such as reference tracking, disturbance attenuation, noise rejection, etc.

Considering the control system shown in Fig. 2.1 again, we always denote:

- $L_y := GK$ the *output loop transfer function*
- $S_y := (I_p + GK)^{-1} = (I_p + L_y)^{-1}$ the *output sensitivity function* which is the closed-loop system from r (reference) to e (tracking error)
- $T_y := (I_p + GK)^{-1}GK = (I_p + L_y)^{-1}L_y$ the *output complementary sensitivity function* which is from r to y (plant output)
- $L_u := KG$ the *input loop transfer function*
- $S_u := (I_m + KG)^{-1} = (I_m + L_u)^{-1}$ the *input sensitivity function* which is from d (disturbance) to $u + d$ (actual control input)
- $T_u := (I_m + KG)^{-1}KG = (I_m + L_u)^{-1}L_u$ the *input complementary sensitivity function* which is from d to u (control input)

where subscripts p and m are dimensions of y and u respectively.

Meanwhile, performance objectives of are usually given using transfer matrices defined above. Then, minimization of the norms (the gain) of these transfer matrices means the meet of corresponding control specifications. For example, good tracking performance is achieved if the norm $\|S_y\|_\infty$ is minimized.

In general, weighting functions (weights) are usually used in the minimization to select the frequency range where the performances are to be improved. For instance, instead of minimizing the *output sensitivity function* S_y alone, we always try to minimize $\|w_e S_y\|_\infty$. Here, w_e is a weight used to specify the tracking requirements.

2.2.5 General H_∞ control problem

Let us consider the general control configuration in Fig. 2.3 where

$$(P): \quad \begin{bmatrix} \dot{x} \\ z \\ y \end{bmatrix} = \left[\begin{array}{c|cc} A & B_1 & B_2 \\ \hline C_1 & D_{11} & D_{12} \\ C_2 & D_{21} & D_{22} \end{array}\right] \begin{bmatrix} x \\ w \\ u \end{bmatrix} \tag{2.8}$$

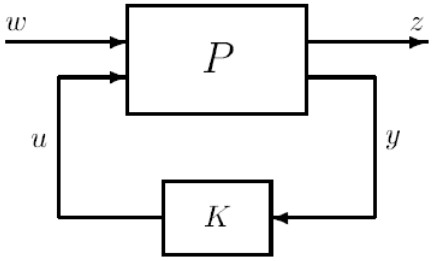

Figure 2.3: The general control configuration

and

$$u = Ky \tag{2.9}$$

where $x \in \mathbb{R}^n$ concatenates the state vector of the system and the state vector of the weights (performance weighting functions), $u \in \mathbb{R}^{n_u}$ is the vector of control inputs, $y \in \mathbb{R}^{n_y}$ is the vector of plant outputs, $w \in \mathbb{R}^{n_w}$ presents the vector of exogenous inputs (reference, disturbances, noise, etc.), $z \in \mathbb{R}^{n_z}$ presents the vector of controlled outputs to be minimized/penalized, P is called the generalized plant or interconnected system.

Remark: in the H_∞ approach, the required performances are represented as some dynamic systems (referred to as weights) and are connected to the exogenous inputs or controlled outputs of the plant. P is then the interconnected system.

Based on the configuration of Fig. 2.3, an H_∞ control problem is referred to as finding a controller K which minimize the H_∞ norm of the transfer function from w to z. That is to find a controller that solves:

$$\min_K \|F_l(P, K)\|_\infty$$

2.2.6 Uncertainty and robustness

Most control designs are based on a plant model which is used to describe the system to be investigated. In fact, there will be differences (mismatches) between models and actual systems. These differences are referred to as uncertainties.

A control system is said to be robust if it remains stable and owns a certain performance in the presence of possible uncertainties, and the robust control problem is to find such a robust controller.

To account for uncertainties, $G_p(s)$ is generally used to denote the actual system with subscript p stands for perturbed in contrast to $G(s)$ which is the nominal model description of the actual system. Also, $\Delta(s)$ denote the normalized perturbation with

H_∞ norm less than 1.

2.2.6.1 Uncertainties

Factors that contribute to model uncertainty include: unmodelled high frequency dynamics, linear approximation, reduced order model order, neglected dynamics, system parameter variations due to environmental changes or torn-and-worn factors, etc. The various sources of uncertainty can be divided into three groups (see Sánchez (2003), Skogestad & Postlethwaite (2007), Gu et al. (2005), Scherer (2001*b*) and Zhou & Doyle (1998))

- **Parametric uncertainties**

  Parametric uncertainty is of interest when the structure of the model is known, but some of the parameters are uncertain. It is assumed that each uncertain parameter α_p is within a region of $[\alpha_{min}, \alpha_{max}]$. Then, parameter sets can be expressed as:

  $$\alpha_p = \bar{\alpha}(1 + r_\alpha \Delta)$$

  where $\bar{\alpha}$ is the mean parameter value, $r_\alpha = \frac{\alpha_{max} - \alpha_{min}}{\alpha_{max} + \alpha_{min}}$ is the relative uncertainty in the parameter, and Δ is any real scalar satisfying $|\Delta| \leq 1$.

- **Neglected and unmodelled dynamics uncertainties**

  Neglected and unmodelled dynamics uncertainty is mainly caused by insufficient understanding of the actual system or/and simplified description of the plant (for instance when when sensor and actuator dynamics are neglected).

  Quantification of such uncertainty is realized with complex perturbations which are normalized such that $\|\Delta(s)\|_\infty \leq 1$

- **Lumped uncertainty**

  Lumped uncertainty is a combination of other two uncertainty group mentioned above. It represents one or several sources of parametric or/and unmodelled dynamics uncertainty combined into a single lumped perturbation of either multiplicative structure or additive structure.

  Fig. 2.4 shows a perturbed plant, with lumped multiplicative uncertainty, which can be described as:

  $$G_p(s) = G(s)(I + w_I(s)\Delta_I(s))$$

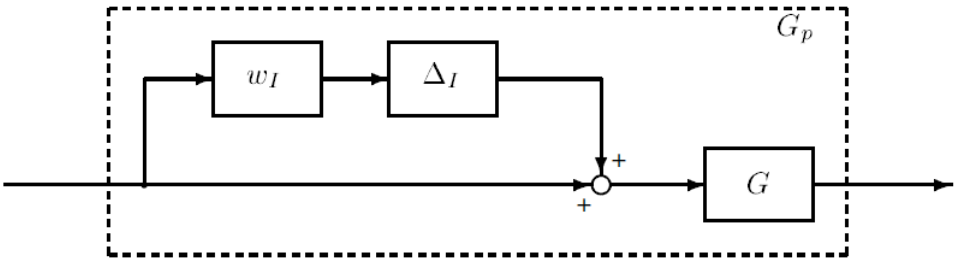

Figure 2.4: Plant with multiplicative uncertainty

where $\Delta_I(s)$ is any stable transfer matrix with H_∞ norm less than 1, subscript I denotes input, $w_I(s)$ is the weight describing the uncertainty level along frequencies.

If the lumped uncertainty is desired in additive form, the perturbed plant will be described as:

$$G_p(s) = G(s) + w_A(s)\Delta_A(s)$$

2.2.6.2 General control configuration with uncertainty

Once the plant uncertainties are identified, they can be pulled out into a block-diagonal matrix:

$$\Delta = diag\{\Delta_i\} = \begin{bmatrix} \Delta_1 & & & \\ & \ddots & & \\ & & \Delta_i & \\ & & & \ddots \end{bmatrix}$$

where each Δ_i represents a specific source of uncertainties, and can be full block or diagonal matrices only.

Furthermore, if the controller K is also pulled out, a generalized plant P, which contains the plant G and the weights (weighting functions used to specify the performance requirements), is considered. Meanwhile, the so-called general control configuration (as structured by Fig. 2.5), which is used for controller synthesis, will be achieved, where all exogenous inputs such as reference, disturbances and noises are denoted by w, z denotes the output signals to be minimized/penalized, y is the measurement, u groups the control signals, u_Δ and y_Δ are input perturbations and output perturbations respectively.

Then, the overall control objective is to design a controller K such that the transfer matrix from w to z is minimized in the H_∞ norm sense.

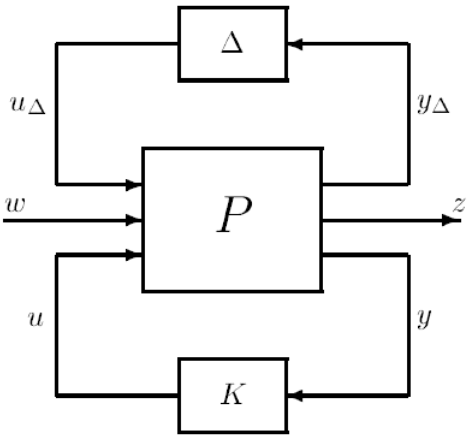

Figure 2.5: General control configuration

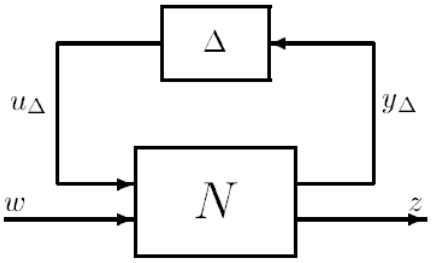

Figure 2.6: $N\Delta$ structure for robust performance analysis

Alternatively, if we only want to analyze the performance of an achieved controller, the $N\Delta$ structure as shown in Fig. 2.6 will be used. Here, N is the Lower LFT of P and K (denoted by $F_l(P,K)$)

$$N = F_l(P,K) = P_{11} + P_{12}K(I - P_{22}K)^{-1}P_{21}$$

based on following mathematical formulation of the structure shown in Fig. 2.5

$$\left[\begin{array}{c} y_\Delta \\ z \\ \hdashline y \end{array}\right] = \left[\begin{array}{c:c} P_{11} & P_{12} \\ \hdashline P_{21} & P_{22} \end{array}\right] \left[\begin{array}{c} u_\Delta \\ w \\ \hdashline u \end{array}\right]$$

The closed-loop transfer function from w to z is related to N and Δ by an upper LFT $F_u(N,\Delta)$

$$F_u(N,\Delta) = N_{22} + N_{21}\Delta(I - N_{11}\Delta)^{-1}N_{12}$$

with

$$\begin{bmatrix} y_\Delta \\ z \end{bmatrix} = \left[\begin{array}{c|c} N_{11} & N_{12} \\ \hline N_{21} & N_{22} \end{array}\right] \begin{bmatrix} u_\Delta \\ w \end{bmatrix} \tag{2.10}$$

2.2.6.3 Robust stability

Definition: A controller K provides Robust Stability (RS) if the closed-loop system is internal stable for all perturbed plants G_p with respect to the nominal model $G(s)$, up to the worst-case model uncertainty.

Let us assume the $N\Delta$ system in Fig. 2.6 owns Nominal Stability (NS) (when $\Delta = 0$), that is, N is internally stable. RS of the system is equivalent to the stability of the $M\Delta$ structure shown in Fig. 2.7 where $M = N_{11}$ is the transfer function from the output perturbations to the input of the perturbations (refer to Fig. 2.6 and (2.10)).

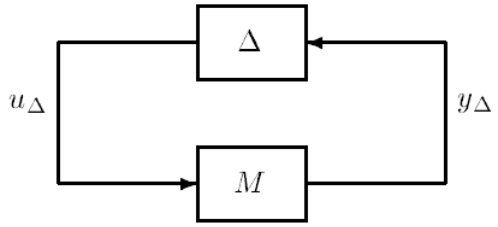

Figure 2.7: $M\Delta$ structure for robust stability analysis

Using the Small Gain Theorem (refer to Zhou et al. (1996)), assume that M and Δ are stable, the $M\Delta$ system shown in Fig. 2.7 is stable for all perturbations Δ satisfying $\|\Delta\|_\infty \leq 1$ (i.e. we have RS) if and only if

$$\|M\|_\infty < 1$$

2.2.6.4 Robust performance

Definition: A controller K provides Robust Performance (RP) if the performance specifications are satisfied for all perturbed plants G_p with respect to the nominal model $G(s)$, up to the worst-case model uncertainty.

If the $N\Delta$ system in Fig. 2.6 owns NS (when $\Delta = 0$), that is, N is internally stable. RP of the system is satisfied if and only if

$$\|F_u(N, \Delta)\|_\infty < 1, \qquad \forall \|\Delta\|_\infty \leq 1$$

2.2.7 Linear Matrix Inequality (LMI) techniques

Linear Matrix Inequality (LMI) is a powerful formulation and design tool for a large variety of control problems. Indeed when the analytical solution of a control problem can not be obtained, the objective is to reformulate the given control problem as an optimization problem. When such a problem is convex, it amounts to find solutions to a set of LMIs, which leads to the reliable numerical solution.

Recently, intensive researches on LMIs have resulted in resolutions of many control problems such as the H_∞ control in Gahinet & Apkarian (1994) and Chilali & Gahinet (1996), H_2 control in Rotea (1993), mixed H_2/H_∞ control in Khargonekar & Rotea (1991) and Scherer (1996), etc.

A LMI owns the form

$$F(x) = F_0 + \sum_{i=1}^{m} x_i F_i > 0$$

where $x \in \mathbb{R}^m$ is the vector of variables, and the symmetric matrices $F_i = F_i^T \in \mathbb{R}^{n\times n}$ are known. The inequality symbol $>$ means that $F(x)$ is positive define, i.e., $u^T F(x) u > 0$ for all nonzero $u \in \mathbb{R}^n$, see Scherer & Weiland (2000) and Boyd et al. (1987) for more information on LMIs and its application for control.

There are also non-strict LMIs which own the form

$$F(x) \geq 0$$

2.3 LMI-based H_∞ control synthesis

2.3.1 LMIs solution to H_∞ controller design

If the output feedback controller K in Fig. 2.3 is defined as

$$\begin{bmatrix} \dot{x_c} \\ u \end{bmatrix} = \begin{bmatrix} A_c & B_c \\ C_c & D_c \end{bmatrix} \begin{bmatrix} x_c \\ y \end{bmatrix}$$

where $x_c \in \mathbb{R}^n$, $y \in \mathbb{R}^{n_y}$, $u \in \mathbb{R}^{n_u}$.

Solution of the H_∞ control problem can be obtained by solving the following LMIs in $(X, Y, \tilde{A}, \tilde{B}, \tilde{C}, \tilde{D})$, while minimizing γ, see Scherer et al. (1997) and Poussot-Vassal

(2008).

$$\begin{bmatrix} M_{11} & * & * & * \\ M_{21} & M_{22} & * & * \\ M_{31} & M_{32} & M_{33} & * \\ M_{41} & M_{42} & M_{43} & M_{44} \end{bmatrix} < 0$$

$$\begin{bmatrix} X & I_n \\ I_n & Y \end{bmatrix} > 0$$

where

$$M_{11} = AX + XA^T + B_2\tilde{C} + \tilde{C}^T B_2^T$$

$$M_{21} = \tilde{A} + A^T + C_2^T \tilde{D}^T B_2^T$$

$$M_{22} = YA + A^T Y + \tilde{B}C_2 + C_2^T \tilde{B}^T$$

$$M_{31} = B_1^T + D_{21}^T \tilde{D}^T B_2^T$$

$$M_{32} = B_1^T Y + D_{21}^T \tilde{B}^T$$

$$M_{33} = -\gamma I_{n_u}$$

$$M_{41} = C_1 X + D_{12}\tilde{C}$$

$$M_{42} = C_1 + D_{12}\tilde{D}C_2$$

$$M_{43} = D_{11} + D_{12}\tilde{D}D_{21}$$

$$M_{44} = -\gamma I_{n_y}$$

Then, the controller K can be constructed based on

$$D_c = \tilde{D}$$

$$C_c = (\tilde{C} - D_c C_2 X)M^{-T}$$

$$B_c = N^{-1}(\tilde{B} - YB_2 D_c)$$

$$A_c = N^{-1}(\tilde{A} - YAX - YB_2 D_c C_2 X - NB_c C_2 X - YB_2 C_c M^T)M^{-T}$$

where M and N are defined such that $MN^T = I_n - XY$

2.4 LMI-based LPV/H_∞ control synthesis

2.4.1 General problem formulation

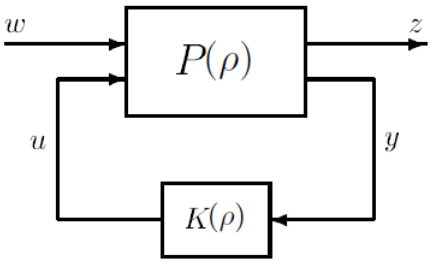

Figure 2.8: Generalized LPV/H_∞ configuration

The generalized LPV/H_∞ configuration is depicted in Fig. 2.8 with the external inputs denoted by w, the controlled outputs to be minimized denoted by z, the control inputs denoted by u and the measured outputs denoted by y. $P(\rho)$ is refered to as the interconnected system which contains the LPV system defined in (2.3) and the weights (performance weighting functions). x concatenates the state vector of the system and the state vector of the weights (performance weighting functions).

Based on such a configuration which can be formulated as

$$(P(\rho)): \quad \begin{bmatrix} \dot{x} \\ z \\ y \end{bmatrix} = \left[\begin{array}{c|cc} A(\rho) & B_1(\rho) & B_2(\rho) \\ \hline C_1(\rho) & D_{11}(\rho) & D_{12}(\rho) \\ C_2(\rho) & D_{21}(\rho) & D_{21}(\rho) \end{array}\right] \begin{bmatrix} x \\ w \\ u \end{bmatrix} \tag{2.11}$$

and

$$u = K(\rho)y \tag{2.12}$$

where $x \in \mathbb{R}^n$, $y \in \mathbb{R}^{n_y}$, $u \in \mathbb{R}^{n_u}$, $w \in \mathbb{R}^{n_w}$ and $z \in \mathbb{R}^{n_z}$.

A LPV/H_∞ control problem is referred to as finding a LPV dynamical controller $K(\rho)$ which minimize the H_∞ norm of the transfer function from w to z, that is to solve:

$$\min_K \|F_l(P(\rho), K(\rho))\|_\infty, \qquad \forall \rho$$

2.4.2 LMIs solution to LPV/H_∞ controller design

If the output feedback controller $K(\rho)$ in Fig. 2.8 is defined as

$$\begin{bmatrix} \dot{x_c} \\ u \end{bmatrix} = \begin{bmatrix} A_c(\rho) & B_c(\rho) \\ C_c(\rho) & D_c(\rho) \end{bmatrix} \begin{bmatrix} x_c \\ y \end{bmatrix}$$

where $x_c \in \mathbb{R}^n$, $y \in \mathbb{R}^{n_y}$ and $u \in \mathbb{R}^{n_u}$.

Solution to the LPV/H_∞ controller can be obtained by solving the following LMIs in $(X(\rho), Y(\rho), \tilde{A}(\rho), \tilde{B}(\rho), \tilde{C}(\rho), \tilde{D}(\rho))$, while minimizing γ, see Poussot-Vassal (2008).

$$\begin{bmatrix} M_{11} & * & * & * \\ M_{21} & M_{22} & * & * \\ M_{31} & M_{32} & M_{33} & * \\ M_{41} & M_{42} & M_{43} & M_{44} \end{bmatrix} < 0, \qquad \forall \rho$$

$$\begin{bmatrix} X(\rho) & I_n \\ I_n & Y(\rho) \end{bmatrix} > 0, \qquad \forall \rho$$

where

$$M_{11} = A(\rho)X(\rho) + X(\rho)A(\rho)^T + B_2(\rho)\tilde{C}(\rho) + \tilde{C}(\rho)^T B_2(\rho)^T + \frac{\partial X(\rho)}{\partial \rho}\dot{\rho}$$

$$M_{21} = \tilde{A}(\rho) + A(\rho)^T + C_2(\rho)^T \tilde{D}(\rho)^T B_2(\rho)^T$$

$$M_{22} = Y(\rho)A(\rho) + A(\rho)^T Y(\rho) + \tilde{B}(\rho)C_2(\rho) + C_2(\rho)^T \tilde{B}(\rho)^T + \frac{\partial Y(\rho)}{\partial \rho}\dot{\rho}$$

$$M_{31} = B_1(\rho)^T + D_{21}(\rho)^T \tilde{D}(\rho)^T B_2(\rho)^T$$

$$M_{32} = B_1(\rho)^T Y(\rho) + D_{21}(\rho)^T \tilde{B}(\rho)^T$$

$$M_{33} = -\gamma I_{n_u}$$

$$M_{41} = C_1(\rho)X(\rho) + D_{12}(\rho)\tilde{C}(\rho)$$

$$M_{42} = C_1(\rho) + D_{12}(\rho)\tilde{D}(\rho)C_2(\rho)$$

$$M_{43} = D_{11}(\rho) + D_{12}(\rho)\tilde{D}(\rho)D_{21}(\rho)$$

$$M_{44} = -\gamma I_{n_y}$$

Then, the controller $K(\rho)$ for $\frac{\partial X(\rho)}{\partial \rho}\dot{\rho} = 0$ can be constructed based on

$$D_c(\rho) = \tilde{D}(\rho)$$

$$C_c(\rho) = (\tilde{C}(\rho) - D_c(\rho)C_2(\rho)X(\rho))M(\rho)^{-T}$$

$$B_c(\rho) = N(\rho)^{-1}(\tilde{B}(\rho) - Y(\rho)B_2(\rho)D_c(\rho))$$

$$A_c(\rho) = N(\rho)^{-1}(\tilde{A}(\rho) - Y(\rho)A(\rho)X(\rho) - Y(\rho)B_2(\rho)D_c(\rho)C_2(\rho)X(\rho)$$

$$-N(\rho)B_c(\rho)C_2(\rho)X(\rho) - Y(\rho)B_2(\rho)C_c(\rho)M(\rho)^T)M(\rho)^{-T}$$

where $M(\rho)$ and $N(\rho)$ are defined such that $M(\rho)N(\rho)^T = I_n - X(\rho)Y(\rho)$

Since the solution presented above depends on the parameters, it results in an infinite dimension problem due to infinite values of ρ. There are mainly two kinds of approaches that are used to relax it into finite dimension problems:

- **the polytopic approach**
- and, **the Linear Fractional Transformation (LFT) approach**

2.4.2.1 Polytopic approach

The polytopic approach can be used when the dependency of the LPV system w.r.t. the parameter vector ρ is affine (as defined in (2.5)). Then ρ remains inside a polytope (parameter convex set) $\mathcal{P}_\rho$ defined by:

$$\mathcal{P}_\rho := \mathbf{Co}\{\omega_1, \cdots, \omega_N\}$$

where N is the number of vertices of $\mathcal{P}_\rho$ ($N = 2^l$, with l the dimension of ρ). ω_i, which denotes the i^{th} vertices of $\mathcal{P}_\rho$, is a vector composed of a combination of the lower bound $\underline{\rho_i}$ and upper bound $\overline{\rho_i}$ of the varying parameters with $i = 1, \cdots, l$.

At each time instant t, the value of ρ is given by:

$$\rho = \sum_{i=1}^{N} \alpha_i \omega_i$$

with $\alpha_i \geq 0$, $\sum_{i=1}^{N} \alpha_i = 1$, where α_i are the polytopic coordinates of the parameters.

Then the LPV system can be described as the convex combination of the N vertices matrices

$$\begin{bmatrix} A(\rho) & B(\rho) \\ C(\rho) & D(\rho) \end{bmatrix} = \sum_{i=1}^{N} \alpha_i \begin{bmatrix} A(\omega_i) & B(\omega_i) \\ C(\omega_i) & D(\omega_i) \end{bmatrix}$$

After connecting the specified weighting functions to the polytopic model achieved above, the interconnected system $P(\rho)$ (as given by (2.11) and the generalized LPV/H_∞ control configuration (as depicted in Fig. 2.8) will be obtained. And, the polytopic H_∞ control problem boils down to find a controller $K(\rho)$ of form:

$$K(\rho): \quad \begin{bmatrix} A_c(\rho) & B_c(\rho) \\ C_c(\rho) & D_c(\rho) \end{bmatrix} = \sum_{i=1}^{N} \alpha_i \begin{bmatrix} A_c(\omega_i) & B_c(\omega_i) \\ C_c(\omega_i) & D_c(\omega_i) \end{bmatrix}$$

that minimizes the H_∞ norm of the closed-loop LPV system formed by the interconnection of $P(\rho)$ and $K(\rho)$ at each vertex. Such a controller is obtained by solving a LMI problem.

Since this dissertation will adopt another approach (the LFT one), the details of LMI algorithm for polytopic approach will not given, interested reader can refer to Apkarian et al. (1995), Sename et al. (2013), Roche (2011) and Poussot-Vassal (2008) for more information.

2.4.2.2 The Linear Fractional Transformation (LFT) approach

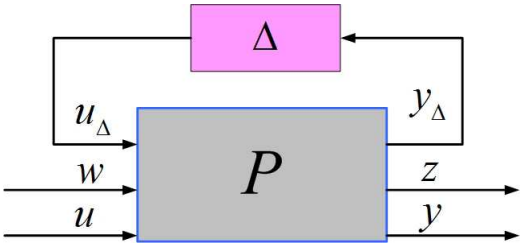

Figure 2.9: Interconnected LPV/LFT system

Let us consider the interconnected LPV/LFT system (the required performance are represented as weights and connected to the LPV system described by Fig. 2.2 and (2.6)) in Fig. 2.9 formulated by:

$$(P): \quad \begin{bmatrix} x^+ \\ y_\Delta \\ z \\ y \end{bmatrix} = \left[\begin{array}{c|ccc} A & B_\Delta & B_1 & B_2 \\ \hline C_\Delta & D_{\Delta\Delta} & D_{\Delta 1} & D_{\Delta 2} \\ C_1 & D_{1\Delta} & D_{11} & D_{12} \\ C_2 & D_{2\Delta} & D_{21} & D_{22} \end{array}\right] \begin{bmatrix} x \\ u_\Delta \\ w \\ u \end{bmatrix} \tag{2.13}$$

and

$$u_\Delta = \Delta y_\Delta, \qquad \Delta = diag(\rho_1 I_{r_1} \cdots \rho_l I_{r_l}) \tag{2.14}$$

where $u_\Delta, y_\Delta \in \mathbb{R}^r$, $r = r_1 + \cdots + r_l$, $x \in \mathbb{R}^n$, $y \in \mathbb{R}^{n_y}$, $u \in \mathbb{R}^{n_u}$, $w \in \mathbb{R}^{n_w}$ and $z \in \mathbb{R}^{n_z}$, all matrices A, B_Δ, B_1, B_2, C_Δ, $D_{\Delta\Delta}$, $D_{\Delta 1}$, $D_{\Delta 2}$, C_1, $D_{1\Delta}$, D_{11}, D_{12}, C_2, $D_{2\Delta}$, D_{21} and D_{22} are time-invariant, x^+ denotes either $\dot{x}$ for continuous-time systems, or x_{k+1} for discrete-time ones.

As seen in Fig. 2.9, the LPV model of LFT interconnection splits the system into two

distinct part: (1) the known LTI plant P independent of the varying parameters, and (2) the uncertain part Δ which is some block diagonal time-varying operator specifying how varying parameters enters the plant dynamics. Note that Δ is traditionally referred to as the uncertainty structure, y_Δ and u_Δ can be interpreted as the inputs and outputs of the time-varying operator Δ, see Apkarian & Gahinet (1995).

With such a structure, the upper LFT representation of the system becomes:

$$\begin{bmatrix} z \\ y \end{bmatrix} = F_u(P, \Delta) \begin{bmatrix} w \\ u \end{bmatrix} \tag{2.15}$$

Consistently with (2.15), we seek a LPV/LFT controller of the form:

$$u = F_l(K, \Delta) y \tag{2.16}$$

where the LTI K specifies the LFT dependency of the LPV/LFT controller on the measurements of Δ with (2.16) giving the rule for updating the controller, see Apkarian & Gahinet (1995).

Remark: the controller could also be scheduled with a subset of Δ, as explained in Scherer (2001*a*).

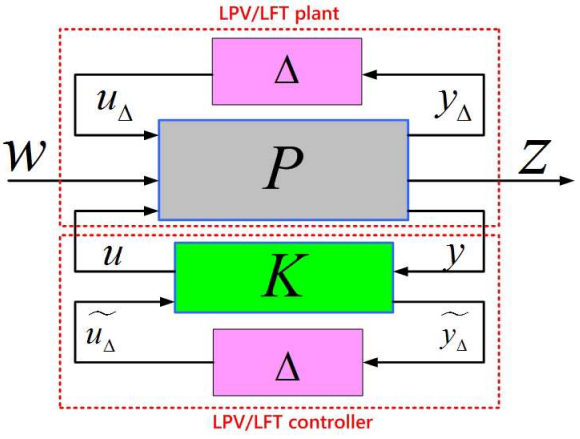

Figure 2.10: LPV/LFT control scheme

Based on the overall LPV/LFT control scheme presented in Fig. 2.10, the closed-loop operator from w to z is:

$$T_{zw} = F_l(F_u(P, \Delta), F_l(K, \Delta)) \tag{2.17}$$

As stated in section 2.2.5, given a LTI plant P, the usual H_∞ control problem is concerned with finding an internally stabilizing LTI controller K such that:

$$\|F_l(P,K)\|_\infty < \gamma$$

where γ is some prescribed performance level. The H_∞/LFT control problem has a similar statement, except that both the plant and the controller are now LPV instead of LTI, see Apkarian & Gahinet (1995). Then, the objective of a H_∞/LFT controller is to guarantee some closed-loop performance $\gamma > 0$ from w to z for all admissible parameter Δ.

Assuming Δ is bounded, the H_∞/LFT control of a LPV/LFT systems boils down to find a control structure K such that the following conditions are satisfied

- the closed-loop system (2.17) is internally stable for all possible parameter Δ
- and, $\|T_{zw}\|_\infty < \gamma$

The methodology used for the synthesis of such a controller in a discrete-time form will be based on the framework of LMIs resolution described in Apkarian & Gahinet (1995). With a discrete-time LPV plant $P(z)$ of LFT form, if we let N_R and N_S denote bases of the null spaces of $(B_2^T, D_{\Delta 2}^T, D_{12}^T, 0)$ and $(C_2, D_{2\Delta}, D_{21}, 0)$ respectively, the H_∞/LFT problem is solvable if and only if there exist pairs of symmetric matrices (R, S) in $\mathbb{R}^{n\times n}$ and (L_3, J_3) in $\mathbb{R}^{n_\Delta \times n_\Delta}$ and a scalar $\gamma > 0$ such that:

$$N_R^T \begin{pmatrix} ARA^T - R + B_\Delta J_3 B_\Delta^T & \star & \star & \star \\ C_\Delta RA^T + D_{\Delta\Delta} J_3 B_\Delta^T & C_\Delta RC_\Delta^T + D_{\Delta\Delta} J_3 D_{\Delta\Delta}^T - J_3 & \star & \star \\ C_1 RA^T + D_{1\Delta} J_3 B_\Delta^T & C_1 RC_\Delta^T + D_{1\Delta} J_3 D_{\Delta\Delta}^T & C_1 RC_1^T + D_{1\Delta} J_3 D_{1\Delta}^T - \gamma I & \star \\ B_1^T & D_{\Delta 1}^T & D_{11}^T & -\gamma I \end{pmatrix} N_R < 0$$

$$N_S \begin{pmatrix} A^TSA - S + C_\Delta^T L_3 C_\Delta & \star \\ B_\Delta SA + D_{\Delta\Delta}^T L_3 C_\Delta & B_\Delta^T SB_\Delta + D_{\Delta\Delta}^T L_3 D_{\Delta\Delta} - L_3 \\ B_1^T SA + D_{\Delta 1} L_3 C_\Delta & B_1^T SB_\Delta + D_{\Delta 1}^T L_3 D_{\Delta\Delta} \\ C_1^T & D_{1\Delta} \end{pmatrix}$$
$$\begin{pmatrix} \star & \star \\ \star & \star \\ B_1^T SB_1 + D_{\Delta 1}^T L_3 D_{\Delta 1} - \gamma I & \star \\ D_{11} & -\gamma I \end{pmatrix} N_S < 0$$

$$\begin{pmatrix} R & I \\ I & S \end{pmatrix} \geq 0$$

$$L_3\Delta = \Delta L_3, J_3\Delta = \Delta J_3, \begin{pmatrix} L_3 & I \\ I & J_3 \end{pmatrix} \geq 0$$

Given any solution (R, S, L_3, J_3) of the LMIs above, the state space data of some γ suboptimal discrete-time controller $K(z)$ can be achieved where:

$$\Omega = \begin{pmatrix} A_K & B_{K1} & B_{K\Delta} \\ C_{K1} & D_{K11} & D_{K1\Delta} \\ C_{K\Delta} & D_{K\Delta 1} & D_{K\Delta\Delta} \end{pmatrix}$$

with $K(z)$ be denoted by:

$$K(z) = \begin{pmatrix} D_{K11} & D_{K1\Delta} \\ D_{K\Delta 1} & D_{K\Delta\Delta} \end{pmatrix} + \begin{pmatrix} C_{K1} \\ C_{K\Delta} \end{pmatrix} (zI - A_K)^{-1} \times (B_{K1}, B_{K\Delta})$$

More information and example of LPV/LFT model and H_∞/LFT controller synthesis can be found in Apkarian & Gahinet (1995), Sename et al. (2013), Roche (2011), Briat et al. (2009), Packard (1994) and Scherer (2001*a*).

2.5 Concluding remarks

Since H_∞ control and H_∞/LFT control will be the main approaches of this dissertation w.r.t. battery estimation and EMS (Energy Management Strategy) development; the LMIs are the main tool of controller synthesis. This chapter has presented some brief introductions associated with the H_∞ robust control, the H_∞/LFT LPV controller, the LMI techniques and related algorithms for controller synthesis.

The LMI-based solutions stated in this chapter will then be used for the synthesis of the H_∞ battery fault observer presented in chapter 5, the robust fault-tolerant EMS controller proposed in chapter 7, the gain-scheduled EMS controller proposed in section 8.1, and the LPV EMS regulator achieved in section 8.2.

Part I

BATTERY MODELING AND ESTIMATION

The first part of this dissertation is focused on the power battery: in particular, modeling and estimation of the Lithium-ion (Li-ion) batteries in Hybrid Electric Vehicles (HEVs).

Chapter 3 is mainly devoted to the Electric Equivalent Circuit (EEC) battery modeling, where the battery configuration and principle of operation, as well as the battery classification are included. Also, an overview of the battery modeling technique is presented.

Based on the battery model achieved in chapter 3, battery State of Charge (SOC) estimation is implemented in chapter 4 using Kalman filter. Besides, a novel method is proposed for battery capacity estimation, which is based on the Least Mean Squares (LMS) algorithm.

Chapter 5 presents a novel battery fault (battery ageing) estimation method based on the H_∞ observer minimizing the effect of temperature and battery input current on the estimation accuracy.

The following contributions are given in this part

1. The LMS algorithm, which is more simple and less time-consuming than the KF/EKF based approach in terms of parameter estimation, is adopted for battery capacity estimation in chapter 4.

2. An H_∞ battery fault observer is presented in chapter 5, where an extended battery model, considering the temperature change, which have influences on battery parameters, as a disturbance, is adopted for the fault estimator development.

Meanwhile, the related method and results of chapter 5 have been published in:

- *H_∞ observer-based battery fault estimation for HEV application* (T.-H. Wang, J.J. Martinez-Molina and O. Sename), in 2012 IFAC Workshop on Engine and Powertrain Control, Simulation and Modeling (E-COSM'12).

Chapter 3

Lithium-ion Battery Model

A battery model of sufficient accuracy and complexity is required for both battery estimation and Energy Management Strategy (EMS) development. Therefore, this chapter will contribute to present the mathematical formulations with respect to the behaviors of the Lithium-ion battery. In section 3.1, the configuration and principle of operation of a Lithium-ion cell is given first, then the classification of Lithium-ion battery is given followed by some basic battery notions. A methods overview in terms of battery modeling is presented in section 3.2.1. The Equivalent Electric Circuit (EEC) battery model is constructed in section 3.2.2, where model assumption and parameters are also given.

As already stated in chapter 1, the main objective of this dissertation is not to present a detailed methodology on modeling and control of batteries, but to account for related battery items in the EMS development of HEVs. Therefore, for detailed model explanations, interested readers are encouraged to refer to related references that should be useful, which will then be given in associated section of this chapter. It is also important to notice that the model presented in this chapter is not a new contribution in the field of battery modeling, and all model parameters are inferred from the experiments by Codecà (2008) and Codecà et al. (2008).

3.1 Introduction to Lithium-ion battery

As depicted in Fig. 3.1, a Lithium-ion (Li-ion) battery cell is composed of a positive electrode (cathode), a negative electrode (anode), a separator, copper current collector on the side of negative electrode and aluminium current collector on the side of positive electrode, with the battery cell connected to an external circuit via the current collectors.

The electrolyte conducts lithium ions, but insulates electrons, providing a medium for lithium ions to travel between the electrodes and keeping electrons within the exter-

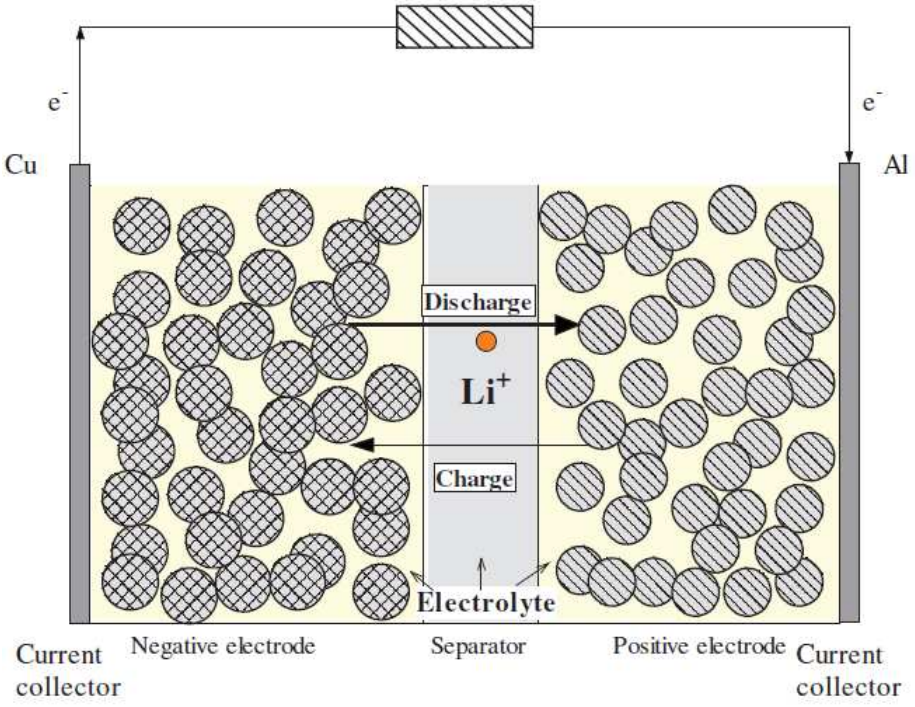

Figure 3.1: Schematic of a Lithium-ion cell (source: Fang et al. (2010))

nal circuit.

During discharge, lithium ions travel from the anode (negative electrode) to the cathode (negative electrode) through the electrolyte. Accumulative lithium ions makes the cathode more positive, and the potential difference between the cathode and the anode results in the current flow through the external circuit. During charge, the opposite effect occurs. The current propels lithium ions to move from the cathode to the anode. The lithium ions accumulate in the anode, and the battery is charged, refer to Fang et al. (2010) and Lam (2011) for more detail.

According to the material of cathode, Li-ion battery can be classified into, refer to Battery University (2013) and Radio-Electronics (2013):

- the **Lithium Cobalt Oxide (LCO)** consisting of a lithium cobalt oxide ($LiCoO_2$) cathode and a graphite carbon anode.
- the **Lithium Manganese Oxide (LMO)** that uses lithium manganese oxide ($LiMn_2O_4$) as its cathode material
- the **Lithium Iron Phosphate (LFP)** that adopts a nano-scale phosphate cathode ($LiFePO_4$) material

- the **Lithium Nickel Manganese Cobalt Oxide (NMC)** that uses a cathode comprising of a combination of nickel, manganese and cobalt ($LiNiMnCoO_2$)
- the **Lithium Nickel Cobalt Aluminum Oxide (NCA)** that uses a cathode comprising of a combination of nickel, aluminum and cobalt ($LiNiCoAlO_2$)

There are many important terms associated with the states and properties of the battery. For sake of sufficient understanding on the properties of various Li-ion battery types, the following related terms of the battery will be defined before going further on battery modeling (presented in section 3.2.1) and estimation (presented in the next immediate two chapters).

- **Battery capacity**

  Battery capacity is a measure of the charge stored in a battery. Battery nominal capacity represents the amount of charge that can be withdrawn from a battery under certain conditions. However, the actual battery capacity varies significantly from the nominal one, since it depends strongly on the usage history and the operating conditions, e.g., discharging/charging currents and internal temperatures, of the battery. Generally, the capacity of a battery is expressed using ampere-hour (Ah).

- **C-rate**

  C-rate is a measure of the current rate at which a battery is discharged/charged. A current of 1C rate means that the battery is ideally charged or discharged in one hour, C/2 in two hours and 2C in half an hour. This means that the current of 1C for a battery with nominal capacity of 160Ah is 160A, see Lam (2011).

- **Internal resistance**

  Internal resistance of a battery is defined as the opposition to the current flow within a battery. The internal resistance of a battery depends on many factors such as C-rate of discharging/charging, battery temperature, battery state of charge and battery state of health which will be defined later. Increased internal resistance resulted in lower battery efficiency since more battery energy is converted into heat.

- **State of charge (SOC)**

  SOC is an expression of the present battery capacity as a percentage of the nominal battery capacity with 100% means the battery is full charged, and 0% means the

battery is empty. Generally, SOC is achieved based on current integration over charging/discharging time.

- **Depth of discharge (DOD)**

  DOD is the opposite of SOC. It is a percentage of the battery capacity that has been discharged. SOC of 20% means the DOD is up to 80%.

- **State of health (SOH)**

  SOH, which can also be described as the age of a battery, represents the health state of a battery. In other words, SOH indicates how much the battery is corrupted. In the application of XEVs, SOH mainly relates to the ability of a battery to perform a particular discharge/charge function at an instantaneous moment, see Haifeng et al. (2009). The range of SOH is defined from 0% to 100% with 100% means the battery is totally new, and 0% means the battery can not meet the power demand of the vehicle usage any more.

  In particular, SOH is usually quantified by estimating the power fade or/and the capacity fade of a battery. The power fade refers to the phenomenon of increasing battery internal resistance as the battery ages. This increasing resistance results in a drop of the power that can be sourced/sunk by the battery. The capacity fade refers to the phenomenon of decreasing battery capacity as the battery ages, see Plett (2004*c*).

- **Specific energy**

  Specific energy is defined as battery capacity per unit mass. The specific energy of a battery/battery cell is expressed using Wh/kg. An high specific energy means lower vehicle burden associated with battery weight for required driving range, as well as guarantees less energy consumption of the vehicle.

- **Specific power**

  Specific power is the available power per unit mass of a battery/battery cell given with W/kg. It determines the battery weight with respect to the performance requirement of a vehicle. A battery can have lower specific energy but higher specific power and vice versa.

- **Cycle life**

  Battery cycle life is defined as the number of charge/discharge cycles that a battery can offer before it fails to meet a specific performance requirement. The definition

of battery cycle life must be related to a certain scenario since the actual cycle life of a battery is affected by environmental impacts and operation profiles such as temperature, C-rate, DOD etc.

For the application of Li-ion batteries to XEVs, the trend will be the use of LFP batteries for reasons of:

- the LFP offers good electrochemical performance with low resistance, high specific power, high current rating (not true for the LCO) and long cycle life (not true for the LMO)
- compared to NCA and the NMC, the LFP owns enhanced safety and good thermal stability, since it does not experience the thermal runaway (accelerated by increased temperature, in turn releasing energy that further temperature increases), which may result in fatal hazard
- the LFP has superior safety and almost no fire hazard, since no oxygen is released at high temperatures
- the LFP is not expensive, since neither nickel nor cobalt is used

Interested readers can refer to Battery University (2013), Radio-Electronics (2013) and Lam (2011) for more information on Li-ion battery and the LFP.

3.2 Battery modeling

This section is devoted to present the model used to describe the dynamic behaviors of a Li-ion cell. But, in practice, all on-board batteries are packs that are composed of multiple battery cells placed in series and parallel; scaling up of single battery cell to battery pack of multiple cells introduces several complications in battery modeling, and is beyond the scope of this dissertation. So, for simplicity, it is assumed in this work that battery cells are connected in series; all battery parameters are times of that of a battery cell.

3.2.1 Methods overview

Several battery models with diverse degrees of complexity and accuracy are proposed in the literature. Each kind is focused on specific battery behaviors for specific purposes: from battery design and performance estimation to circuit simulation, Codecà (2008).

Basically, battery models can be classified into:

- black-box models
- electrochemical models
- Equivalent Electric Circuit (EEC) battery models

Black-box models use transfer functions to describe the behavior of batteries without rebuilding the underlying physicochemical processes, Dong et al. (2011).

Examples of such kind of model include the one proposed by Shepherd in Shepherd (1965), Peukert's law in Durr et al. (2006), fuzzy logic model by Salkind et al. (1999), and model using artificial neural network in Shen et al. (2002) and Shen (2007), etc.

Most of the black-box models are only suitable for specific applications. For example, as stated in Doerffel & Sharkh (2006), Peukert's equation just works for batteries that are discharged under constant temperature and current. Especially, it is not applicable to Li-ion batteries whose capacity is strongly dependent on battery temperature, environmental conditions and discharge current.

Similarly, for Shepherd equation, parameters could only be achieved by experimental discharge with constant current. Subsequently, the applicability of such kind of model is limited to temperature range between $10^{\circ}C$ and $30^{\circ}C$, Pattipati et al. (2011).

Electrochemical models, refer to Doyle et al. (1993), Dees et al. (2002) and Gu & Wang (2000) etc., accounts for the full physicochemical processes by means of a set of partial differential equations.

Electrochemical model, see Chaturvedi et al. (2010), on one hand, is a time consuming task since it requires lots of complex electrochemical equations for a complete system description, and, on the other hand, is mainly used to optimize the physical design aspects of batteries, characterize the fundamental mechanisms of power generation and relate battery design parameters.

Taking He et al. (2011), Yann Liaw et al. (2004) and Gao et al. (2002) for example, EEC battery models are typically described by circuits composed of passive components such as resistors, inductances, and capacitances which are configured to match the frequency response of the battery impedance, Chiang & Sean (2009).

Specifically, all EEC models can be divided into Thevenin and impedance-based ones. Impedance-based models, refer to Dong et al. (2011), Chen & Rincon-Mora (2006) and Buller et al. (2003) for example, are extracted from electrochemical impedance spectroscopy (EIS) measurements on a battery cell, within a large range of frequencies. Each circuit component of the impedance-based model corresponds with one or more electrochemical processes of the battery, and the model will be more accurate if a circuit of higher order is used, Lam (2011).

Thevenin models, refer to Salameh et al. (1992), Liaw et al. (2005), Haifeng et al. (2009), Codecà et al. (2008) and Hu et al. (2011) for example, are more commonly used to describe the voltage behavior of a battery. By measuring voltage response with respect to current variations, the electrical circuit model of a battery is constructed. The circuit order is determined by taking into account the tradeoff between model complexity and accuracy, Lam (2011).

3.2.2 Equivalent Electric Circuit (EEC) battery model

The EEC models, based on the combinations of voltage sources, resistances and capacitance, whose parameters have physical meanings, are commonly used for control design, and are particularly suitable for co-design and co-simulation with other electrical circuits or systems. Also, for electrical applications, this kind of model is more intuitive, useful, and easy to handle. Therefore, the EEC model which owns a good compromise between computation time and simulation accuracy is adopted in this work.

3.2.2.1 Model structure and dynamical equations

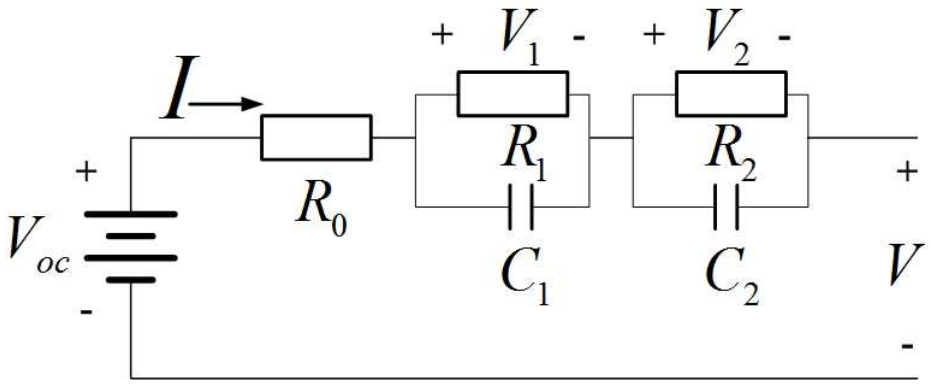

Figure 3.2: EEC battery model structure

Fig. 3.2 shows the 2^{nd} order Thevenin model adopted in this dissertation, which catches better all main static and dynamic phenomena of a Li-ion battery, see Do et al. (2009) and Codecà et al. (2008), with:

- V_{oc} stands for the Open Circuit Voltage (OCV) of the battery, which mainly depends on the SOC defined as the available capacity in a battery expressed as a percentage of the battery's nominal capacity
- R_0 is the internal resistor which represents electrolyte and connection resistances

- the other two RC parallel circuits represent the charge transfer phenomenon and the diffusion phenomenon respectively
- V_1 and V_2 are the voltages over R_1C_1 and R_2C_2 parallel circuits respectively
- V is the terminal voltage of the battery
- I is the current drawn from the battery

The EEC battery model shown in Fig. 3.2 can be described by following dynamic equations applying the voltage-current law.

$$\dot{V}_1 = -\frac{1}{C_1R_1}V_1 + \frac{1}{C_1}I \tag{3.1}$$

$$\dot{V}_2 = -\frac{1}{C_2R_2}V_2 + \frac{1}{C_2}I \tag{3.2}$$

$$V = V_{oc}(SOC) - V_1 - V_2 - R_0I \tag{3.3}$$

Meanwhile, the SOC, which is defined as the available battery capacity expressed as a percentage of the battery's nominal capacity, is related to I and can be formulated as:

$$SOC = 1 - \frac{\int_0^t Idt}{Cb} \tag{3.4}$$

so, there is:

$$\dot{SOC} = -\frac{1}{Cb}I \tag{3.5}$$

where Cb denotes the nominal battery capacity.

As shown in Fig. 3.3, V_{oc} is usually represented as a monotonically increasing function of SOC. Furthermore, the relation between V_{oc} and SOC owns strong linearisation widely, except for ranges of very high or very low SOCs. So it is reasonable that a linear function as shown in (3.6) be used as a approximation of V_{oc} with the consideration that the SOC of battery for HEV application will never be too high nor too low.

$$V_{oc}(SOC) = k \cdot SOC + b \tag{3.6}$$

where k and b can be achieved easily based on two points picked within the linear range of Fig. 3.3 ($SOC \in [0.1 \quad 0.9]$).

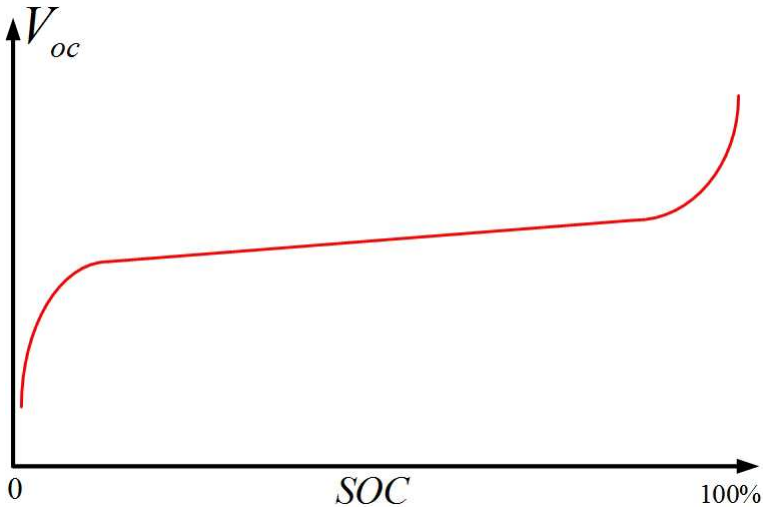

Figure 3.3: V_{oc} vs. SOC

Note that this representation (Fig. 3.3 or (3.6)) depends on the battery ageing and operation conditions such as the temperature.

Then, another description showing more explicit relation between V and SOC can be obtained by substituting (3.6) into (3.3)

$$V = k \cdot SOC + b - V_1 - V_2 - R_0 I \tag{3.7}$$

In fact, the predicted OCV (based on the estimated SOC), evaluated after a charge or a discharge, is always greater or smaller than the "true" OCV, due to the so-called electro-chemical hysteresis, see Codecà (2008).

This electro-chemical hysteresis is well defined in Srinivasan et al. (2001) as the characteristic of a system in which a change in the direction of an independent variable (for example the current flow direction) leads to the dependent variable failing to retrace the path it passed in the forward direction.

The effect of the electro-chemical hysteresis on the OCV of a battery can be illustrated by the charge/discharge curves shown in Fig. 3.4, where the OCV for discharge is the dash curve, and the OCV for charge the solid curve.

As seen from the model formulations presented previously, the voltage hysteresis is not taken into account in this work. Therefore, for battery model including voltage hysteresis, interested readers are encouraged to refer to Codecà (2008), Plett (2004*b*), Xuyun & Zechang (2008), Roscher et al. (2011).

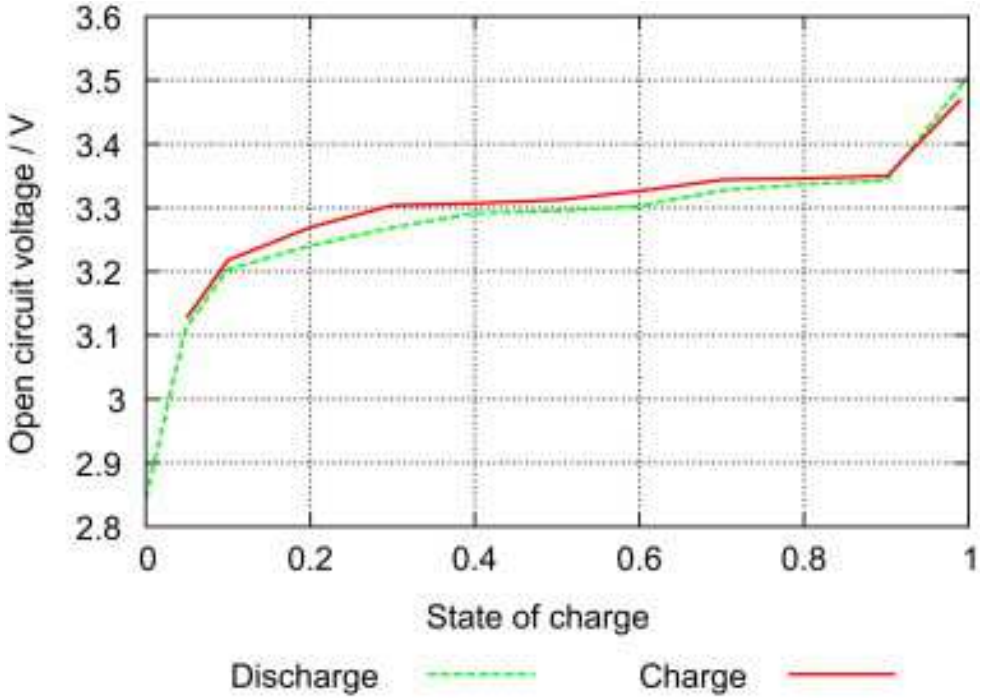

Figure 3.4: V_{oc} curves of a LFP battery during charging and discharging (source: Schwunk et al. (2012))

3.2.2.2 Model parameters and assumptions

Table 3.1 presents the parameters of a battery cell, which will be used for battery estimation and EMS design under the following assumptions:

- all the parameters are with respect to the situation of $T = 40°C$, $I = 10A$ and $SOC = 0.5$
- the parameters are independent of current direction, C-rate, temperature and SOC

Table 3.1: Battery cell parameters

Cell parameters	
R_0	0.00867Ω
R_1	0.0124Ω
R_2	0.0123Ω
C_1	$2239F$
C_2	$41831F$
Cb	$2.3Ah$
k	$1/3$
b	3.05

The author have to emphasis that the parameters in Table 3.1 are inferred thanks to the identification and validation results of an A123-M1 Li-ion cell proceeded in Codecà (2008).

3.3 Concluding remarks

One of the main reason related to battery modeling is its need to estimate some battery states that are difficult to measure or sometimes impossible to measure, e.g., the SOC and SOH of the battery. If the battery model includes these states, the model can be used for their estimation.

In fact, the battery model presented in section 3.2.2 is a battery cell model. For simplicity, it is assumed, in this work, that the battery is composed of battery cells connected in series. Then the battery model can be achieved by scaling up of the cell model presented in section 3.2.2 with all parameters given in Table 3.1 multiplied by the cell number of the battery pack, and be used for battery estimation and EMS design.

The battery model presented in this chapter is a basic one that does not take into account the influences of battery temperature and other factors, such as the hysteresis effect, current direction and C-rate. The influence of temperature changes and battery ageing will be considered as additive uncertainties on the battery parameters in chapter 5 and chapter 8.

Chapter 4

Battery State of Charge Estimation and Parameter estimation

Accurate battery understanding, based on the estimation of battery State of Charge (SOC) and battery parameters, such as battery capacity and battery internal resistances, which indicate the health state (State of Health (SOH)) of a battery, is on one hand one of the requirements related to the optimal Energy Management Strategy (EMS) development of the XEVs, and, on the other hand, is the core of proper battery usage that guarantees acceptable cycle life and safety of the battery.

This chapter is mainly devoted to the estimation of battery SOC and parameters based on the Electric Equivalent Circuit (EEC) Li-ion battery model presented in section 3.2.2. The method considered for battery SOC estimation will be the Kalman Filter (KF) that are widely used in the literature related to the estimation of Li-ion and other kinds of batteries. Besides, this chapter will propose a novel method for battery capacity estimation based on the Least Mean Squares (LMS) algorithms, which is more simple and less time-consuming than the KF based approach.

In details, section 4.1 gives the definitions and the state of the art of both SOC estimation and parameter estimation. In section 4.2, introduction of KF and Extended Kalman Filter (EKF) is given and followed by the application of KF to SOC estimation tackled in section 4.2.2. Finally, a novel method, which is based on the LMI techniques, is introduced and applied for battery parameter estimation in section 4.3.

Since, in this dissertation, battery capacity will be the only battery parameter that is used to schedule the Linear Parameter Varying (LPV) EMS controller (one of the main contributions of this work, which will be presented in chapter 8, all parameter estimations referred to in this chapter will be the capacity estimation. Therefore, it must

be noticed that capacity is not the only parameter that could be used to indicate battery SOH; the estimation methods (EKF, KF, LMS) may be used for other battery parameters, e.g., battery resistances, see Plett (2004*c*), Haifeng et al. (2009) and Do et al. (2009) for example.

4.1 State of the art

4.1.1 Battery State of Charge (SOC) estimation

Larsson et al. (2011) illustrated the crucial influence of battery SOC on the quality of an EMS. However, the fact is that SOC is not measurable. When developing an EMS, the SOC must therefore be estimated using observers or online estimation technics.

Almost as long as rechargeable batteries have existed, systems able to give an indication of the available amount of charge inside a battery (i.e. the SOC of a battery) have been used. It was the Curtis Instruments who pioneered gauges to monitor the SOC of vehicle traction batteries, see Pop et al. (2005). And, during that period, all proposed methods and algorithms of SOC estimation were only based on the voltage average evaluation, see Dreer (1984) for example. However, it is concluded by Lerner et al. (1970), that the only reliable way of estimating the SOC is to use a current-sharing method.

The current was taken into account for the first time in Brandwein & Gupta (1974), where in addition to voltage measurements, the current that flows into and out of the battery is also measured and used for SOC indication of Nickel Cadmium (NiCd) batteries.

Christianson & Bourke (1975) developed a method of SOC indication based on the evaluation of the Open Circuit Voltage (OCV) that is directly proportional to the battery SOC, and can be calculated using the following equation:

$$OCV = V_T + IR$$

where V_T is the terminal voltage of the battery, I is the battery current with a positive value during discharge and a negative value during charge and R is the internal resistance of the battery.

In Dowgiallo (1975) and Zaugg (1982), the Electrochemical Impedance Spectroscopy (EIS), which was used for the first time on batteries in 1941 as described in Rodrigues et al. (2000), was used to estimate the SOC and other battery parameters.

In 1984, Peled developed a method for SOC determination of Li-ion batteries based on the usage of look-up tables. After applying a current step and a short rest period,

the OCV (as a function of temperature) of a battery is measured and compared with a corresponding predetermined value stored in a look-up table. Then the SOC can be inferred from the comparison, see Peled et al. (1984). Similarly, a method aiming at determining the SOC of Nickel Metal Hydride (NiMH) batteries in notebook applications is presented in Bowen et al. (1994), with discharge/charge rate as another additional input of the look-up tables compared to the method in Peled et al. (1984).

Table 4.1: History of SOC algorithm development, Pop et al. (2005)

Year	**Researcher/Company**	**Method**
1963	Curtis	Voltage measurements
1970	Lerner	Comparison between two batteries (one has a known SoC)
1974	York	Threshold in voltage levels
1974	Brandwein	Voltage, temperature and current measurements
1975	Christianson	OCV
1975	Dowgiallo	Impedance measurements
1975	Finger	Coulomb counting
1978	Eby	OCV and voltage under load
1980	Kikuoka	Book-keeping
1981	Finger	Voltage relaxation
1984	Peled	Look-up tables based on OCV and temperature measurements
1985	Muramatsu	Impedance spectroscopy
1986	Kopmann	Look-up tables based on OCV, temperature and current measurements
1988	Seyfang	Book-keeping and adaptive system
1992	Aylor	OCV, OCV prediction and Coulomb counting
1997	Gerard	Voltage and current measurements, artificial neural networks
1999	Salkind	Coulomb counting, EIS, fuzzy logic
2000	Garche	Voltage and current measurements, KF
2000	Bergveld	Book-keeping, overpotential, maximum capacity learning algorithm

SOC estimations using Coulomb counting, which is based on the integration of battery current, are presented in Aylor et al. (1992) and Richter & Meissner (2000). The method developed in Aylor et al. (1992) is a combination of the previously described OCV method and Coulomb counting, and only hold for Lead-acid batteries. Verbrugge et al. (2000) presented the applications of Coulomb counting relates to NiMH batteries and other battery technology such as Lead-acid, Li-ion, etc., operating in the powertrain of an HEV. In addition to Coulomb counting, the systems presented by Kikuoka et al.

(1980) and Seyfang (1988) also compensate for temperature, charging efficiency of the battery, self-discharge and battery ageing, see Pop et al. (2005).

Some adaptive methods of SOC estimation are presented in Gérard et al. (1997), Garche & Jossen (2000) and Salkind et al. (1999). In Gérard et al. (1997), an algorithm based on the neural networks is used, while the fuzzy logic is used in Salkind et al. (1999). In Garche & Jossen (2000), the KF is used to implement an adaptive algorithm, where the SOC estimation is performed comparing the estimated battery voltage on the basis of the current and temperature measurements with the measured value of the battery voltage.

The most important points of the SOC estimation history is summarized in Table 4.1, and more related details can be found in Pop et al. (2005).

The actually implemented solutions with respect to battery SOC estimation can be classified as follows, see Codecà (2008), Di Domenico et al. (2011), Piller et al. (2001), Pattipati et al. (2011) and Bhangu et al. (2005):

- **Coulomb counting (Ampere hour (Ah) counting)**

  Ah counting, see Lin et al. (2006), Ng et al. (2009), Alzieu et al. (1997) and Codecà (2008) for example, is the most commonly used technique, requiring dynamic measurement of the current flowing inside and outside of the battery, the time integral of which is considered to provide a direct indication of SOC.

- **Open Circuit Voltage (OCV)**

  OCV, see Pang et al. (2001) and Verbrugge & Tate (2004) for example, is usually related to the SOC of batteries. Letting the battery rest for enough time, then all relaxation dynamics inside the battery are completed, and the SOC can be evaluated.

- **Impedance Spectroscopy and internal resistance**

  Impedance Spectroscopy, see Huet (1998) and Rodrigues et al. (2000) for example, is also called Electrochemical Impedance Spectroscopy (EIS). It is implemented applying an Alternating Current (AC) on the battery, recording meanwhile the battery voltage response. The voltage-current ratio (also called the impedance) over frequency is related to the SOC and other battery characteristics, e.g., battery ageing and the SOH.

  Internal resistance is essentially an EIS, but implemented only with Direct Current (DC).

- **Black-box methods**

  Black-box methods, concerned by the application of SOC estimation, include the fuzzy logic, refer to Salkind et al. (1999) and Singh et al. (1998), and artificial neural network, see Bo et al. (2008) and Shen (2007).

- **Kalman Filter (KF) and Extended Kalman Filter (EKF)**

  KFs are designed to estimate unknown states of systems from some input and output measurements. Optimum KF can be used to determine the SOC of batteries based on a numeric battery model description with SOC as one of its states. Then, on the basis of the current, temperature and other input measurements, the measured value of the battery voltage is used as correction comparison with the estimated output voltage of the battery model. Such an approach can also be used for the prediction of battery parameters, see Plett (2004*c*) for example. KFs can only be designed for linear systems, while actual battery models often contain nonlinearities of different level, then EKFs can be used instead, see Vasebi et al. (2008) and Santhanagopalan & White (2006).

However, as stated in Codecà (2008), not all the methods summarized above are suited for XEVs applications.

Impedance Spectroscopy and **internal resistance** are offline tests, which means batteries have to be disconnected to the vehicle to perform certain tests. This is obviously not possible for XEVs, where the battery has to be always available to store or provide electrical power.

Open Circuit Voltage (OCV) is widely used in small-power electronic applications, thanks to the predictable working conditions and the controlled environment. Moreover, due to the large characteristic time associated with the battery relaxation, the OCV-based SOC estimation is unavailable in automotive applications, see Pang et al. (2001) and Verbrugge & Tate (2004).

Coulomb counting, i.e. current integration, provides the simplest method to detect SOC variations, since it is a good information source for SOC. However, it is affected by inaccuracy of the initial SOC condition, accumulated battery capacity degradation with battery ageing, see Di Domenico et al. (2011) and Hansen & Wang (2005).

Neural network and **fuzzy Logic** usually provide good online estimation performances, and there is no need to disconnect batteries. However, the learning process of **Black-box methods** is computationally heavy, even they can reach high estimation accuracy.

Similarly, **Kalman Filter (KF)** owns good performance for online SOC estimations. Meanwhile, it can provide a robust estimation with respect to noisy measurements, inaccurate initializations and model uncertainties, which will be seen in section 4.2.

4.1.2 Battery parameters and State of Health (SOH) estimation

The performance of batteries degrades with battery usage, since active material on the battery plates gradually degrades by mechanisms such as loss of plate active surface area due to repeated dissolution and recrystallization, loss of electrical contact between metallic grids and active materials, and growth of large inactive crystals of lead sulphate, see Bhangu et al. (2005) and Lam (2011). SOH is then used to quantify the performance fade (power fade or/and capacity fade) of a battery.

The methodologies, proposed in the literature, for SOH estimation can be categorized into two groups (see Chiang & Sean (2009)):

- one is based on the performance fading model that continuously monitor the changes in performance values of a battery such as voltage, power and capacity, taking into account all/some of the degradation factors such as temperature, C-rate and depth of discharge.

- another one is to search the sensitive parameters with strong correlation to the performance fades.

Some kinds of methods on battery SOH modeling can be found in Lam (2011), Schmidt et al. (2010), Pattipati et al. (2008) and Ramadass et al. (2003). As seen, modeling of the performance fade is not a trivial work.

In fact, the most direct and simple way for SOH estimation is to estimate the electrical characteristics of the battery that can be modeled by the Electric Equivalent Circuit (EEC) that is mostly composed of a series of resistor and capacitors. It means that the parameter estimation of the EEC model can facilitate the SOH estimation, see Chiang & Sean (2009), Liaw et al. (2005) and Sun et al. (2007) for example.

Meanwhile, it is widely proved that battery resistance and battery capacity are two main electrical characteristics of the battery that are related to the SOH (ageing level) of a battery. So, in practice, SOH estimation is usually boiled down to the parameter estimation problem in terms of battery capacity and/or battery resistance. And, most of the algorithms use for battery parameter estimation are based on the EKF that provide robust estimations in spite of noisy measurements and model uncertainties, by modeling

the battery system to include the wanted battery parameters in its state description, see Plett (2004c), Bhangu et al. (2005) and Do et al. (2009) for example.

4.2 Battery SOC estimation based on Kalman Filter (KF)

The section is focused on the realization of KF methods on battery estimation. An introduction to KF and EKF problem is given first, then SOC estimation is tackled using KF.

4.2.1 Introduction to Kalman Filter and Extended Kalman Filter

4.2.1.1 Kalman Filter

The Kalman Filter is named after R. E. Kalman who described a recursive solution to the discrete-data linear filtering problem in Kalman et al. (1960). Essentially, KF is a set of mathematical equations that implement a predictor-corrector type estimator that is optimal in the sense that it minimizes the estimated error covariance when some presumed conditions are met, Bishop & Welch (2001).

For a discrete-time lumped linear dynamic systems:

$$\begin{cases} x_{k+1} = Ax_k + Bu_k + w_k \\ y_k = Cx_k + Du_k + v_k \end{cases} \tag{4.1}$$

where $x_k \in \mathbb{R}^n$ is the state vector at time index k, $u_k \in \mathbb{R}^p$ is the known input to the system, $w_k \in \mathbb{R}^n$ is the stochastic process noise or disturbance that models some unmeasured input which affects the state of the system. $y_k \in \mathbb{R}^m$ is the output of the system, $v_k \in \mathbb{R}^m$ models sensor noises that affect the measurement of the system output, but does not affect the system state, matrices $A \in \mathbb{R}^{n\times n}$, $B \in \mathbb{R}^{n\times p}$, $C \in \mathbb{R}^{m\times n}$ and $D \in \mathbb{R}^{m\times p}$ describe the dynamics of the system.

KFs address the problem of estimating the unmeasurable state x_k of the system (4.1), given knowledge of the system's measured input and output signals.

Also, it is assumed that w_k and v_k are independent of each other, with zero mean and covariance matrices of known value:

$$E\left[w_n\, w_k^T\right] = \begin{cases} Q, & n = k \\ 0, & n \neq k \end{cases} \quad E\left[v_n\, v_k^T\right] = \begin{cases} R, & n = k \\ 0, & n \neq k \end{cases} \tag{4.2}$$

where Q is the process noise covariance and R is the sensor noise covariance.

The KF problem is then: using the entire observed input data $\{u_0, u_1, \cdots u_k\}$ and measurement data $\{y_0, y_1, \cdots y_k\}$, find the minimum mean squared error estimate $\hat{x}_k$ of the true state x_k, based on the system by (4.1) and assumptions (4.2) on w_k and v_k, Plett (2004*a*).

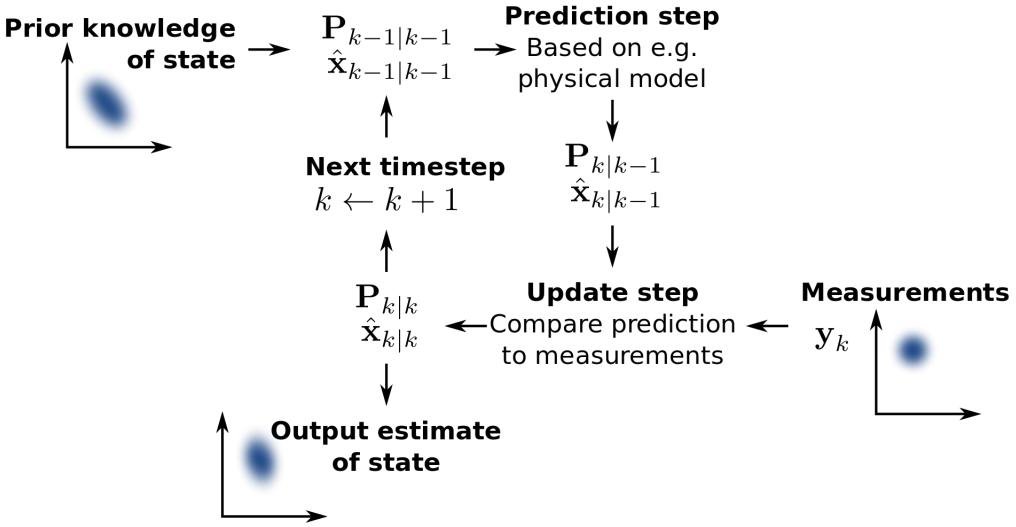

Figure 4.1: Kalman Filter cycle (source: wikipedia)

The solution to this problem is illustrated in Fig. 4.1, which adopts the form of feedback control. As seen, for each time step, the KF computes two state estimates ($\hat{x}_{k|k-1}$ and $\hat{x}_{k|k}$) as well as two covariance matrices ($P_{k|k-1}$ and $P_{k|k}$) of the state estimate error.

The first state estimate, $\hat{x}_{k|k-1}$, is computed before any measurements are made, and is called the a priori state estimate, $\hat{x}_k^-$. The second state estimate $\hat{x}_{k|k}$ updates the first estimate after measuring the system output y_k, and is called the a posteriori state estimate $\hat{x}_k$. $P_{k|k-1} = E\left[e_k^- \ (e_k^-)^T\right]$, which corresponds to the a priori estimate error, $e_k^- = x_k - \hat{x}_k^-$, is called the a priori estimate error covariance, P_k^-. $P_{k|k} = E\left[e_k \ e_k^T\right]$, which corresponds to the a posteriori estimate error, $e_k = x_k - \hat{x}_k$, is called the a posteriori estimate error covariance, refer to Greg & Gary (2006) and Plett (2004*a*).

For realization, the KF is initialized with prior knowledge of the state x_0,

$$\hat{x}_0 = E\left[x_0\right] \tag{4.3}$$

$$P_0 = E\left[(x_0 - \hat{x}_0) \ (x_0 - \hat{x}_0)^T\right] \tag{4.4}$$

Following initialization, the KF repeatedly performs two steps: prediction step and

update step. During the prediction step, it predicts the value of the present state $\hat{x}_{k|k-1}$ and the error covariance $P_{k|k-1}$. During the update step, it corrects the state estimate $\hat{x}_k$ and the error covariance P_k using the measurement of system output y_k.

1. **Prediction step**:

   The following equations are used for the prediction step:

$$\hat{x}_{k|k-1} = A\hat{x}_{k-1} + Bu_{k-1} \tag{4.5}$$

$$P_{k|k-1} = AP_{k-1|k-1}A^T + Q \tag{4.6}$$

2. **Update (Correction) step**:

   Then, the predicted state $\hat{x}_{k|k-1}$ is corrected based on the measurement of the system output y_k

$$\hat{x}_k = \hat{x}_{k|k-1} + L_k \left[y_k - \left(C\hat{x}_{k|k-1} + Du_k \right) \right] \tag{4.7}$$

   where $C\hat{x}_{k|k-1} + Du_k$ is the predicted output $\hat{y}_k$, the measurement difference $y_k - \hat{y}_k$ is weighted by the Kalman gain

$$L_k = P_{k|k-1}C^T \left[CP_{k|k-1}C^T + R \right]^{-1} \tag{4.8}$$

   and the error covariance is corrected using

$$P_{k|k} = \left(I - L_k C \right) P_{k|k-1} \tag{4.9}$$

4.2.1.2 Extended Kalman Filter

As described in section 4.2.1.1, the KF is a tool for state estimate of a discrete-time linear system. For a nonlinear system:

$$\begin{cases} x_{k+1} = f\left(x_k, u_k\right) + w_k \\ y_k = g\left(x_k, u_k\right) + v_k \end{cases} \tag{4.10}$$

where $x_k \in \mathbb{R}^n$, $u_k \in \mathbb{R}^p$, $w_k \in \mathbb{R}^n$, $y_k \in \mathbb{R}^m$, $v_k \in \mathbb{R}^m$, a linearization process can be used to approximate the nonlinear system with a Linear Time Varying (LTV) system which is

then used in the KF, resulting in an EKF on the true nonlinear system, see Greg & Gary (2006) for more details.

The EKF is very similar to the KF, except that:

- A of KF is replaced by the linearized matrix $\hat{A} = \frac{\partial f(x_k, u_k)}{\partial x_k}$ for prediction step
- C of KF is replaced by the linearized matrix $\hat{C} = \frac{\partial g(x_k, u_k)}{\partial x_k}$ for correction step

4.2.2 KF based SOC estimation

By modeling the battery system with SOC as one of its states, the SOC estimation can then be achieved using Kalman filter.

The battery model achieved in section 3.2.2 can be converted to the discrete-time form

$$\begin{pmatrix} V_{1,k+1} \\ V_{2,k+1} \\ SOC_{k+1} \end{pmatrix} = \begin{pmatrix} e^{\frac{-Ts}{R_1C_1}} & 0 & 0 \\ 0 & e^{\frac{-Ts}{R_2C_2}} & 0 \\ 0 & 0 & 1 \end{pmatrix} \begin{pmatrix} V_{1,k} \\ V_{2,k} \\ SOC_k \end{pmatrix} + \begin{pmatrix} R_1(1 - e^{\frac{-Ts}{R_1C_1}}) \\ R_2(1 - e^{\frac{-Ts}{R_2C_2}}) \\ -Ts/Cb \end{pmatrix} I_k + w_k \quad (4.11)$$

$$V_k = k \cdot SOC_k + b - V_{1,k} - V_{2,k} - R_0 I_k + v_k \quad (4.12)$$

where Ts is the sample period, k is the sample point, w_k and v_k are the process noise vector and the sensor noise vector of the system respectively. According to the KF assumptions, w_k and v_k are uncorrelated zero-mean Gaussian white sequences.

Table 4.2: Battery parameters for battery SOC estimation

Battery parameters	
R_0	0.5202Ω
R_1	0.744Ω
R_2	0.738Ω
C_1	$134340F$
C_2	$2509860F$
Cb	$496800Ah$
k	22.5
b	177.75

Treating battery current I_k as the input and battery terminal voltage V_k as the output measurement, and assuming all parameters, R_0, R_1, R_2, C_1, C_2, Cb, k, b are time-invariant with values given in Table 4.2. Then the KF algorithm presented previously can be used for battery SOC estimation based on (4.11) and (4.12).

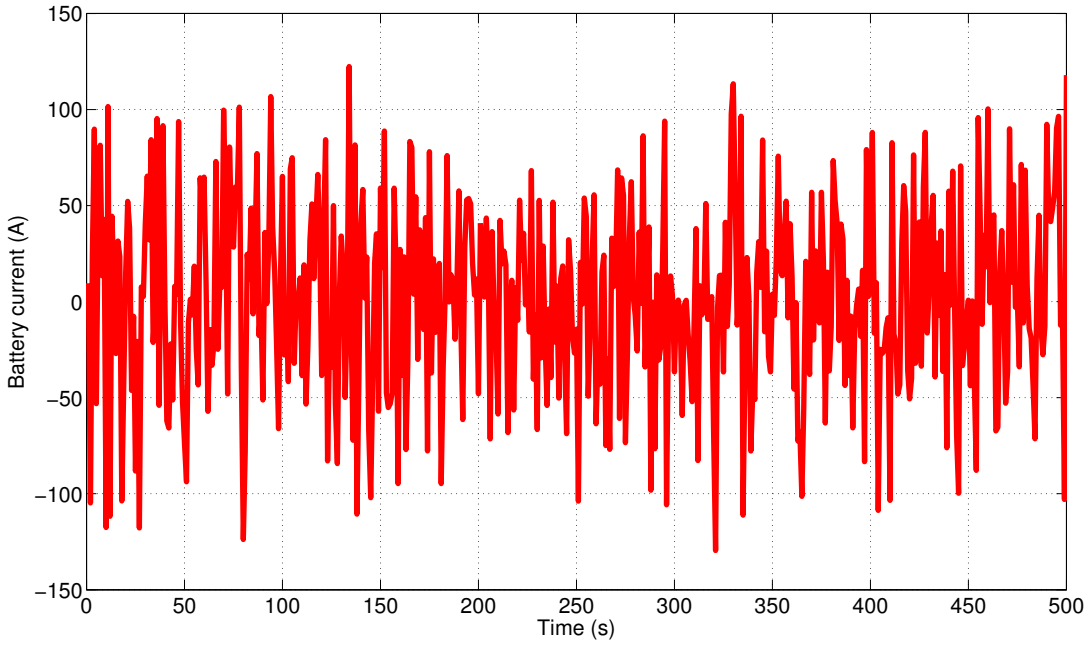

Figure 4.2: Battery current profile

Information on the system noise is contained in Q and R as defined in (4.2). Often, the selection of Q, R is complicated due to the fact that knowledge on the statistic property of system noises is limited.

Here, Q=R=10 is firstly chosen, and the testing current as shown in Fig. 4.2 is applied as the input to the Kalman filter.

A comparison of the actual battery terminal voltage and the estimated one by the KF is shown in Fig. 4.3, where well convergence can be seen. Fig. 4.4 shows the result of Kalman filter for battery SOC estimation. As seen, the estimated SOC owns excellent consistency with the real one.

In essence, Q and R influence the accuracy of the KF's performance, since, as seen in 4.6 and 4.8, they determine the action of the estimation error covariance matrix $P_{k|k-1}$ and KF gain matrix L_k. The impact of Q and R on the performance of the KF are shown in Fig. 4.5 and Fig. 4.6. It can be seen from Fig. 4.5 that R has trivial influence on the estimated battery terminal voltage, while Q has a significant influence. As seen from Fig. 4.6, both Q and R have remarkable influence on SOC estimation error, where R has more influence.

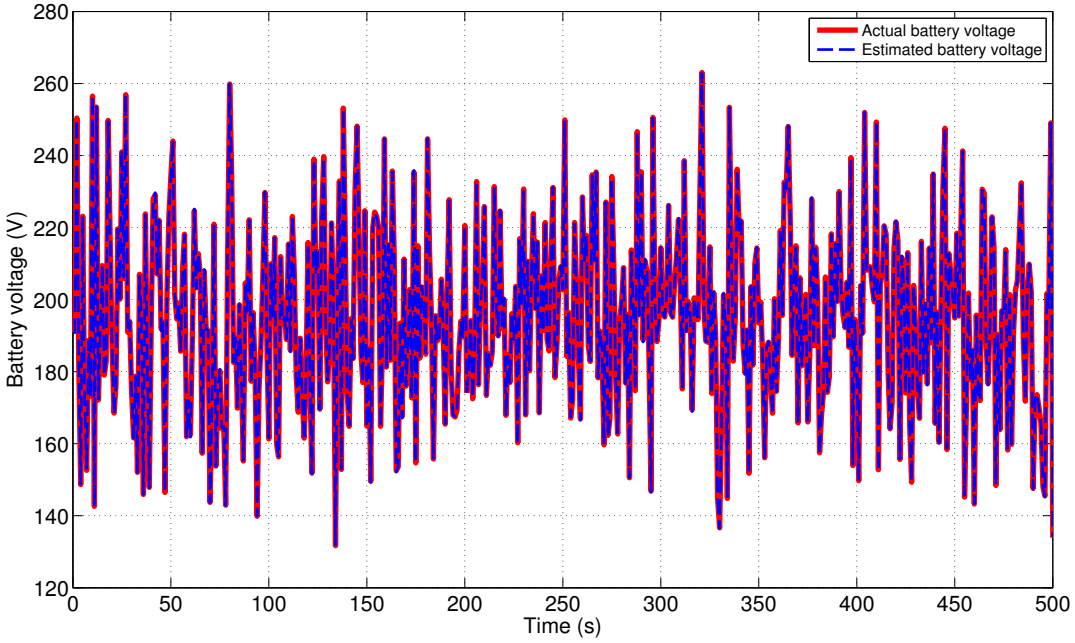

Figure 4.3: Estimated and actual battery terminal voltage

4.3 LMS based battery parameter estimation

It is important to remind that the KF-based SOC estimation achieved above is implemented based on the assumption that all battery parameters are time-invariant. However, there exists variation, which gets larger as the battery ages, in some crucial battery parameters, such as battery resistance and capacity. So, the method used to estimate SOC might be adapted to time-varying battery parameters.

The method, which is called the joint estimation, can then be adopted to estimate both the state and the time-varying cell parameters by augmenting the state vector of the battery model with expected battery parameters and estimating the values of this augmented state vector. Since such an extension of state vector results in non-linearity of system model, the EKF algorithm must be adopted instead of the KF one, refer to Do et al. (2009) and Barlak & Ozkazan (2009) for more details and examples on modeling of battery parameter variations and the realization of joint estimation methods.

Due to the high dimensionality of the resulting augmented battery model, the joint estimation method has the disadvantage of large matrix operations. Meanwhile, it is apparent that the descriptive quantities of the present battery condition exist on two time scales. The SOC changes very fast on its entire range (between 100% and 0%) within minutes. Battery parameters, such as cell capacity, change very slowly, which might change as little as 20% in a decade or more of regular use, see Plett (2004*c*).

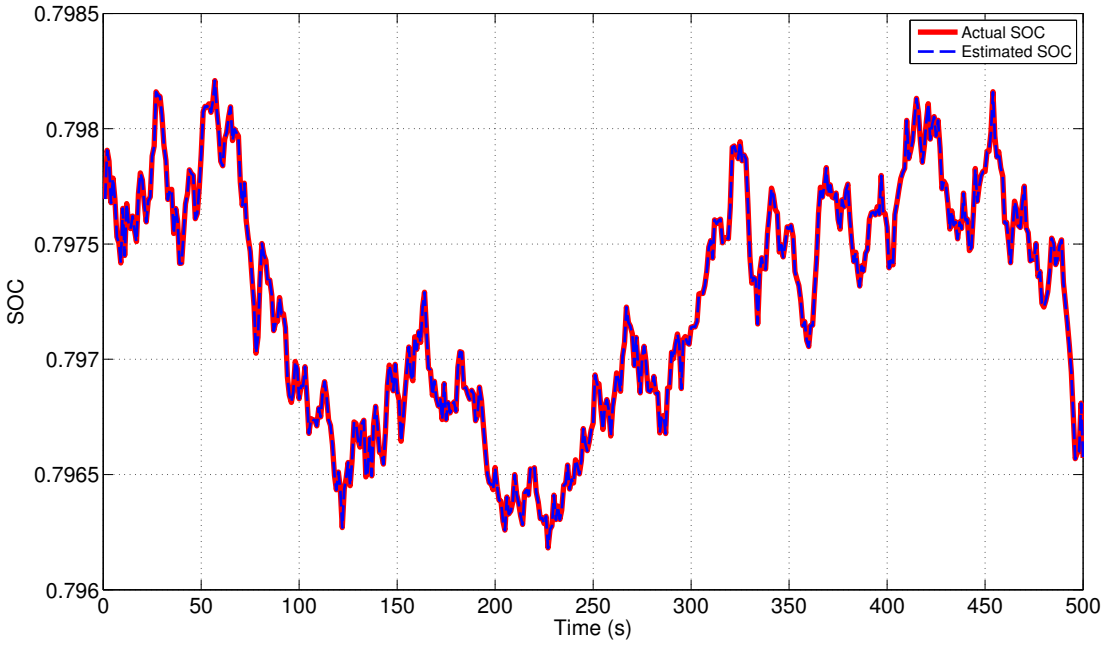

Figure 4.4: Estimated and actual battery SOC

Plett (2004*c*) and Lee et al. (2008) proposed the dual EKF estimation method to estimate both the SOC and the battery parameters, which combines two EKFs, one of which is the state filter, which estimates the SOC, and the other is the weight filter, which estimates the battery parameters. At each sample point, the state filter uses an a priori value of the weight filter, while the weight filter uses an a priori value of the state filter. Therefore, the two EKFs are calculated concurrently to estimate the SOC and battery parameters, and the matrix operations become simpler.

In this section, the similar principle is adopted, where the connection between SOC estimation and battery capacity estimation is depicted in Fig. 4.7, except that the Least Mean Squares (LMS) algorithm, which is more simple and direct than the EKF one, is adopted for battery parameter estimation. Also, different cycle periods are assigned for SOC estimation and battery capacity estimation. In detail, the SOC is estimated always to catch the rapid battery dynamic, while battery capacity is estimated occasionally to ensure the optimization of the SOC estimation, and to provide the indication of battery age/health state (SOH).

4.3.1 Introduction to LMS technique

The LMS algorithm introduced by Bernard Widrow, see Widrow (1971) and Widrow & Stearns (1985), is a kind of adaptive filter that has gained much popularity due to

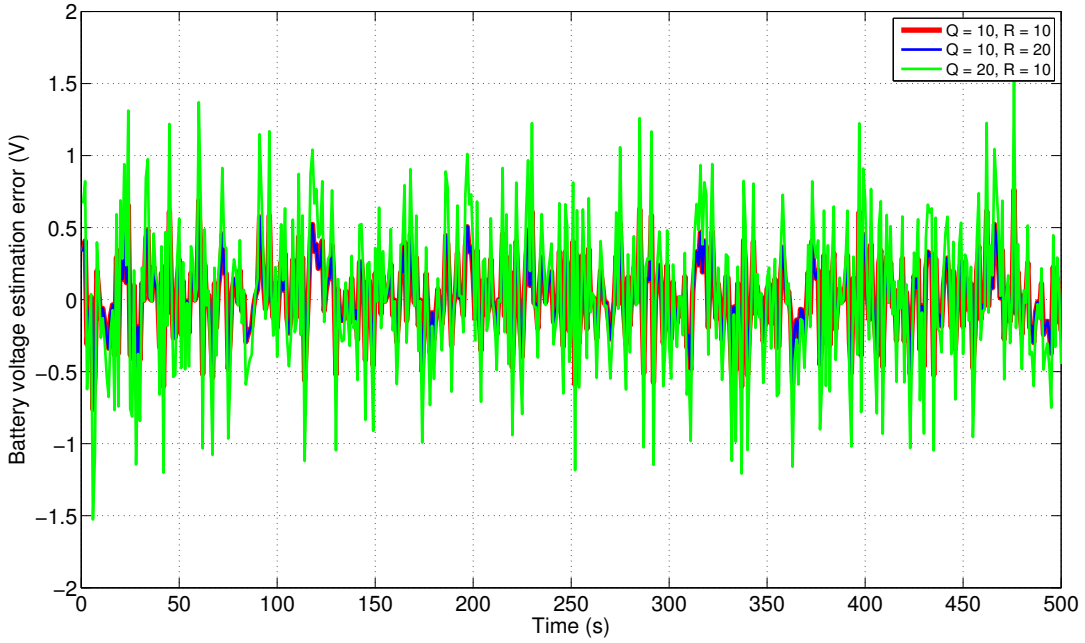

Figure 4.5: Impact of Q and R on estimated battery terminal voltage

the advantages of simplicity in its underlying structure, ease of implementation and robustness, see Slock (1993), Feng et al. (1998), Duttweiler (2000) and Pradhan et al. (2005) for example.

The LMS filter is structured in Fig. 4.8, where X_k is the vector of input signals at time index k, y_k is the vector of desired signals, $\hat{y}_k$ represents the estimate of y_k, e_k is the vector of estimation error.

The basic idea behind LMS filter is to update the filter weight W_k in a manner to converge to an optimum filter weight that minimize the cost function

$$J_k = E[e_k^2]$$

where E denotes the expectation operation, $e_k = y_k - \hat{y}_k$.

The cost function J_k is a Mean Square Error (MSE), and is minimized by the algorithm, which results in that the LMS gets its name.

In detail, the algorithm starts by assuming a small weight W_0 (zero in most cases), and the weight W_k is updated at each iteration k using

$$W_{k+1} = W_k - \mu \nabla(J_k) \tag{4.13}$$

where μ is the adaptation parameter, ∇ is the gradient operator. The negative sign indicates that we need to change the weights in a direction opposite to that of the gradient

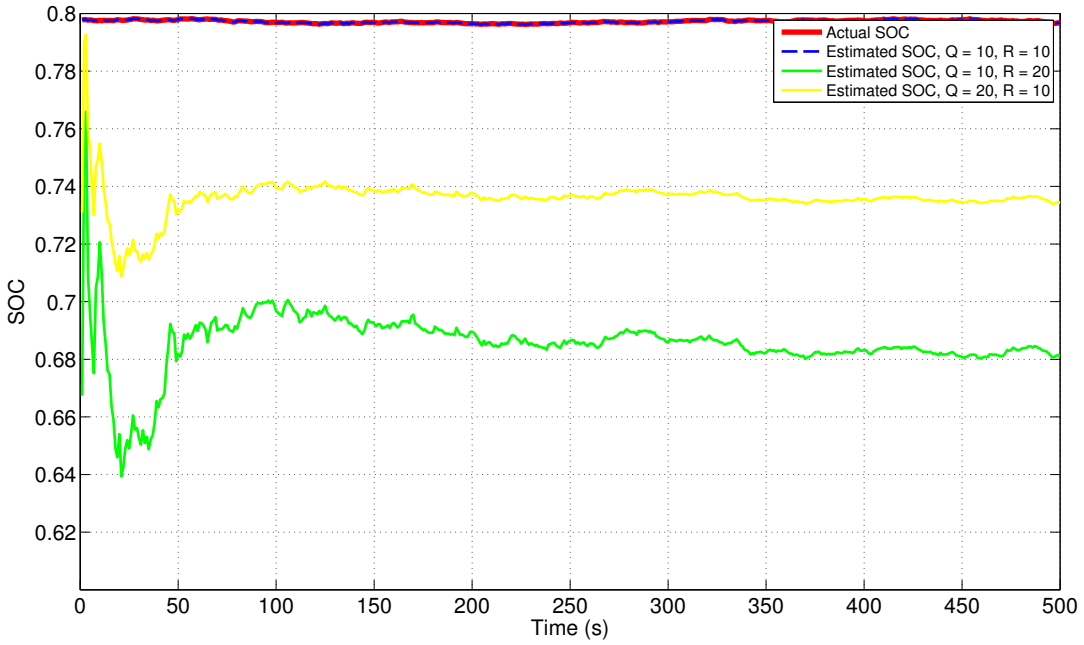

Figure 4.6: Impact of Q and R on battery SOC estimation

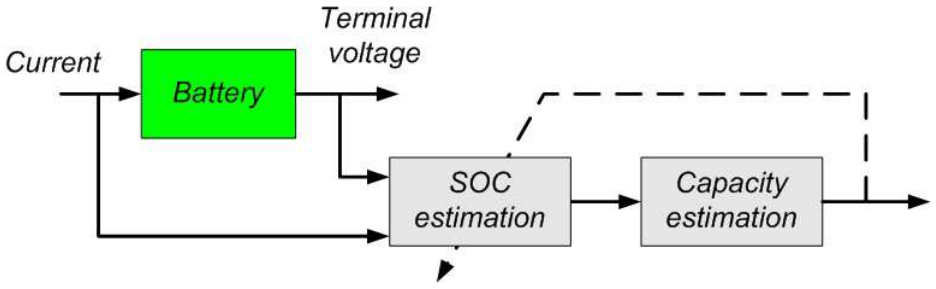

Figure 4.7: Interaction between battery SOC estimation and capacity estimation

slope. That is, when the MSE-gradient is positive, the error would keep increasing positively if the same weight is used for further iterations, which means we need to reduce the weight. Similarly, if the MSE-gradient is negative, we need to increase the weight.

Then the LMS algorithm proceeds by first computing the error signal e_k which is then used to compute the updated filter weight W_k, and this cycle is performed until steady-state conditions are attained. The convergence of such a algorithm is governed by the selection of μ which should satisfy the condition

$$0 \prec \mu \prec \frac{2}{\lambda_{max}}$$

where λ_{max} the greatest eigenvalue of $E\,[X_k\ X_k]$. If this condition is not fulfilled, the algorithm becomes unstable. And, When μ is small, the LMS algorithm takes more time

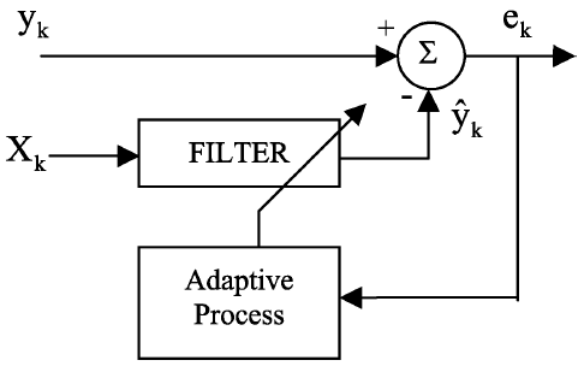

Figure 4.8: LMS filter structure, Pradhan et al. (2005)

to learn about its input with minimum mean square error and vice versa, see Pradhan et al. (2005).

4.3.2 Battery capacity estimation

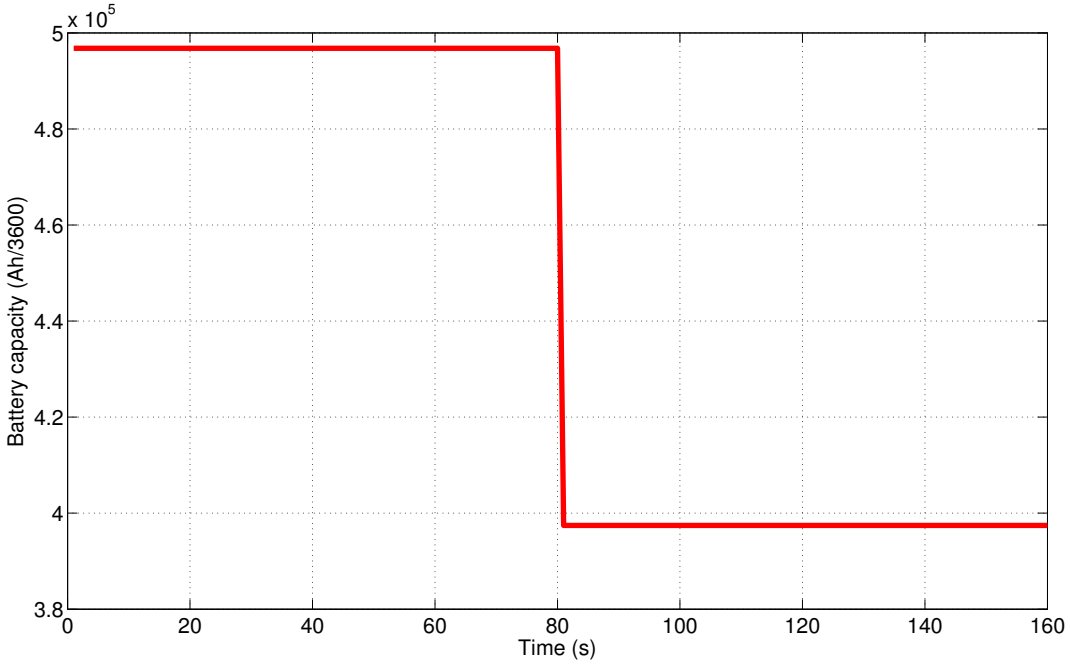

Figure 4.9: Evolution of the battery capacity

To estimate battery capacity using the LMS, the following simple model, which is a reformulation of the SOC state equation picked out from the discrete-time battery model

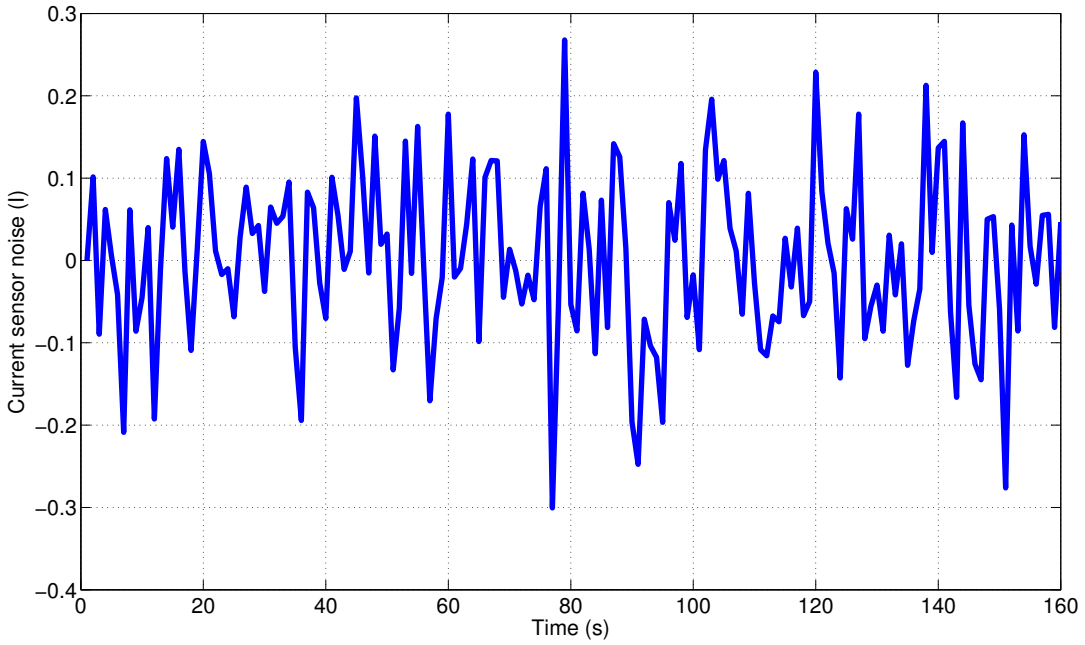

Figure 4.10: Current sensor noise

given by (4.11), is adopted

$$-I_{k-1}Ts = Cb_{k-1}(SOC_k - SOC_{k-1} + n_w) + n_v \tag{4.14}$$

where Ts is the sample period, k is the sample point, I is the battery current that is measurable, Cb is the battery capacity needed to be estimated, SOCs inherit the estimated values using the KF as stated in section 4.2.2, n_w is used to accounting for the SOC estimation error, n_v represents the sensor noise input.

With respect to the filter illustrated by Fig. 4.8 and the LMS algorithm presented in section 4.3.1, we

- treat battery capacity Cb as the filter weight W_k that owns the initial value of $W_0 = 0$, which means the first capacity estimation is $Cb_0 = 0$.
- define $X_k = SOC_k - SOC_{k-1}$ as the input
- define $\hat{y}_k = SOC_k - SOC_{k-1} + n_w$
- define $y_k = -I_{k-1}Ts$

Then, for each iteration step k, $\hat{y}_k$ is compared with y_k, and the difference $e_k = y_k - \hat{y}_k$ is used to correct W_k (the capacity estimation Cb_k) based on (4.13) aiming at minimizing the MSE $E[e_k^2]$.

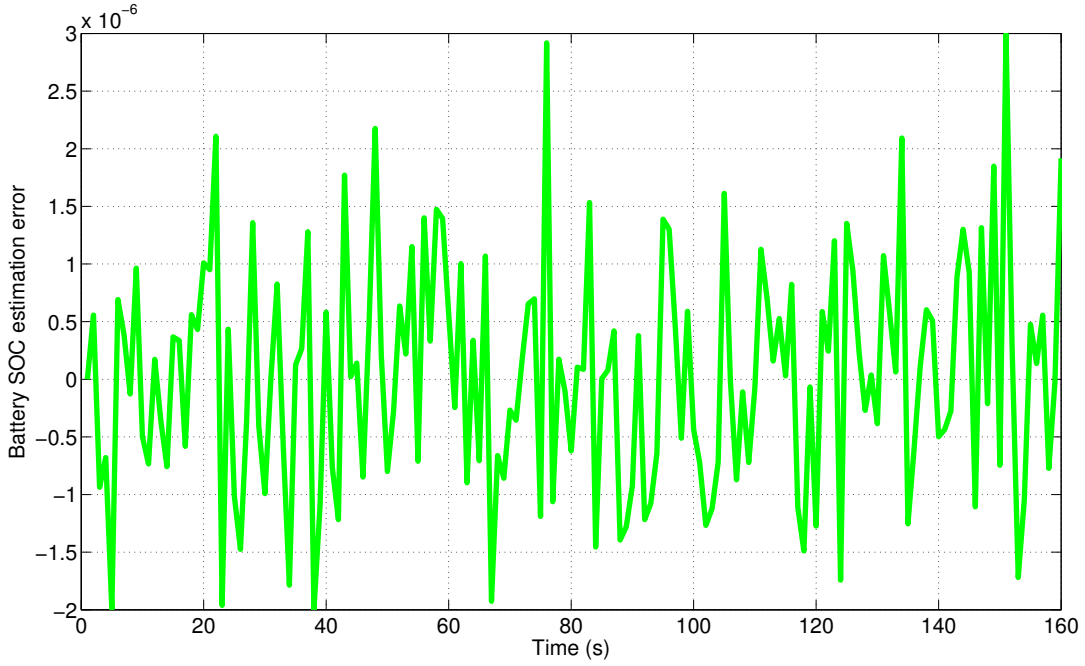

Figure 4.11: Uncertainty on battery SOC estimation

Fig. 4.9 presents the scenario used to test the efficiency of the LMS algorithm for battery capacity estimation based on the system description (4.14). It can be seen, a sudden capacity jump is given at $t = 80s$ with the final value of 80% of the initial one. The related n_w and n_v is specified by Fig. 4.11 and Fig. 4.10 respectively.

Then, the capacity estimation is implemented based on the LMS method stated previously, with the estimation result presented by Fig. 4.12. It is obvious that the estimated capacity converges to the actual value quickly.

Fig. 4.13 gives the capacity estimation errors with respect to three n_w of different amplitude levels. As seen, the estimation error is significantly impacted by the SOC uncertainty, and well SOC estimation is the basis of correct battery capacity estimation, since SOC values are directly inherited from the estimation results using the KF as stated in section 4.2.2.

4.4 Concluding remarks

In this chapter, the state of the art of both SOC estimation and battery parameter estimation is given. The estimation of battery SOC is tackled using the Kalman filter based on the discrete-time Electric Equivalent Circuit (EEC) battery model achieved in chapter 3, while, a novel method that is based on the Least Mean Squares (LMS) algorithm is used

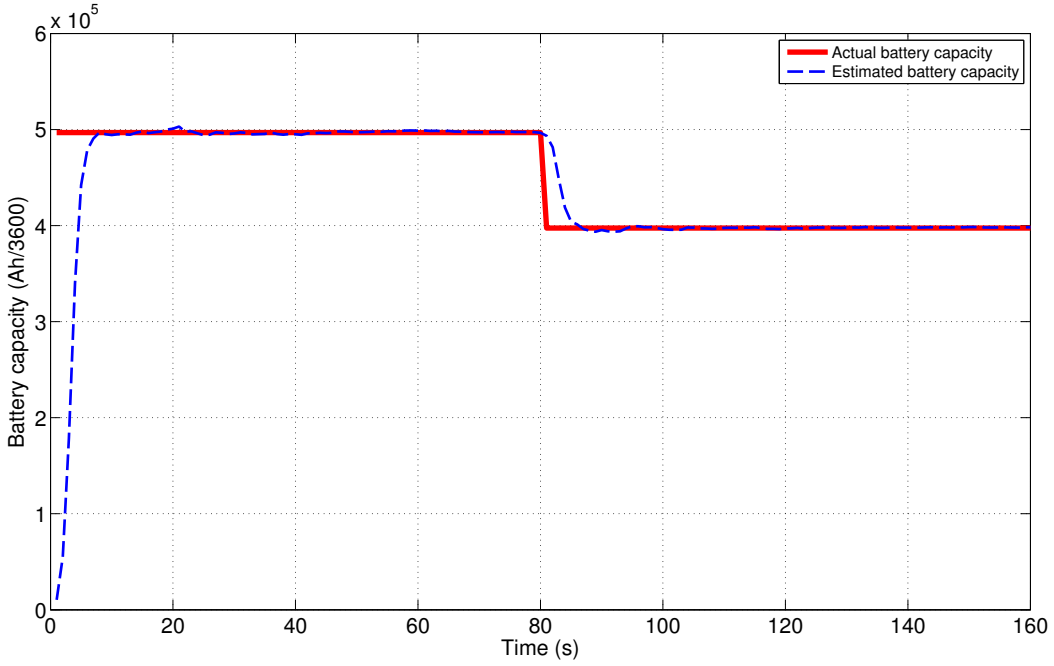

Figure 4.12: Battery capacity estimation based on LMS

for battery capacity estimation, where a simple model, which reformulates the SOC state equation given by (4.11), is adopted.

Then, the estimation results based on the methods presented in this chapter can be used for the development of Energy Management Strategy (EMS) in Hybrid Electric Vehicles (HEV) aiming at improve the control performance, as well as achieve proper battery usage that guarantees acceptable cycle life and safety of the battery.

Since just basic battery model is used in this work, further work is expected to get a more complex battery model that takes into account the influences of the battery temperature and other factors, such as the hysteresis effect, current direction and C-rate, which will result in more accurate estimation for both battery SOC and capacity.

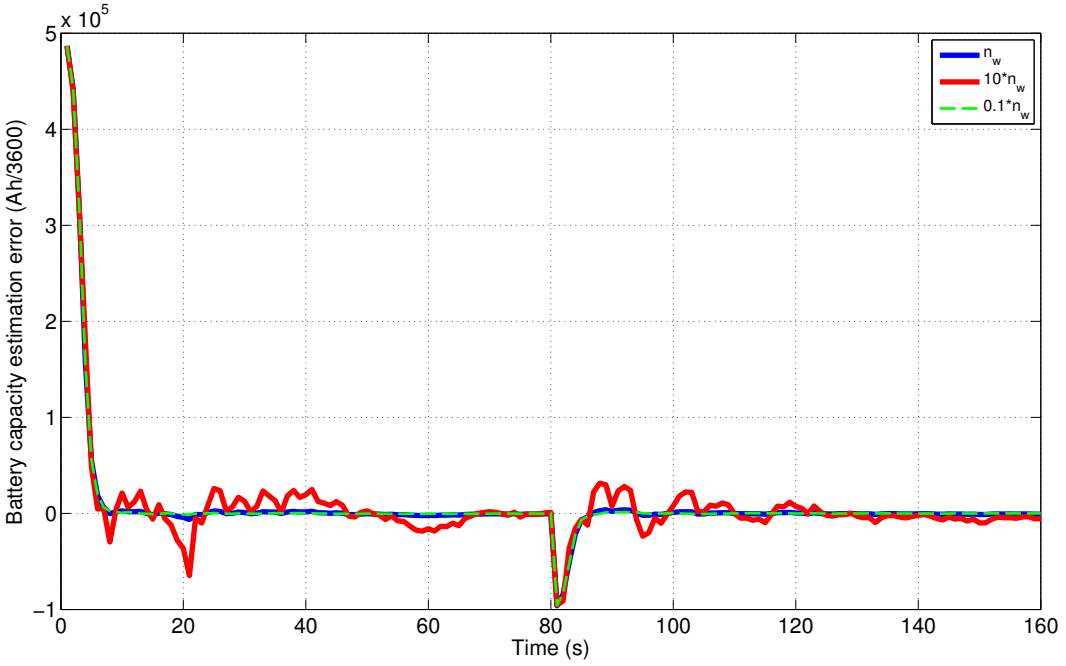

Figure 4.13: Impact of SOC uncertainty on the accuracy of battery capacity estimation

Chapter 5

H_∞ Observer Based Battery Fault Estimation

No matter how the battery technology will progress and how advanced the battery will be, the battery ageing and its rate is significantly affected by environmental impacts, such as environmental temperature, and operation profiles, such as charge/discharge current rate (C-rate). Therefore, it is important to detect the underlying battery degradation aiming at, on one hand predicting how soon the battery will fail or reach a level that cannot guarantee satisfactory performances (see Zhang & Lee (2011)) and on the other hand preventing the whole system from unexpected severe failures or even breakdown, since, as the core component, the battery has a primary effect on the performance of XEVs.

As a sub-field of the control engineering, fault diagnosis concerns monitoring a system, identifying if a fault has occurred, pointing the type of fault and locating the fault that is defined as an unexpected change in a system with component malfunction or variation in operating condition. Faults in a dynamic system can take many forms, such as actuator faults, sensor faults and abrupt changes of some parameters, see Zhang & Huang (2011). In literature related to fault detection, there has been significant research activity in the design and analysis of model-based diagnostic schemes, see Chen & Patton (1999), Blanke (2003) and Isermann (2006), including parity relations, observer-based methods, and parameter identification techniques. Among these methods, observer-based fault detection is one of the most effective methods and has obtained much more attention.

For battery fault detection, the well-known and widely used approach is Kalman filter based battery parameter identification method as stated in the previous chapter.

Although the fault information of a battery inferred from battery estimation is valuable, experimental results have shown significant variations of battery parameters under different environments, especially under different ambient temperatures.

This chapter is devoted to the development of a novel fault estimation method for the Li-ion battery based on the H_∞ observer taking into account the environment variations, where battery ageing is treated as the fault. First, the influence of temperature changes and battery ageing on battery resistance and capacity are considered and modeled as additive variations from the nominal values of battery parameters, based on the 2^{nd} order EEC battery model achieved in chapter 3. Then, the principle of fault estimation is stated, the fault observer owning the general H_∞ configuration is depicted, and the extended model, considering temperature changes as a disturbance and battery ageing effect as a fault, is used to develop the H_∞ estimator minimizing the influence of the disturbance on the fault detection. Finally, the H_∞ fault observer, including weighting functions for performance specifications, is derived and simulation results both in frequency domain and time domain are given.

5.1 Battery model used for fault estimation

5.1.1 Nominal battery model

Let us recall the battery model achieved in chapter 3, based on the model structure depicted in Fig. 3.2

$$\dot{V}_1 = -\frac{1}{C_1 R_1} V_1 + \frac{1}{C_1} I \tag{5.1}$$

$$\dot{V}_2 = -\frac{1}{C_2 R_2} V_2 + \frac{1}{C_2} I \tag{5.2}$$

$$\dot{SOC} = -\frac{1}{Cb} I \tag{5.3}$$

$$V = k \cdot SOC + b - V_1 - V_2 - R_0 I \tag{5.4}$$

with all battery parameters are specified in Table 3.1.

5.1.2 Influences of temperature on battery parameters

Practical experiments have shown that battery parameters are sensitive to variation of environment situations such as temperature, SOC, C-rate, etc.

In this work, the influence of temperature, which owns significant impact on battery parameters, as well as that of battery ageing will be emphasized.

5.1.2.1 Influence on battery resistances

The effect of temperature on the internal resistance with respect to a specific kind of Sony commercial Li-ion polymer battery (UP393562) which has a nominal capacity of $800mAh$ is illustrated in Fig. 5.1. As seen clearly, battery internal resistance decreases with increasing temperature, see Gomez et al. (2011).

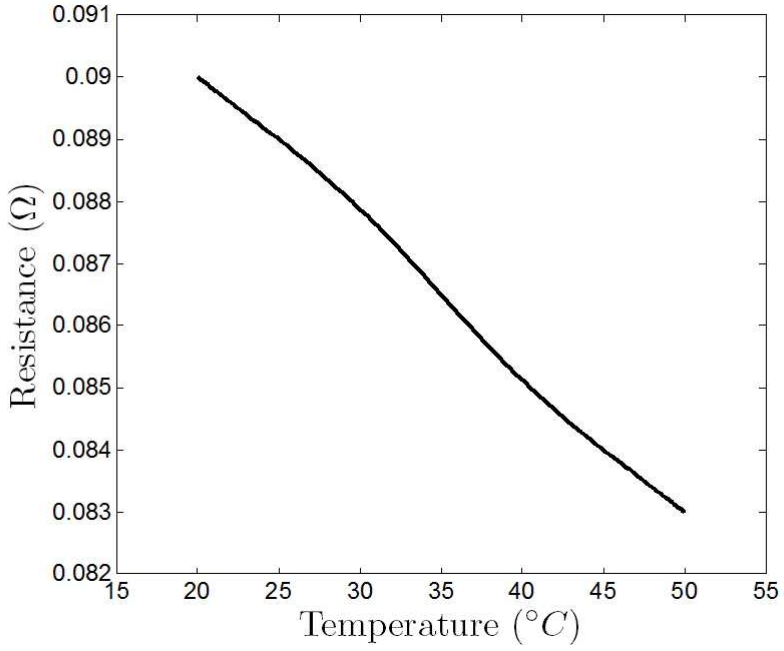

Figure 5.1: Effect of temperature on battery internal resistance

In fact, beside the internal resistance, both the charge transfer resistance and the diffusion resistance decrease simultaneously with temperature increase too, see Johnson et al. (2001).

5.1.2.2 Influence on battery capacity

Table 5.1: Percent battery capacity as a function of temperature

Temperature, °C	Percent of nominal battery capacity, %
−20	65
0	84
25	100
40	110
55	120

In addition to the dependence of battery resistances on temperature, battery capacity also varies with temperatures. Table 5.1 shows the variation of battery capacity as a function of temperature for a kind of GENESIS battery, see Jana (2000). As seen from the table, battery capacity rises at higher temperatures and falls at lower temperatures.

5.1.3 Influence of battery SOH on battery parameters

As defined previously, battery SOH, which can also be described as the age of a battery, represents the health state of a battery. In other words, SOH indicates how much the battery is corrupted.

5.1.3.1 Influence on resistance

During the ageing process, the charge transfer resistance and diffusion resistance of battery vary slightly, while the internal resistance increases significantly. And, it is said the resistance increases up to 160% of its initial value at the same condition (same temperature and same SOC) when the battery reaches the end of life, which means the maximum power of a battery decreases to 60% of its initial maximum power at the same condition (same temperature and same SOC), refer to Haifeng et al. (2009).

5.1.3.2 Influence on battery capacity

According to the definition of battery death with respect to battery capacity degradation, the capacity of a dead battery (with SOH of 0%) decreases to the 80% of its initial maximum capacity at the same condition (same temperature and same SOC), which means battery capacity decreases with decreasing SOH, see Picciano (2007).

5.1.4 Extended battery model for fault observation

In this part, the influences of temperature and SOH on battery parameters will be parametrized as additive variations from the nominal values specified in Table 3.1.

$$\tilde{R_0} = R_0 + \Delta R_{0,T} + \Delta R_{0,A} \tag{5.5}$$

$$\tilde{R_1} = R_1 + \Delta R_{1,T} \tag{5.6}$$

$$\tilde{R_2} = R_2 + \Delta R_{2,T} \tag{5.7}$$

$$\tilde{Cb} = Cb + \Delta Cb_T + \Delta Cb_A \tag{5.8}$$

where R_* denote nominal resistances, Cb denotes the nominal battery capacity, $\Delta R_{*,T}$ and ΔCb_T denote battery resistance and capacity variations, resulted from temperature changes, respectively, while $\Delta R_{*,A}$ and ΔCb_A denote that resulted from battery ageing, $\tilde{R_*}$ and $\tilde{Cb}$ denote updated battery resistances and capacity, including influence of temperature changes and battery ageing, respectively.

In this preliminary study, the temperature change ΔT is treated as a system disturbance d, while the battery ageing, which is defined as $1 - SOH$, is treated as the system fault f. Moreover, all the variations are modeled as:

$$\Delta R_{*,T} = k_1 d \tag{5.9}$$

$$\Delta R_{0,A} = k_2 f \tag{5.10}$$

$$\Delta Cb_T = k_3 d \tag{5.11}$$

$$\Delta Cb_A = k_4 f \tag{5.12}$$

Combining the influences of temperature and SOH with the nominal battery model presented in section 5.1.1, the following dynamic non-linear model can be obtained:

$$\begin{cases} \dot{x_i} = g_i(x_1, \cdots, x_i, I, d, f) \\ y = h(x_1, \cdots, x_i, I, d, f) \end{cases} \tag{5.13}$$

where $i = 1, 2, 3$, $x_1 = V_1$, $x_2 = V_2$, $x_3 = SOC$, and

$$\begin{cases} g_1 = -\frac{1}{C_1(R_1+k_1 d)} x_1 + \frac{1}{C_1} I \\ g_2 = -\frac{1}{C_2(R_2+k_1 d)} x_2 + \frac{1}{C_2} I \\ g_3 = -\frac{1}{Cb+k_3 d+k_4 f} I \\ h = k \cdot x_3 + b - x_1 - x_2 - (R_0 + k_1 d + k_2 f) I \end{cases} \tag{5.14}$$

where R_0, R_1, R_2, C_1, C_2, Cb, k and b are time-invariant with values given in Table 4.2, k_* are ratios between the variation of battery parameters and the change of temperature or battery ageing. Take k_1 for example, R_0 varies from 0.0105Ω for temperature of $25°C$ to 0.0075Ω for temperature of $50°C$, then:

$$k_1 = \frac{0.0075 - 0.0105}{50 - 25} \tag{5.15}$$

Using the tangent linearisation method, the following linear model, which is adopted for fault observer design presented in the coming section, can be obtained around the operation point specified by x_{op}, I_{op}, d_{op} and f_{op}

$$\begin{cases} \dot{\bar{x}} = A\bar{x} + B\bar{I} + E_x\bar{d} + F_x\bar{f} \\ \bar{y} = C\bar{x} + D\bar{I} + E_y\bar{d} + F_y\bar{f} \end{cases} \tag{5.16}$$

where $\bar{x} = x - x_{op}$, $\bar{I} = I - I_{op}$, $\bar{d} = d - d_{op}$, $\bar{f} = f - f_{op}$, $\bar{y} = y - y_{op}$, A, B, E_x, F_x, C, D, E_y and F_y are linearized system matrices with respect to the specified linear operation point.

5.2 Fault observer design

5.2.1 Problem statement

As the core and most expensive component of XEVs, knowledge on battery ageing is critical to system reliability and safety. So, some kind of observer that is adopted to follow the ageing process of a battery is of great importance.

In fact, the battery system is affected by various factors besides the battery ageing, such as current and temperature variations, which will induce deviation on estimation accuracy in terms of battery ageing. Therefore, robustness becomes the most important issue for battery fault (ageing) observation.

5.2.2 Problem formulation

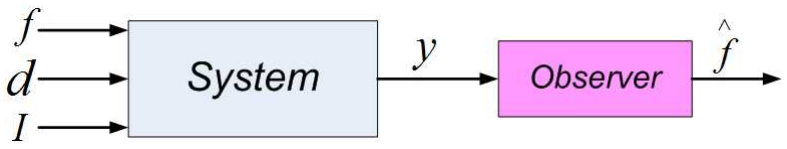

Figure 5.2: Observer scheme

Fig. 5.2 depicts the fault observer proposed in this work, where the system is described by (5.16), d is the disturbance, f is the battery fault (ageing), and $\widehat{f}$ is the fault estimation.

5.2.2.1 Problem definition

$$\begin{cases} \dot{x}_0 = A_0 x_0 + B_0 y \\ \widehat{f} = C_0 x_0 + D_0 y \end{cases} \tag{5.17}$$

An observer of the form like (5.17), where $x_0 \in \mathbb{R}^{n_0}$, is said to be an H_∞ robust observer-based fault estimator for system (5.16) if:

- $\widehat{f} \longrightarrow f$ when $I = 0$ and $d = 0$.
- $\left\| \dfrac{\widehat{f} - f}{f} \right\|_\infty < \gamma$ for some non zero I and d, and fixed attenuation level $\gamma > 0$.

Remark: of course we will look for the minimal γ.

5.2.2.2 Problem description with standard H_∞ form

The fault observation problem stated above is considered here in the following standard H_∞ problem as depicted in Fig. 5.3, where w is the vector of external inputs, z denotes the vector of output signals to be minimized/penalized, y is the vector of measurements available to the observer O and $\widehat{f}$ is the fault observation. P is called the generalized plant or interconnected system where all weights that specify the performance requirements are included.

Then, the objective is to find a stabilizing observer O which minimizes the H_∞ norm of the transfer function from w to z.

Since $z = F_l(P, O)w$, where $F_l(P, O)$ is the lower Linear Fractional Transformation of P and O, the design objective becomes:

$$min \left\| F_l(P, O) \right\|_\infty \tag{5.18}$$

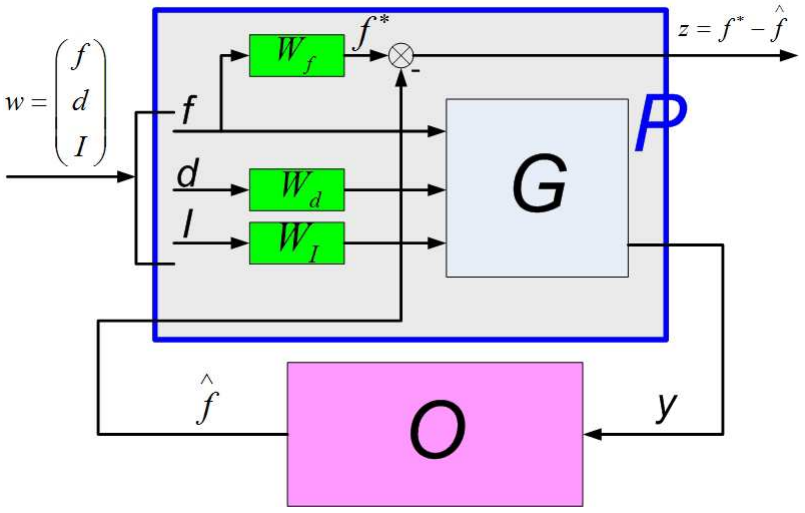

Figure 5.3: Observer scheme on standard H_∞ form

and is referred to as the H_∞ optimization problem.

5.2.3 Observer synthesis

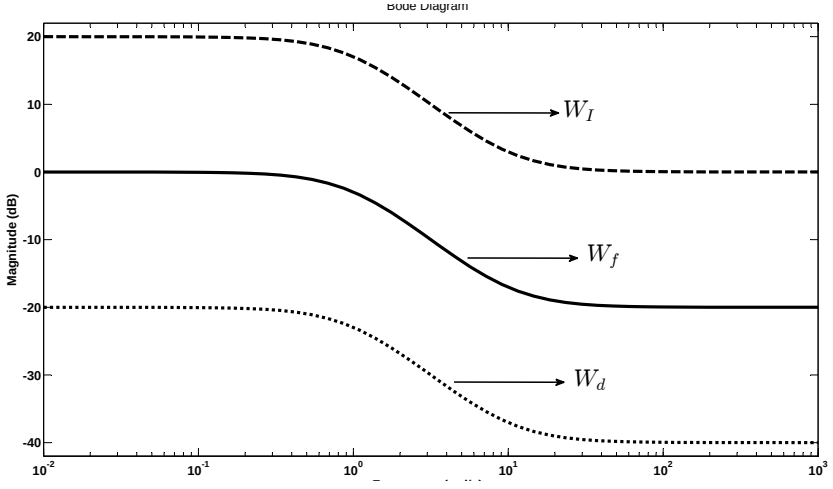

Figure 5.4: Weighting functions for fault estimation

The related weights given in Fig. 5.3 have been chosen as:

$$\begin{cases} W_f = \dfrac{0.1s+1}{s+1} \\ W_d = \dfrac{0.01s+0.1}{s+1} \\ W_i = \dfrac{s+10}{s+1} \end{cases} \tag{5.19}$$

As seen from Fig. 5.4, the weighting functions give the attenuation levels that the

fault observer should meet with respect to different system inputs within specified frequency range.

Then, based on the system description of G by (5.16), where

$$A = \begin{bmatrix} -0.036 & 0 & 0 \\ 0 & -0.0019 & 0 \\ 0 & 0 & 0 \end{bmatrix}, B = \begin{bmatrix} 0.0004 \\ 0 \\ -0.4348 \end{bmatrix}, E_x = \begin{bmatrix} 0 \\ 0 \\ 0.0174 \end{bmatrix}, F_x = \begin{bmatrix} 0 \\ 0 \\ -0.8696 \end{bmatrix},$$

$$C = \begin{bmatrix} -1 & -1 & 0.3333 \\ 0 & 0 & 1 \\ 0 & 0 & 0 \\ 0 & 0 & 0 \end{bmatrix}, D = \begin{bmatrix} -0.0087 \\ 0 \\ 1 \\ 0 \end{bmatrix}, E_y = \begin{bmatrix} 0.0012 \\ 0 \\ 0 \\ 1 \end{bmatrix}, F_y = \begin{bmatrix} 0 \\ 0 \\ 0 \\ 0 \end{bmatrix},$$ and the weights specified above, the H_∞ optimization problem (5.18) is solved using the LMI approach. The achieved fault observer owns the attenuation level of γ=0.000185.

5.3 Simulation and discussion

5.3.1 Sensitivity functions for observer

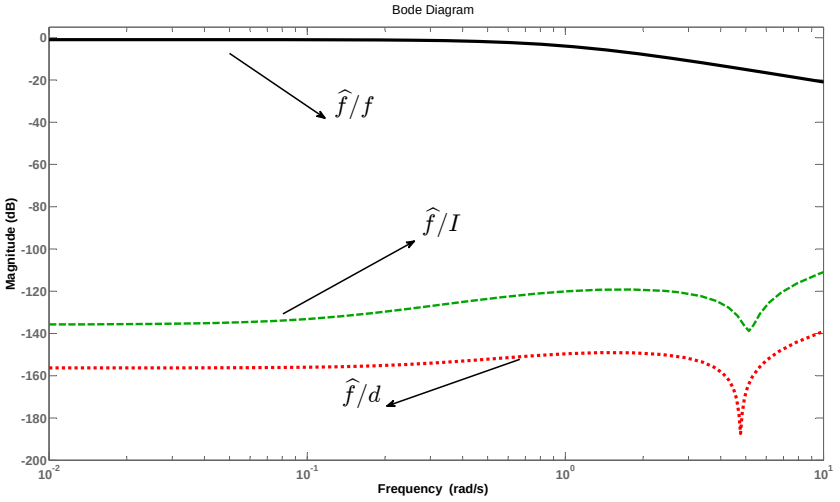

Figure 5.5: Sensitivity functions of fault estimation

The sensitivity functions are shown in Fig. 5.5, where the solid line presents the transfer between the estimated fault $\widehat{f}$ and the the real f, the dashed line presents the transfer between the estimated fault $\widehat{f}$ and the input current I, the dotted line presents the transfer between the estimated fault $\widehat{f}$ and the disturbance d.

It can be clearly seen from Fig. 5.5 that attenuation of the system input is greater than $100dB$, attenuation of the disturbance is greater than $140dB$. Meanwhile, the fault

estimation is correctly obtained within low frequency range (range from $0.01 rad/s$ to $1 rad/s$) where the real battery fault belongs to.

5.3.2 Time domain results

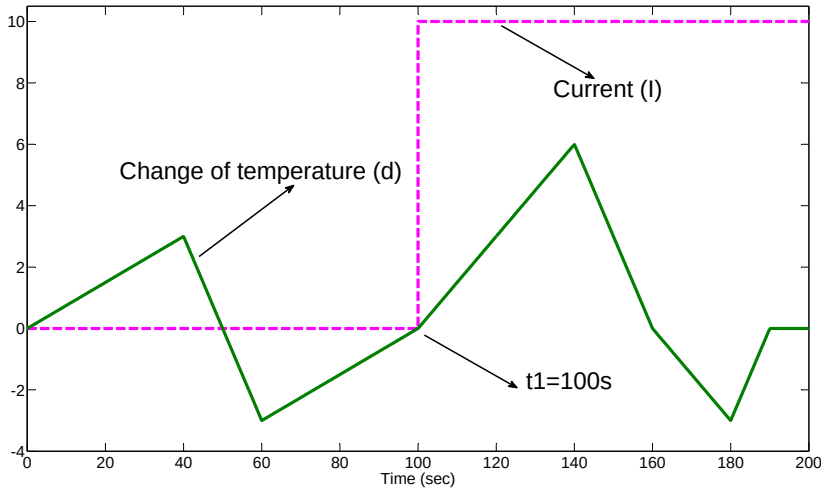

Figure 5.6: Evolution of the current and temperature

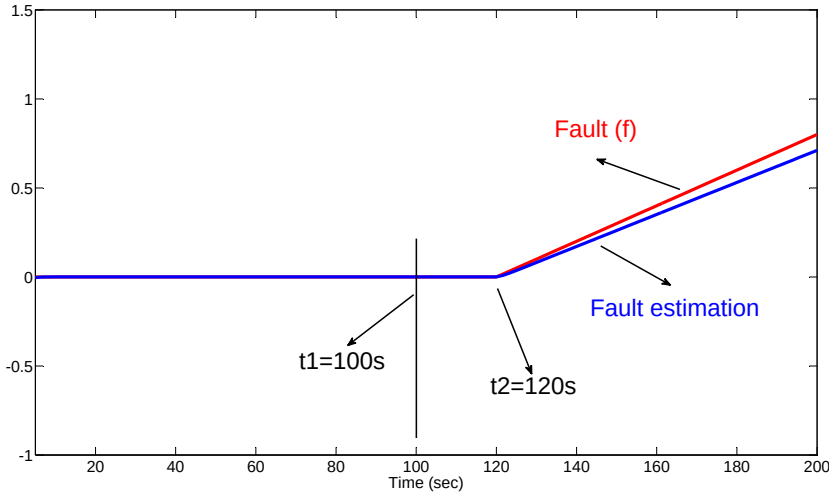

Figure 5.7: Fault estimation with respect to slow battery ageing (case 1)

Based on the system specified in section 5.2.3, time domain simulations are performed to check the tracking performance of the achieved fault observer with respect to the actual battery fault (battery ageing) of different type.

The scenario, as depicted in Fig. 5.6, is specified for the test, where the dashed line presents the variation of the input current I that steps at time t1=100s and remains at

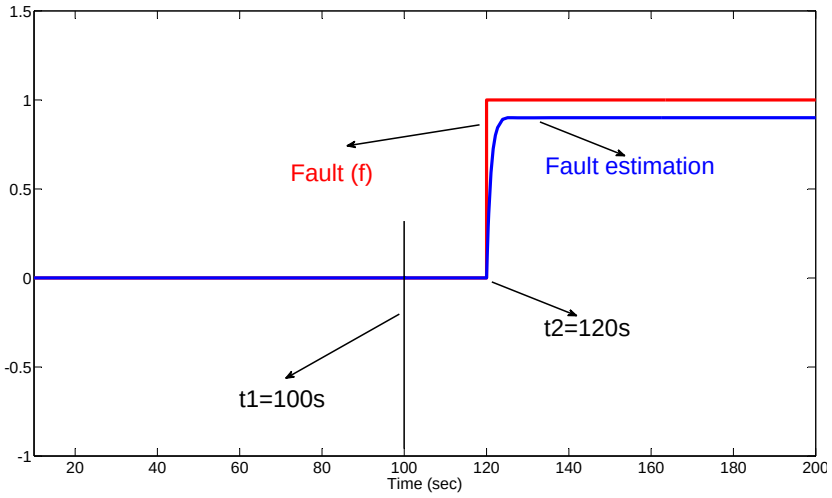

Figure 5.8: Fault estimation with respect to abrupt battery fault (case 2)

a constant value $10A$ all along, the solid line presents the evolution of the temperature during the test, which is treated as the disturbance d.

Then, two case studies are implemented

- **Case 1: estimation for slow battery ageing**

  The read line in Fig. 5.7 defines a process of the battery ageing that arises at time t2=120s and evolves slowly over time. The blue line presents the related estimation with respect to specified battery fault by the read line.

  It can be seen that the fault observer can not only detect the happen of the battery fault (at t2 moment) immediately, but also follows the trend of the fault evolution (time range from t2 to 200s) in spite of other influences such as the input current I described by the dashed line in Fig. 5.6 and the temperature variation described by the solid line in Fig. 5.6.

- **Case 2: estimation for abrupt battery ageing**

  The read line in Fig. 5.8 defines a sudden battery fault that happens at time t2=120s. The blue line presents the related estimation with respect to the abrupt battery ageing process.

  As seen, the achieved observer can not only track the slow but also the abrupt battery ageing process.

Since the battery ageing f and the battery SOH are connected by SOH=1-f, the method proposed here can be used to evaluate the battery health. For example, it can

be concluded form Fig. 5.8 that the battery is dead (SOH=0), then the SOH information can be used to adopt the energy control law in the Hybrid Electric Vehicle (HEV).

5.3.3 Robustness Analysis

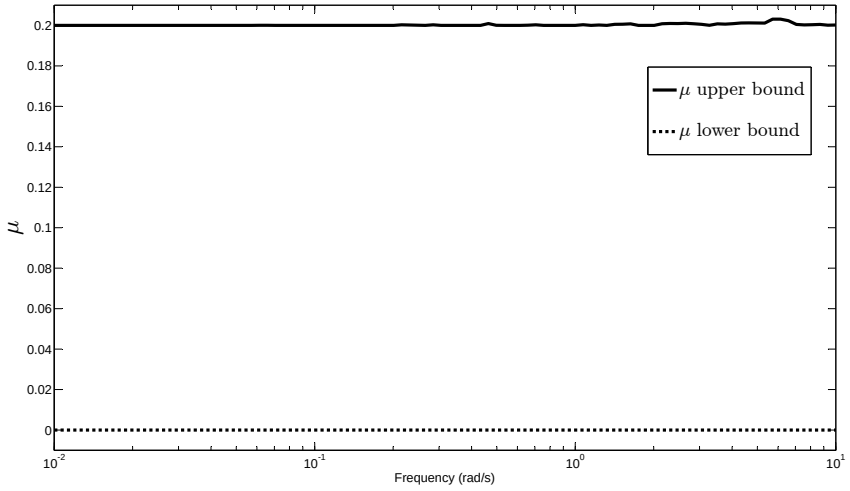

Figure 5.9: μ plot for robust stability analysis

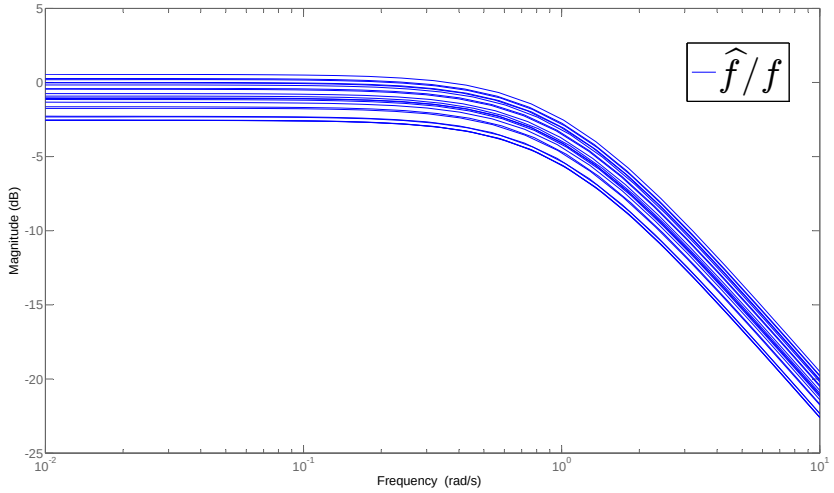

Figure 5.10: $\widehat{f}/f$ for perturbed battery

The μ analysis method, see Skogestad & Postlethwaite (2007), is used to conclude on the robustness properties of the proposed controller. Fig. 5.9 shows the lower and upper bounds of the structured singular value μ when the considered uncertainties are 120% of the nominal battery parameters of $R_0 = 0.00876$, $R_1 = 0.0124$, $R_2 = 0.0123$, $C_1 = 2239$,

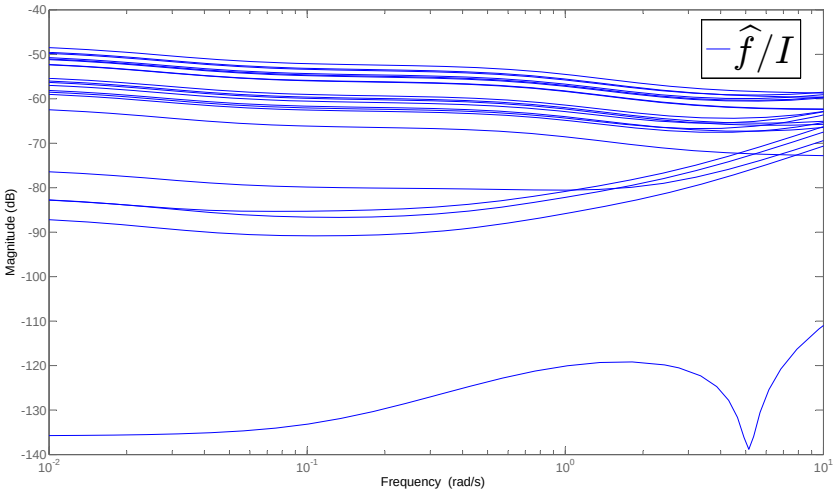

Figure 5.11: $\widehat{f}/I$ for perturbed battery

$C_2 = 41831$. As seen, the upper bound is always less than 1 for all frequencies which ensures the robust stability of the closed-loop system.

Also, Fig. 5.10, Fig. 5.11 and Fig. 5.12 show sensitivity functions $\widehat{f}/f$, $\widehat{f}/I$ and $\widehat{f}/f$ with respect to perturbed battery parameters within the same range as defined for Fig. 5.9, respectively, which verify robustness of the proposed algorithm.

5.4 Concluding remarks

Reliability of the battery for XEVs applications has been a concern for long time, since batteries tend to age under severe utility situation such as lower thermal stability, high current apply, frequent change of current direction etc. Therefore, it is important to estimate the battery ageing level aiming at prolonging the battery age and maintain the system safety as long as possible.

In this chapter, the extended battery model taking into account the influences of temperature and battery ageing on model parameters is presented. An H_∞ observer-based fault estimation method is proposed, that also to estimate continuously ageing effect while minimizing the disturbance effects such as the temperature. The battery fault estimator proposed here then can be combined with the conventional control scheme of an HEV, which ensures the energy control strategy adapting to the battery ageing evolution.

Since the fault observer achieved here is based on the linearisation of the system description, the estimation performance is limited with respect to the real non-linear

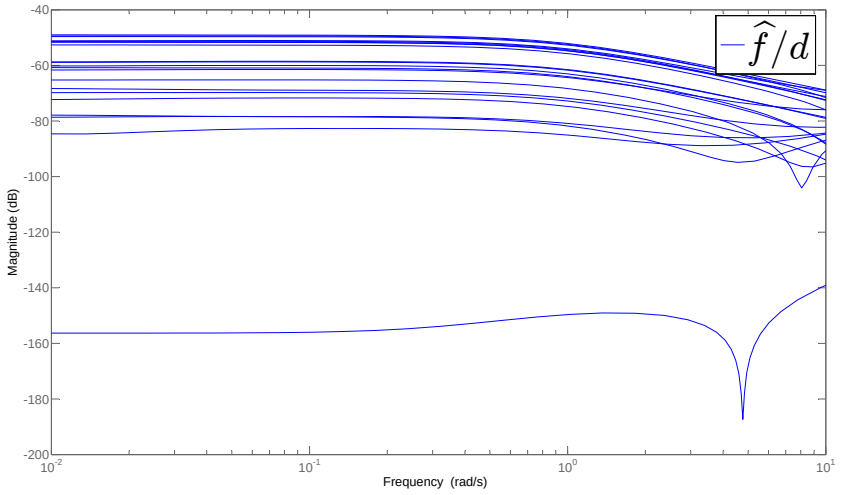

Figure 5.12: $\widehat{f}/d$ for perturbed battery

system as described by 5.14. So, it will be interested to do future works aiming at designing a Linear Parameter Varying (LPV) observer that is more suitable for the real battery systems.

Part II

POWERTRAIN MODELING AND ENERGY MANAGEMENT STRATEGY DESIGN

The second part of this dissertation is focused on Hybrid Electric Vehicles (HEVs): in particular, the powertrain modeling and Energy Management Strategy (EMS) developments of the HEV based on the H_∞ and Linear Parameter Varying (LPV) approaches.

Chapter 6 is exclusively concerned by the mathematical descriptions of the main components of a specific Parallel Hybrid Electric Vehicle (PHEV). Chapter 7 mainly contributes to a preliminary study on the influence of battery ageing on the control strategy in a PHEV, where the robust H_∞ approach is used for the EMS development. The objective of such a EMS is to determine the power split ratio between the engine and the battery that maintains the battery state within a reasonable range to prolong the battery life. In chapter 8, the LPV/H_∞ approach is adopted for the EMS developments and improvement.

The main contributions of this part include:

1. Not only vehicle dynamics but also battery behaviors are taken into account for EMS developments in chapter 7 and chapter 8.

2. Systems considered in chapter 8 are modeled as LPV ones of LFT form, accounting for variant velocity and battery capacity.

3. A gain-scheduled EMS controller is proposed in section 8.1 aiming at minimizing the fuel consumption and prolonging the battery life in the presence of battery capacity degradation (battery ageing). While, a LPV regulator is achieved in section 8.2 for a parallel hybrid electric vehicle, which determine the regulating quantity of battery current and the power split ratio with respect to the ones by the already existed EMS, according to the driving cycle variation and battery capacity degradation.

Meanwhile, the main method and results of this part have been published in:

- *H_∞ based supervisory control strategy for a parallel HEV with battery fault accommodation* (T.-H. Wang, O. Sename and J.J. Martinez-Molina), in 8th International Federation of Automatic Control (IFAC) Symposium SAFEPROCESS-2012: Fault Detection, Supervision and Safety for Technical Processes.

- *A LPV EMS regulator for the parallel HEV with battery life prolongation* (Tinghong Wang, Olivier Sename and John-jairo Martinez-molina), in 21st Mediterranean Conference on Control and Automation (MED'13).

- *A LPV/H_∞ approach for fuel consumption minimization of the PHEV with battery life prolongation* (T.-H. Wang, O. Sename and J.J. Martinez-Molina), in 7th IFAC International Symposium on Advances in Automotive Control (IFAC-AAC 2013)

Chapter 6

Hybrid Electric Vehicle Model

The aim of this chapter is not to provide an accurate model for simulation of Hybrid Electric Vehicle (HEV) behavior but to some classical control-oriented models that will allow us to develop our proposed energy management strategies, coordinated with the battery state of health. In terms of system modeling, four main components of the HEV are modeled: the engine, the electric motor, the driveline and the battery. For engine and motor, the Willans method proposed by Rizzoni et al. (1999) and Guzzella & Sciarretta (2007) is adopted to consider the corresponding energy conversion efficiencies. The achieved driveline model captures the inertial dynamics and the torque-speed relations of related powertrain components, as well as is capable of representing the longitudinal motion and the road load of the HEV. In addition, the battery dynamics are incorporated into the system description aiming at taking into account the battery age item into EMS developments. In this chapter, some basic introduction on the classification of HEV models is given first, whose characteristics are specified for each kind of models. Then, mathematical representations of the main components with respect to a Parallel Hybrid Electric Vehicle (PHEV) are given based on the specific powertrain architecture.

6.1 Introduction

Compared with conventional vehicles, there exist additional components for Hybrid Electric Vehicles (HEVs), such as electric motors and batteries. Moreover, conventional Internal Combustion Engine (ICE) and mechanical subsystems, such as the gear box and the final differential, still present. The development and analysis of the Energy Management Strategy (EMS) of an HEV rely on the mathematical models of the vehicle that capture the behavior of these components and take into account the dynamic interactions among these components.

Mathematical models are constitutionally inaccurate representations of real systems, and the level of accuracy depends on the model complexity. Usually, sophisticated HEV models require extensive computational resources and are time consuming to simulate. Therefore, a typical HEV model is often focused on the system dynamics that have significant impacts on the behaviors of the interest variables. According to the level of model complexities and accuracies, an HEV model may be static, quasi-static or dynamic, see Koprubasi (2008), Gao et al. (2007) and Serrao (2009).

The main objectives of static and quasi-static models are to evaluate the fuel economy and exhaust emissions of HEVs with respect to specific driving cycles. For example, Wipke et al. (1999) presents a static model using the simulation environment ADVISOR (ADvanced VehIcle SimulatOR), and a quasi-static model is achieved in Rousseau et al. (2006) using the Powertrain System Analysis Toolkit (PSAT) tool.

The main advantage of static or quasi-static models is the computation efficiency, while their disadvantage is the inaccuracy for dynamic simulation. On the contrary, dynamic models provide further insight into driveline and vehicle dynamics that have impact on the performance of a vehicle, which is useful for the development an effective EMS. For example, models by Syed et al. (2006) and Powell et al. (1998) are well suitable for studies of both the mechanical dynamic and the electrical dynamic sub-systems of an HEV.

Mixed models are used to combine the quasi-static and dynamic component models. Such a kind of model generally aim at dealing with specific purposes, e.g., to corporate dynamic models of driveline components (such as the transmission and the tires) in addition to a number of quasi-static models that characterize the behavior of the components upstream from the transmission (such as the engine and the electric motor), see Koprubasi (2008) and Amrhein & Krein (2005). A mixed model can be found in Waltermann (1996), where a simplified longitudinal drivetrain model of a series HEV is combined with detailed lateral dynamics and adopted for the development of a vehicle stability controller.

The PHEV model considered in this work is a mixed one: (1) the quasi-static Willans line models are used to describe the engine and the electric motor, representing the input-output power relationships with different efficiencies and power losses that depend on the operating speeds and torques; (2) constant efficiencies and gear ratios are assigned for the gear box and the final differential to describe the input-output torque-speed relations; (3) the battery is described using the dynamic equations achieved in chapter 3; (4) the rotational speed of the vehicle is dynamically calculated based on the tractive force generated by the powertrain and the road load by the vehicle.

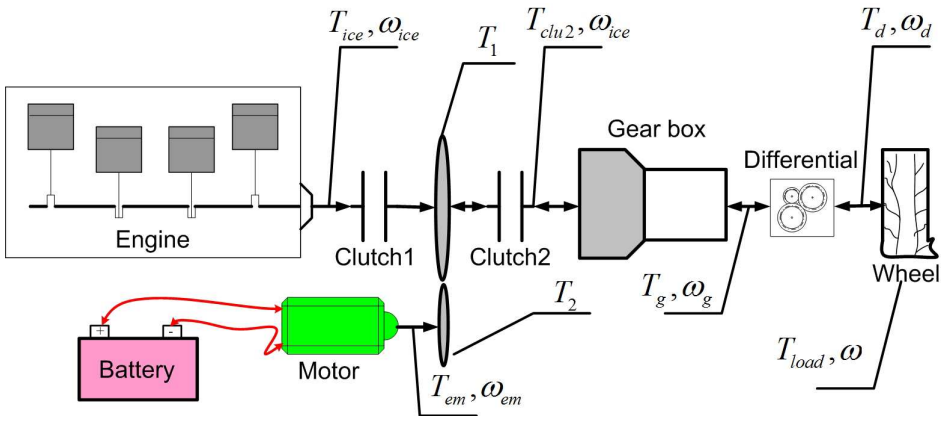

Figure 6.1: Topology of the PHEV under consideration

6.2 Vehicle topology and system modeling

6.2.1 Vehicle topology and fundamental assumptions

Architecture of the PHEV considered in this dissertation is depicted by Fig. 6.1. As seen, the HEV owns the driveline of a pre-transmission type consisting of the engine, the battery, the electric motor and the transmission components such as the clutches, the gearbox and the final differential. In Fig. 6.1, T_* are torques, ω_* are rotational speeds, *ice* denotes the engine, *em* the electric motor, *g* the gear box, *d* the final differential, and *load* the road load.

Regarding the vehicle model, the following fundamental assumptions are made:

- only longitudinal vehicle dynamics are taken into account, and all indirect coupling effects due to vertical and lateral motions are neglected.
- power losses of the driveline are represented by lumped efficiencies applied to relative components.
- only remarkable inertia, such as inertia of the engine, the motor, the clutches and the tires, are taken into account; inertia of the smaller components (e.g. the axles) that have less effect on the dynamics of the system are ignored for simplicity.
- the damping and spring effects to the transmission components are also omitted.

6.2.2 System model and parameters

Based on the vehicle topology and model assumptions presented above, the mathematical descriptions of the engine, electric motor, battery, driveline and vehicle dynamic are given separately in this part.

6.2.2.1 Driveline model

As depicted in Fig. 6.1, the engine torque is applied to a clutch, and combined with the torque from the electric motor via a gear coupling that is used to coordinate the rotational speeds of the engine and the motor, as well as amplify the motor torque. Then the combined torque is applied to another clutch and transmitted to the tires through the rigidly connected gear box and final differential.

As stated already, constant efficiencies and gear ratios are assigned for the gear box and the final differential. Then, the flowing torque-speed relations taking into account simple descriptions of the torque losses with fixed ratios can be achieved based on the input-output connections between the driveline components referred to in Fig. 6.1

$$\omega_d = \omega \tag{6.1}$$

$$\omega_g = \lambda_d \omega_d \tag{6.2}$$

$$\omega_{em} = \lambda_b \omega_{ice} \tag{6.3}$$

$$\omega_{ice} = \lambda_g \omega_g \tag{6.4}$$

$$T_d = \lambda_d T_g \eta_d \tag{6.5}$$

$$T_g = \lambda_g T_{clu2} \eta_g \tag{6.6}$$

Also, the following equations explaining the inertia dynamics of the driveline hold

$$J_{c1}\dot{\omega}_{ice} = T_{ice} - T_1 \tag{6.7}$$

$$J_2\dot{\omega}_{em} = T_{em} - T_2 \tag{6.8}$$

$$J_{c2}\dot{\omega}_{ice} = T_1 + \lambda_b T_2 - T_{clu2} \tag{6.9}$$

$$J_3\dot{\omega} = T_d - T_{load} \tag{6.10}$$

where J_{c1} is the lumped inertia of the engine and the clutch 1, J_{c2} is the inertia of the clutch 2, λ_b is the gear ratio of the dynamic coupling between the engine and the motor, T_{clu2} is the torque at the output shaft of clutch 2, J_2 is the inertia of the motor, J_3 is the lumped inertia of the wheels, ω is the rotational speed of the wheel.

Based on the equations and the torque-speed relations presented above, we can get:

$$\dot{\omega} = A_1 T_{ice} + A_2 T_{em} + A_3 T_{load} \tag{6.11}$$

with $A_1 = \frac{b}{c}$, $A_2 = \frac{\lambda_b b}{c}$, $A_3 = -\frac{1}{c}$, $a = J_1 \lambda_g \lambda_d + J_2 \lambda_b^2 \lambda_g \lambda_d$, $b = \lambda_g \lambda_d \eta_g \eta_d$, $c = ab + J_3$, $J_1 = J_{c1} + J_{c2}$, where J_1 is the lumped inertia of the engine and two clutches. All related coefficients of the driveline are specified in Table 6.1.

Table 6.1: Coefficients of the driveline

Coefficients of the driveline	
λ_d [-]	1
λ_g [-]	4
λ_b [-]	2
η_d [-]	0.98
η_g [-]	0.96
J_1 $[Kg * m^2]$	0.2
J_2 $[Kg * m^2]$	0.1
J_3 $[Kg * m^2]$	222

Note that the parameters presented in Table 6.1 are not from a real vehicle but are inferred (not be directly taken) from the related parameter values in Guzzella & Amstutz (2005), which guarantees acceptable rationality.

6.2.2.2 Engine model

For engine modeling, the Willans method proposed by Rizzoni et al. (1999) and Guzzella & Sciarretta (2007) is adopted due to its outstanding features:

- independence on the availability of specific efficiency maps of the engine.
- owning the property of scalability which gives permission of representing objects (i.e. engines) that belong to the same class using an unique basic model such that the actual models are independent of scales and can be, for example, sized simply by defining a scalar "displacement" or "power rating" parameter.

In the Willans engine model, the energy conversion efficiency is defined as the ratio between the output and input powers, and the output power P_{ice} of the engine can be expressed by

$$P_{ice} = \eta_c P_{chem} - P_{loss} \tag{6.12}$$

where η_c is the intrinsic energy conversion efficiency of the engine, P_{chem} is the input power (chemical power available in the fuel), P_{loss} is power losses due to air pumping, mechanical friction, etc. of the engine.

Accordingly, for each time instant, the following equation hold

$$P_{chem} = \frac{D_1\omega}{D_2 + D_3\omega + D_4\omega^2} T_{ice} + \frac{E_1\omega + E_2\omega^2}{D_2 + D_3\omega + D_4\omega^2} \tag{6.13}$$

with $D_1 = \lambda_g\lambda_d$, $D_2 = e_{ice,0}$, $D_3 = e_{ice,1}\frac{S}{\pi}\lambda_d\lambda_g$, $D_4 = e_{ice,2}(\frac{S}{\pi})^2\lambda_d\lambda_g$, $E_1 = \frac{V_d}{4\pi}\lambda_g\lambda_d k_1\Pi_{e,max}\sqrt{\frac{k_4}{B}}k_2$, $E_2 = \frac{V_d}{4\pi}(\lambda_g\lambda_d)^3 k_1\Pi_{e,max}\sqrt{\frac{k_4}{B}}k_3S^2$.

T_{ice} is the engine torque, ω is the rotational speed of the wheel, λ_* are gear ratios as defined in section 6.2.2.1, $e_{ice,*}$ and k_* are coefficients from experiences, S is the engine stroke, V_d is the engine displacement, B is engine's bore diameter, $\Pi_{e,max}$ is the maximum boost ratio of the engine (different with the compression ratio). All related engine parameters are included in Table 6.2.

The values of $e_{ice,0}$, $e_{ice,1}$, $e_{ice,2}$, k_1, k_2, k_3, k_4, which can be referred to as Willans engine parameters, are obtained using the parameter identification approach in Guzzella & Sciarretta (2007), while other engine parameters are from Guzzella & Amstutz (2005).

For interested readers, more details on the Willans engine model can be found in Pisu & Rizzoni (2004), Rajagopalan et al. (2003), Wei (2004), Guzzella & Sciarretta (2007) and Guzzella & Amstutz (2005).

6.2.2.3 Motor model

The electric motor is modeled using the Willans approach similar to the one used for the engine. Let P_{batt} be the available power from the battery. Then, for each time instant, the following equations hold, refer to Pisu & Rizzoni (2004):

$$P_{batt} = B_1(\omega_{em})P_{em} + B_0(\omega_{em}) \tag{6.14}$$

Table 6.2: Engine parameters

Engine parameters	
S [m]	50×10^{-3}
V_d [m^3]	0.708×10^{-3}
B [m]	45×10^{-3}
$\Pi_{e,max}$ [-]	2
$e_{ice,0}$ [-]	0.3713
$e_{ice,1}$ [-]	0.022
$e_{ice,2}$ [-]	-0.0025
k_1 [-]	1.44×10^5
k_2 [-]	0.46
k_3 [-]	9.1×10^{-4}
k_4 [-]	0.075

$$B_1(\omega_{em}) = \left[\sum_{i=0}^{4} e_{em,i}(r\omega_{em})^i\right]^{-1} \tag{6.15}$$

$$B_0(\omega_{em}) = 2V_r B_1(\omega_{em}) \left[\sum_{j=0}^{4} p_{em,loss_j}(r\omega_{em})^{j+1}\right] \tag{6.16}$$

where ω_{em} is the rotational speed of the motor, P_{em} denotes the output power of the motor, $e_{em,*}$ and $p_{em,loss_*}$ are coefficients from experiences, r is the rotor radius and V_r is the rotor volume.

Table 6.3: Motor parameters

Motor parameters	
r [m]	90×10^{-3}
V_r [L]	4.6×10^{-3}
$e_{em,0}$ [-]	1.1633
$e_{em,1}$ [-]	-0.0692
$e_{em,2}$ [-]	0.004
$e_{em,3}$ [-]	-8.6536×10^{-5}
$e_{em,4}$ [-]	6.3656×10^{-7}
$p_{em,mloss0}$ [-]	4.1815×10^3
$p_{em,mloss1}$ [-]	2.9684×10^3
$p_{em,mloss2}$ [-]	-197.196
$p_{em,mloss3}$ [-]	4.2974
$p_{em,mloss4}$ [-]	-0.031

And, the following equation, which is used to model the motor, can be obtained by substituting (6.1), (6.2), (6.3), (6.4) and $P_{en} = \omega_{em} T_{em}$ into the achieved equations above

$$P_{batt} = \frac{F_0 \omega}{F} T_{em} + \frac{G}{F} \tag{6.17}$$

with $F = F_1 + F_2\omega + F_3\omega^2 + F_4\omega^3 + F_5\omega^4$, $G = G_1\omega + G_2\omega^2 + G_3\omega^3 + G_4\omega^4 + G_5\omega^5$, $F_0 = \lambda_g \lambda_d \lambda_b$, $F_1 = e_{em,0}$, $F_2 = e_{em,1} r F_0$, $F_3 = e_{em,2} r^2 F_0^2$, $F_4 = e_{em,3} r^3 F_0^3$, $F_5 = e_{em,4} r^4 F_0^4$, $G_1 = 2V_r p_{em,loss_0} r F_0$, $G_2 = 2V_r p_{em,loss_1} r^2 F_0^2$, $G_3 = 2V_r p_{em,loss_2} r^3 F_0^3$, $G_4 = 2V_r p_{em,loss_3} r^4 F_0^4$, $G_5 = 2V_r p_{em,loss_4} r^5 F_0^5$.

P_{batt} denotes the electric power from the battery, T_{em} is the motor torque and λ_* are gear ratios. The related motor parameters can be found in Table 6.3, and all Willans motor parameters, $e_{em,*}$ and $p_{em,*}$, presented in Table 6.3 are obtained using the similar method as used for the engine.

6.2.2.4 Battery model

For battery model, equations achieved previously are directly used. More information on battery dynamics is available in section 3.2.

$$\dot{V}_1 = -\frac{1}{C_1 R_1} V_1 + \frac{1}{C_1} I \tag{6.18}$$

$$\dot{V}_2 = -\frac{1}{C_2 R_2} V_2 + \frac{1}{C_2} I \tag{6.19}$$

$$\dot{SOC} = -\frac{1}{Ah_{nom}} I \tag{6.20}$$

$$V = k \cdot SOC + b - V_1 - V_2 - R_0 I \tag{6.21}$$

6.2.2.5 Vehicle dynamic

The vehicle dynamic model represents the longitudinal motion as well as the road load of the vehicle. In such a model, all weight of the vehicle is supposed to be concentrated on the center of gravity. In the direction of motion, the vehicle experiences the following forces, see Guzzella & Sciarretta (2007) and Choi (2008)

- **the aerodynamic friction** caused by the viscous friction of the surrounding air on the vehicle surface, and the pressure difference between the front and the rear of the vehicle.

- **the rolling friction** mainly depending on the rolling friction coefficient, tire pressure and road surface condition.
- **the uphill driving force** induced by gravity when driving on a non-horizontal road.
- **the inertial force** resulted from all rotating parts inside the vehicle.

Since the inertial force of the driveline components has been taken into account separately from (6.7) to (6.10), the road load T_{load} of the vehicle can be approximated by:

$$T_{load} = A_4\omega^2 + A_5 cos(\theta) + A_6 sin(\theta) + A_7\dot{\omega} \tag{6.22}$$

with the first term accounting for the aerodynamic friction, the second term accounting for the rolling friction, the third term accounting for the uphill driving force, the last term accounting for the vehicle acceleration, and

$$A_4 = \frac{1}{2}\rho_{air} C_d A_f r_w^3 \tag{6.23}$$

$$A_5 = mgf_r r_w \tag{6.24}$$

$$A_6 = mgr_w \tag{6.25}$$

$$A_7 = mr_w^2 \tag{6.26}$$

where ρ_{air} denotes the air density, C_d denotes the drag coefficient, A_f denotes the vehicle frontal area, r_w denotes the radius of the wheel, m denotes the vehicle mass, g denotes the gravitational acceleration, f_r denotes the rolling resistance coefficient, θ denotes the slope of the road. All related parameters of the vehicle are specified in Table 6.4, refer to Guzzella & Amstutz (2005).

6.3 Concluding remarks

In this chapter, some basic introduction on the classification of HEV models is given first. Then, mathematical representations of the main components of a PHEV are given based on a specific powertrain architecture. The system model is then available by combining

Table 6.4: Vehicle parameters

Vehicle parameters	
ρ_{air} $[Kg/m^3]$	1.2258
C_d [-]	0.22
A_f $[m^2]$	1.8
r_w [m]	0.3
m [Kg]	950
g $[Kg * m^2]$	0.98
f_r [-]	0.008
θ [rad]	not fixed

required component description, and is used in later chapters for the developments of energy management strategies in HEVs.

However, the model parameters presented in this chapter is not from the real experiments of a specific vehicle. So, intensive tests with a real HEV will be of interest for model validation and identification in future works.

Meanwhile, the development of a more complex HEV model, which contains more dynamic descriptions with respect to the gear box, can lead to more accurate system description, as well as optimal energy control strategy accounting for gear box control.

Chapter 7

H_∞ Based Energy Management Strategy Design

Regardless of the topology, the key point of an Hybrid Electric Vehicle (HEV) is to design a proper Energy Management Strategy (EMS). The EMS should provide an optimal use of the components in order to achieve the fuel consumption and performance criteria. As the most expensive part of an HEV, battery's states should be surely taken into account during the EMS developments. The aim of this chapter is to present some preliminary results on the influence of battery fault on the control strategy in a Parallel Hybrid Electric Vehicle (PHEV) (in particular on the power split between chemical and electrical energies). Here, the battery fault is usually due to battery ageing, and is formulated by considering it as some extent of voltage drop with respect to the normal battery voltage.

Section 7.1 is focused on an overview of the EMS, where the motivation of EMS developments, as well as a general structure of the EMS controller referring to all necessary input signals and control outputs is presented first. Then an introduction and classification of several energy management strategies proposed in literature is given.

Section 7.2 presents the H_∞ energy management approach for a PHEV of specific structure. The main objective of such a EMS is to determine the power split ratio between the engine and the battery, which maintains the State of Energy (SOE) of the battery within a reasonable range to prevent the battery from undesirable breakdown. The system description is given first inheriting the achieved powertrain model in chapter 6. Then the controller is derived based on the specified control system structure, and some simulation results are given.

7.1 Energy management strategy overview

7.1.1 Problem description on energy management strategies

The main benefit of a hybrid electric architecture is the presence of additional energy sources (usually the power battery and its associated electric motor(s)) besides the fuel tank, that can be used to reduce the fuel consumption and/or the vehicle emissions, while sustaining the required performances of the vehicle. Then, for each time instant, the required power by the vehicle can be provided by either one or a combination of these sources.

The key point to use the full potential of the hybridization is to design a proper control strategy, which manages how to split the demanded power between energy sources in the most efficient and optimum way. And, the energy management strategy is adopted to play such a role in hybrid electric vehicles.

The EMS is also called supervisory controller, in contrast to low-level or component-level controllers, that is used to manage associated components so that they behave as dictated by the supervisory controller. In a conventional vehicle, there is no need for a supervisory controller, since engine is the sole power source. The desired power by the driver is directly translated into action of the engine controller (low-level controller) that determines the operation of the engine. In an hybrid electric vehicle, the required power is firstly transmitted to energy management controller (supervisory controller), which decides the power share between the engine and the electric motor, and sends the power requirement signals to engine controller and motor controller. Then the engine and the motor will operate according to the indication by their related component-level controller. As mentioned previously, decisions of the EMS should also tend to minimize the fuel consumption, the pollutant emissions, as well as maintain the vehicle performance, or ensure a compromise among all these goals, see Serrao (2009).

The hierarchical control structure of an hybrid electric vehicle can be represented as in Fig. 7.1. As seen, the EMS indicates the required torque (power) of the engine T_{ice} and the electric motor T_{em} accounting for the required torque T_{req} by the driver, the vehicle speed v and the battery state (usually the State of Energy (SOE) or state of charge). Then, signals on power share are send to the engine controller and motor controller contained in the powertrain (not shown explicitly).

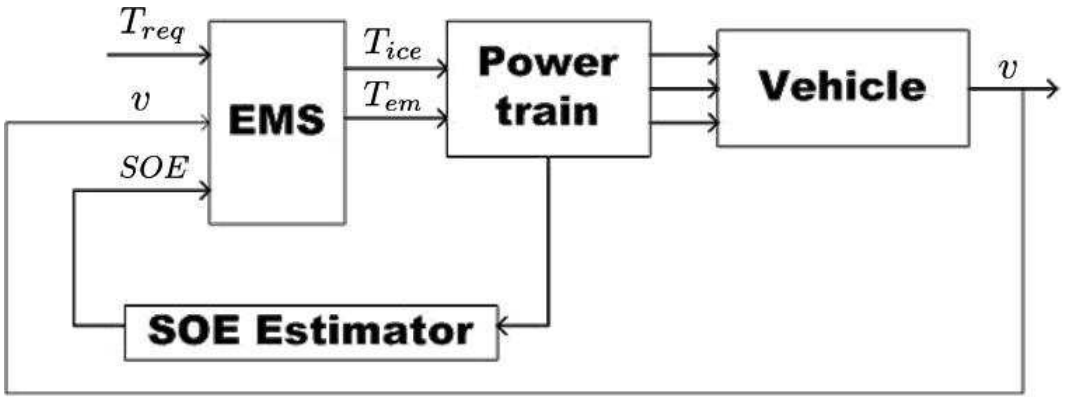

Figure 7.1: Role of the EMS in a hybrid electric vehicle

7.1.2 Energy management strategies in literature

Numerous power management algorithms or supervisory control strategies for hybrid electric vehicles have been proposed in literature. As shown in Fig. 7.2, EMS can be divided into two main groups: rule-based strategies and optimization-based strategies. Rule-based strategies are further categorized into fuzzy rule based methods and deterministic rule based ones. Optimization-based strategies are further categorized into global optimization methods and real-time optimization ones, refer to Desai & Williamson (2009), Salmasi (2007), Gurkaynak et al. (2009) and Çağatay Bayindir et al. (2011).

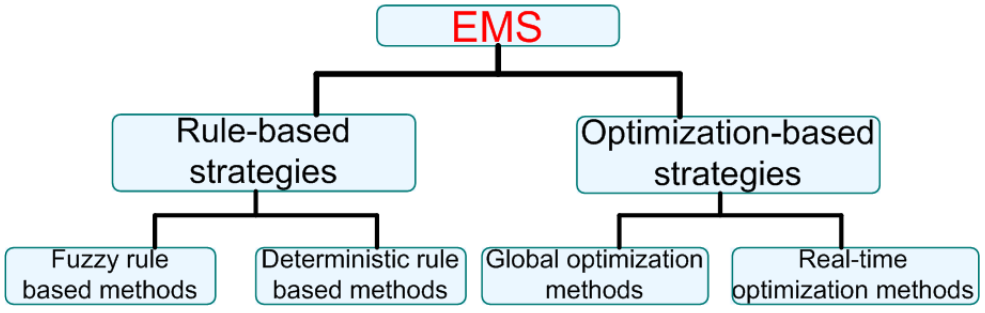

Figure 7.2: Classification of hybrid vehicle control strategies

7.1.2.1 Rule-based strategies

The main aspect involved in rule-based approaches is their effectiveness in real time supervisory control of power flow in a hybrid driveline. The rules are usually based on heuristics, intuition and human expertise, and are generally independent of the priori knowledge of a predefined driving cycle. The main idea of rule based strategies is

commonly based on the concept of load-leveling, see Hochgraf et al. (1996). For each engine speed, the load-leveling strategy shift the engine torque as close as possible to the operating point of optimal efficiency, fuel economy and emissions. The variation between the demanded power by the driver and the power generated by engine will be compensated by the motor, see Salmasi (2007).

The deterministic rules are based on engine maps of efficiency and emission, as well as driving experience. Such kind of rules are generally implemented via static maps, to share the required power between engine and electric motor. Instead of using deterministic rules, the knowledge of experts can be used to form a fuzzy logic, and a real-time energy management strategy can be realized using decision-making quality of the fuzzy logic, see Desai & Williamson (2009).

Jalil et al. (1997) presents a Thermostat (on/off) Control approach to the problem of controlling the electricity generation of Series Hybrid Electric Vehicles (SHEVs) aiming at minimize fuel consumption. Based on knowledge of the generator consumption maps, as well as information on the battery behavior, the achieved algorithm is able to define: whether to continuously keep the generator in the on state or not; when to, if is the case, switch the generator on or off.

Power Follower (Baseline) Control, see Bedir & Alouani (2009) for example, is a popular strategy for energy management in HEVs. The control strategies of famous Toyota Prius and Honda Insight are developed based on such a kind of method. For Power Follower Control strategies, the engine is treated as the primary source of power, while the motor is used to compensate for the power variation between the demanded power and the power generated by the engine. However, the efficiency of the whole power system is not optimized, and the vehicle emissions are not directly taken into account.

In order to improve the Baseline strategy, Johnson et al. (2000) proposed a Modified Power Follower Control strategy, where a cost function representing the overall fuel consumptions and emissions at all candidate operating points is introduced to optimize both energy consumptions and emissions. The strategy continuously selects the "optimal" operating point that is the minimum of this cost function.

State Machine Based Control strategy is adopted in Phillips et al. (2000) for supervisory control of a Parallel Hybrid Electric Vehicle (PHEV). The state machine dictates the operating mode of the HEV which can be Engine (engine propelling the vehicle), Hybrid (both the engine and the motor are used to propel the vehicle), Charging (engine propelling the vehicle and charging the battery), etc. Each operating mode is connected to another one by transition that is activated under certain condition in terms of battery

state of charge, vehicle speed and torque requirement.

Lee & Sul (1998) proposed a Fuzzy Control strategy to minimize emissions while sustaining the battery charge and achieving the vehicle performance, where inputs to the proposed fuzzy controller include the acceleration pedal stroke and the motor speed, and the output is defined as the normalized ratio of motor torque command to rated motor torque. After that, more sophisticated controller are developed by Lee et al. (2000), Rajagopalan et al. (2003), etc.

It is well known that the optimization of fuel efficiency and emissions are two contending goals; in other words, an optimal solution is always a compromise when dealing with efficiency and pollutant emissions, see Salmasi (2007) and Desai & Williamson (2009). An Adaptive Fuzzy Control strategy is used to tackle the conflicting problem in Zhu et al. (2004), where a cost function is defined with adaptively weights assigned to each objective (emission or fuel efficiency) based on their importance in different driving environments. Then, the control strategy is able to control any one of the objectives, by changing the values of relative weights.

7.1.2.2 Optimization-based strategies

Given the inherent rigidity of a rule-based approach, designers have turned their attention to optimization-based strategies that are used to calculate the optimal engine reference torques, motor reference torques and gear ratios for HEVs by minimizing a cost function generally representing the fuel consumption or pollutant emissions. If this optimization is performed for specific drive cycles using past and future (expected) information, a global optimization solution can be achieved. Obviously, this approach cannot be used directly for practical energy management, even the results obtained can be considered as useful benchmarks for analyzing, evaluating and deriving real-time control strategies, see Bernard et al. (2010). On the other hand, a real-time optimization strategy can be found by definition of an instantaneous cost function that depends only on the system variables at the current time. Of course, the solution of such a problem is not globally optimal, but it can be used directly for real-time implementation, see Salmasi (2007), Desai & Williamson (2009) and Wirasingha & Emadi (2011).

Vinot et al. (2007) introduced an energy management strategy using the Linear Programming technique. The problem of optimizing the fuel consumption is considered as a convex nonlinear optimization problem that is finally approximated by a linear programming method.

Dynamic Programming is a global optimization method for EMS developments, see

Brahma et al. (2000), Pisu & Rizzoni (2007) and Serrao (2009). The sequence of choices represents the power split ratio between the engine and motor at successive time steps. The cost corresponds to fuel consumption, emissions and other design objective. Once the grid of possible power splits is created with associated cost for each of the solution candidates, the proceeding goes backwards (i.e., from the end of the driving cycle), the optimal cost-to-go is calculated for each grid point, and stored in a matrix of costs. When the entire cycle has been examined, the path with the lowest total cost represents the optimal solution, see Serrao (2009). Application examples of Dynamic Programming to solve the optimal power management problem of a hybrid electric vehicle can be found in Lin et al. (2003), Liu & Peng (2006) and Pérez et al. (2006).

Table 7.1: Summary of energy management types

EMS	Rule-based strategy		Optimization-based strategy	
	Fuzzy rule based	Deterministic rule based	Global optimization	Real-time optimization
Dynamic Programming			×	
Trip Based Control			×	
Fuzzy Predictive Control	×			
Adaptive Control				×
Genetic Algorithms			×	
Switching Rule		×		
Decoupling Control				×
Predictive Control				×
Game Theory			×	
Thermostat Control		×		
Robust Control				×
Power Follower Control		×		
ECMS (A-ECMS)				×
Modified Power Follower Control		×		
Stochastic Dynamic Programming			×	
State Machine Based Control		×		
Linear Programming			×	
Fuzzy Control	×			
Adaptive Fuzzy Control	×			

The Stochastic Dynamic Programming has been proposed to solve the power management as a stochastic problem in Lin et al. (2004) and Moura et al. (2011). The basic principle of Stochastic Dynamic Programming problem formulation is to model the power command as a discrete-time stochastic dynamic process and this demand can be generated by a stationary Markov chain. Markov driver model predicts the future power demands by generating the probability distribution for them, see Gurkaynak et al. (2009).

These global optimization methods mentioned above require lots of computational time. To outperform these algorithms, another efficient approach based on the optimal control theory is proposed in Delprat et al. (2004). It allows very fast results to be obtained and can be used to evaluate all the other kinds of control strategies, especially those dedicated to real-time control.

Equivalent Consumption Minimization Strategy (ECMS) is a famous and widely-used real-time optimization strategy. ECMS is based on the concept that the battery is only used as an energy buffer, and all energy ultimately comes from the fuel tank. Thus, a virtual fuel consumption should be associated with the use of electrical energy, and a factor which is called the equivalence factor is used to convert the consumed electrical power into the equivalent fuel consumption. The optimality of the achieved EMS strongly depends on this equivalence factor, see Rizzoni & Onori (2012). So, the revised control strategy, which is referred to as the Adaptive Equivalent Consumption Minimization Strategy (A-ECMS), is proposed, see, for instance, Tulpule et al. (2010) and Musardo et al. (2005). It is proved that such strategy promises the near-optimality if the equivalence factors are properly defined with time evolution.

The power management strategy can also be achieved based on Fuzzy Predictive Control (Rajagopalan et al. (2003)), Genetic Algorithms (Piccolo et al. (2001)), Decoupling Control (Barbarisi et al. (2005)), Predictive Control (Borhan et al. (2009)), Switching Rule (Wei et al. (2006)), Game Theory (Gielniak & Shen (2004)), Trip Based Control (Gong et al. (2008)), Adaptive Control (Antoniou & Emadi (2009)), etc. Table 7.1 gives the summary of EMS types referred to previously. Note that there still exists other kinds of EMS that are not mentioned here.

Pisu et al. (2003) and Pisu & Rizzoni (2004) have proposed Robust Control approach to solve the power split problem in PHEV, where the objective is to determine an output feedback controller that minimize fuel consumption with respect to a family of possible torque/power input profiles, e.g. urban driving cycles.

It could be concluded that: rule-based strategies are easier to be implemented in real applications, among which fuzzy rule based control strategies are superior than deterministic rule based ones; optimization based strategies own better performance than rule-based ones, but global optimization methods are typically not feasible in an online application due to their computational demands, as well as needs of priori knowledge on future vehicle power demand (road profile); from the online implementation point of view, optimal real-time and fuzzy rule based methods are highly suitable due to the adaptive and robust characteristics.

In this work, robust control is adopted as the method for EMS developments, main achievements will be presented in coming part of the dissertation.

7.2 H_∞ based EMS with battery fault accommodation

Pisu & Rizzoni (2004) have applied the robust H_∞ approach to the EMS development of a PHEV. However, the battery behavior was not taken into account. As mentioned previously, the usage of battery information is required to improve system performance and lengthen the battery life. So, this part contributes to some preliminary study on the influence of battery fault on the control strategy.

7.2.1 System description

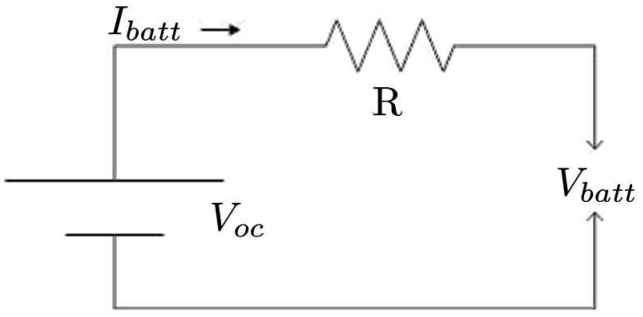

Figure 7.3: Simplified battery model

The PHEV considered here will adopt the architecture depicted by Fig. 6.1. Models of the engine and the motor are directly inherited from the results achieved in 6.2.2.2 and 6.2.2.3.

For battery, a simplified model (as shown in Fig. 7.3), which treats the battery as the combination of a voltage source and a resistance, is adopted. Then, following equations can be obtained according to Kirchhoff voltage law and battery characteristics, see Serrao

(2009):

$$V_{oc} = V_{batt} + RI_{batt} \tag{7.1}$$

$$SOE = \frac{E_{act}}{E_{batt}} = \frac{Q_{act}V_{oc}}{E_{batt}} \tag{7.2}$$

$$Q_{act} = Q_{batt} - \int_0^t I_{batt}(\tau)d\tau \tag{7.3}$$

From the equations above, we can get:

$$SOE = \frac{Q_{batt}V_{oc}}{E_{batt}} - \frac{V_{oc}}{E_{batt}}\int_0^t I_{batt}(\tau)d\tau \tag{7.4}$$

and:

$$\dot{SOE} = -\frac{P_{batt}}{E_{batt}}(1 + \frac{RI_{batt}^2}{P_{batt}}) = -\frac{\epsilon_{batt}}{E_{batt}}P_{batt} \tag{7.5}$$

where V_{oc} denotes the open circuit voltage of the battery, I_{batt} is the battery current, V_{batt} is the battery voltage, E_{batt} denotes nominal battery energy, E_{act} denotes remained battery energy, Q_{batt} denotes nominal charge of the battery, Q_{act} denotes remained battery charge and ϵ_{batt} is treated as a constant which differs from discharge to charge of the battery.

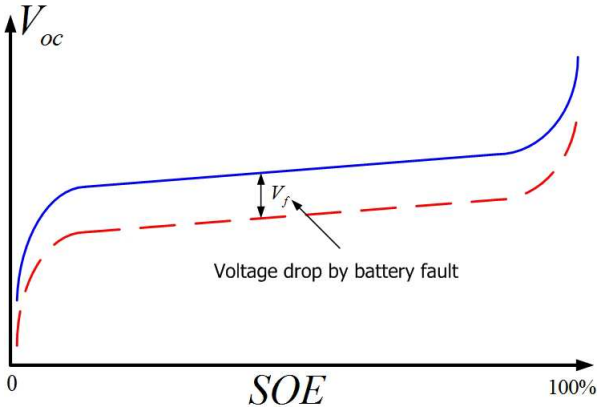

Figure 7.4: Battery voltage Vs. SOE

Fig. 7.4 depicts battery voltages with respect to different SOE, where the solid curve describes the ordinary relation between the voltage and the SOE, while the dashed one roughly shows the voltage loss in the presence of battery fault due to the battery ageing.

In case of the existence of battery fault, following equation is considered:

$$V_{oc} = V_{batt} + RI_{batt} + V_f \tag{7.6}$$

and (7.5) becomes:

$$\dot{SOE}_f = -\frac{\epsilon_{batt}}{E_{batt}} P_{batt} - \frac{I_{batt}}{E_{batt}} V_f \tag{7.7}$$

where V_f is the voltage drop resulted from the battery fault and SOE_f denotes SOE with the existence of battery fault.

7.2.1.1 State space system model

In practice, the following equation holds:

$$T_r = T_{ice} + \lambda_b T_{em} \tag{7.8}$$

where T_r is the required torque by the driver, T_{ice} is the engine torque, T_{em} is the motor torque and λ_b is the gear ratio between the engine and the motor, see Fig. 6.1.

Here, the distribution between chemical and electrical power is modeled by the following ratio which belongs to [0,1]

$$\alpha = \frac{T_{ice}}{T_r} \tag{7.9}$$

In this study, α is considered as the control input that will allow to accommodate the battery fault effect.

Combining the notation above with (6.13), (6.17) and (7.7), we can get:

$$\frac{dE_{chem}}{dt} = -P_{chem} = -\Gamma_1(\omega)\alpha T_r - \Gamma_2(\omega) \tag{7.10}$$

$$\frac{dSOE_f}{dt} = \Gamma_3(\omega)\alpha T_r - \Gamma_4(\omega) T_r - \Gamma_5(\omega) - \Gamma_6 V_f \tag{7.11}$$

where E_{chem} is the remained fuel energy, $\Gamma_1(\omega) = D_1\omega/(D_2 + D_3\omega + D_4\omega^2)$, $\Gamma_2(\omega) = (E_1\omega + E_2\omega^2)/(D_2 + D_3\omega + D_4\omega^2)$, $\Gamma_3(\omega) = \epsilon_{batt}F_0\omega/E_{batt}F\lambda_b$, $\Gamma_4(\omega) = \epsilon_{batt}F_0\omega/E_{batt}F\lambda_b$, $\Gamma_5(\omega) = \epsilon_{batt}G/E_{batt}F$, and $\Gamma_6 = I_{batt}/E_{batt}$.

In this preliminary study, the effect of battery fault is modeled in an additional way.

Meanwhile, the following state space description is adopted for the controller design.

$$\begin{cases} \dot{x}_1 = A(\omega)T_r u + B(\omega) \\ \dot{x}_2 = C(\omega)T_r u - (D(\omega)T_r + E(\omega)) - F_f f \\ y = x_2 \end{cases} \tag{7.12}$$

where $A(\omega)$, $B(\omega)$, $C(\omega)$, $D(\omega)$, $E(\omega)$ and F_f are constant system matrices, $x_1 = E_{chem}$ and $x_2 = SOE_f$ are treated as the state variables, $u = \alpha$ is treated as the control input, y is treated as the system output, $f = V_f$ is treated as the system fault, and T_r is supposed to be a known value.

7.2.2 H_∞ EMS controller synthesis

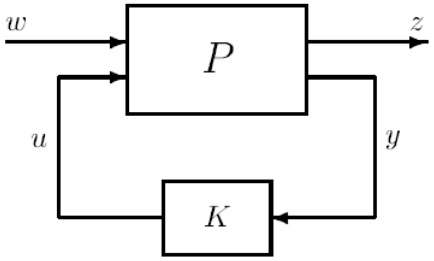

Figure 7.5: The standard H_∞ control problem

Let us recall the standard H_∞ control problem (as depicted in Fig. 7.5) that is already defined in section 2.2.5, where $u \in \mathbb{R}^{n_u}$ is the vector of control inputs, $y \in \mathbb{R}^{n_y}$ is the vector of plant outputs, $w \in \mathbb{R}^{n_w}$ presents the vector of exogenous inputs (reference, disturbances, noise, etc.), $z \in \mathbb{R}^{n_z}$ presents the vector of controlled outputs to be minimized/penalized, P is called the generalized plant or interconnected system where all weighting functions that specify the performance requirements are included.

Based on the configuration of Fig. 7.5, the H_∞ control problem is referred to as finding a controller K such that:

$$\|F_l(P, K)\|_\infty < \gamma$$

where γ is some prescribed performance level.

Based on the the system model described by (7.12), the EMS controller development, accounting for the influence of battery ageing, is considered in the standard H_∞ control problem as illustrated by Fig. 7.6, where Σ is described by (7.12), K is the EMS controller to be designed, f is the system fault, SOE_{ref} is the desired SOE, SOE_f is the measured

output, z_1 and z_2 are controlled outputs to be minimized, w_1 and w_2 are weighting functions.

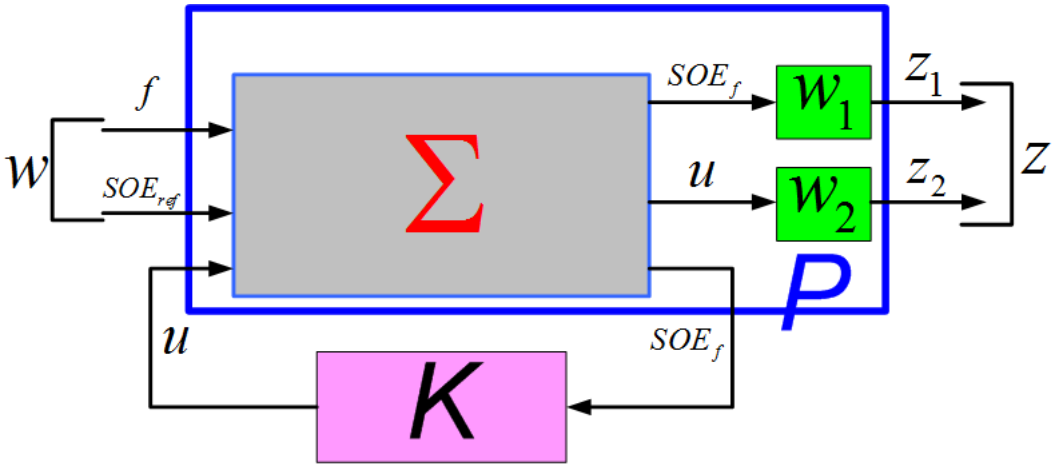

Figure 7.6: Suggested control structure in standard H_∞ control form

Then, the control problem is boiled down to seek the dynamic K for each time instant such that the following objectives are satisfied

- fault accommodation: minimizing the effect of battery fault f on SOE_f.
- limited control action u (torque distribution between T_{ice} and T_{em}) such that $\left\| \frac{u}{SOE_{ref}} \right\| \leq 1$.

To achieve the objectives specified above, the following weighting functions are specified

- $w_1 = \frac{s+1}{s+0.001}$ is used to achieve good fault attenuation in low frequency.
- $w_2 = \frac{s+1000}{0.1s+1000}$ is used to keep u less than 1.

The control problem can be solved using the Linear Matrix Inequality (LMI) based solution stated in section 2.3.

7.2.3 Simulation and discussion

Based on the control structure and weighting functions specified in section 7.2.2, a relative suboptimal EMS controller K is obtained for (7.12) with respect to $\omega = 60$ and $T_r = 28$. The achieved H_∞ performance level is $\gamma = 397.9976$.

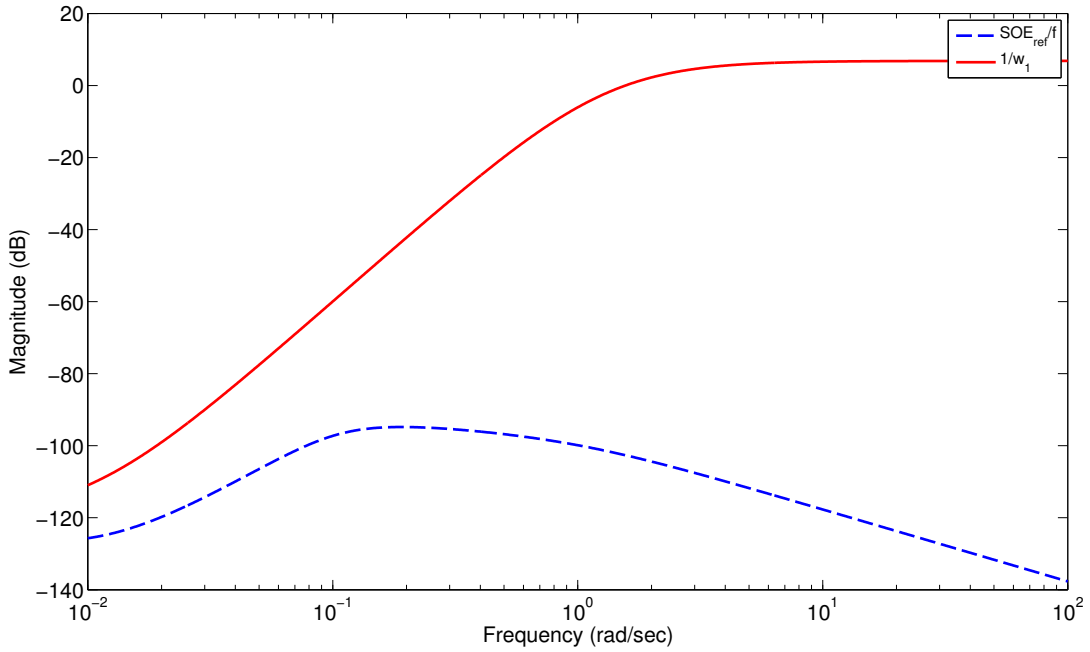

Figure 7.7: Frequency response of SOE_f / f

7.2.3.1 Frequency domain simulation

The dashed line in Fig. 7.7 presents the transfer between the actual SOE SOE_f and the battery fault f, while the dashed line in Fig. 7.8 presents the transfer between the control action u and the desired SOE SOE_{ref}.

As seen in Fig. 7.7, the closed-loop system with achieved controllers owns good fault attenuation within the whole frequency range, where battery fault mainly consists in low frequencies. Also, it can be seen from Fig. 7.8, the achieved controllers own limited control action u as required.

7.2.3.2 Time domain simulation

The time domain simulation concerns the reaction of the control signal u, following the occurrence of battery fault. Note that the fault here means that some cells of the battery pack do not work.

Supposing that the battery owns the initial values of $E_{chem} = 1.935 \times 10^9$ and $SOE_f = 0.78$, and some sudden fault happens to the battery at time t_f (as pointed in the upper part of Fig. 7.9). Then, apply the achieved EMS controller to the system described by (7.12) where $\omega = 60$ and $T_r = 28$. The related simulation results are shown in Fig. 7.9 and Fig. 7.10.

It can be seen, when the fault happens to the battery (at time t_f), a rise of the control

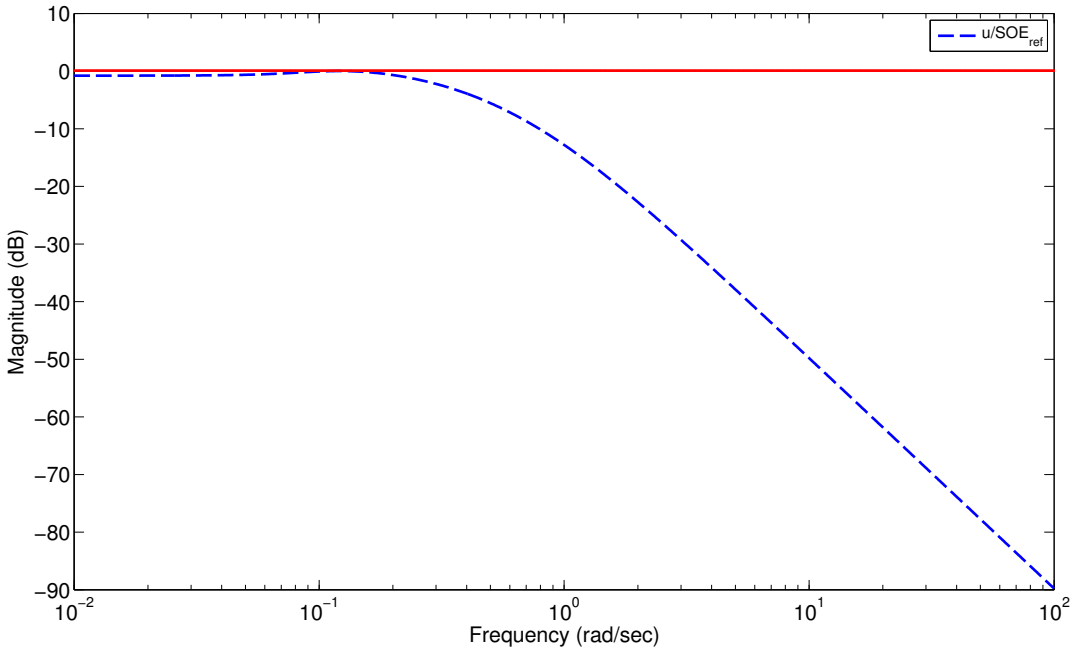

Figure 7.8: Frequency response of u/SOE_{ref}

output u follows (see the bottom part of Fig. 7.9), which results from the reaction of the EMS controller K to the presence of the battery fault. An increase of u means that more fuel will be used. Accordingly, E_{chem} will drop significantly (see the solid line of Fig. 7.10) compared with the non-fault condition (see the dotted line of Fig. 7.10). On the contrary, if another controller is used, which does not take into account the influence of the battery fault, same power split ratio u will be taken for both fault and fault-free conditions. Then, battery SOE may drop significantly, which will results into battery over-discharge that speeds battery aging or even leads to the breakdown of the battery system.

7.2.3.3 Robustness analysis

For systems owning the form like (7.12) where $T_r = 28$, we will provide here a robustness analysis of the achieved controller to the variation of ω belonging to [50,70] rpm.

The μ analysis method (see Skogestad & Postlethwaite (2007)) is used to conclude on the robustness properties of the controller referred to in section 7.2.3.2.

Fig. 7.11 shows the lower and upper bounds of the structured singular value μ. It is clear that the upper bound of μ is less than 1 for all frequencies, which means the robust stability can be satisfied within certain range of ω for the closed-loop system with achieved controller.

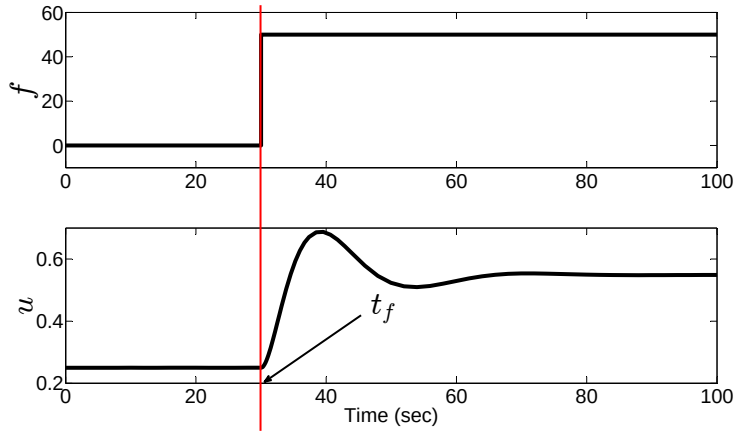

Figure 7.9: Time response of u

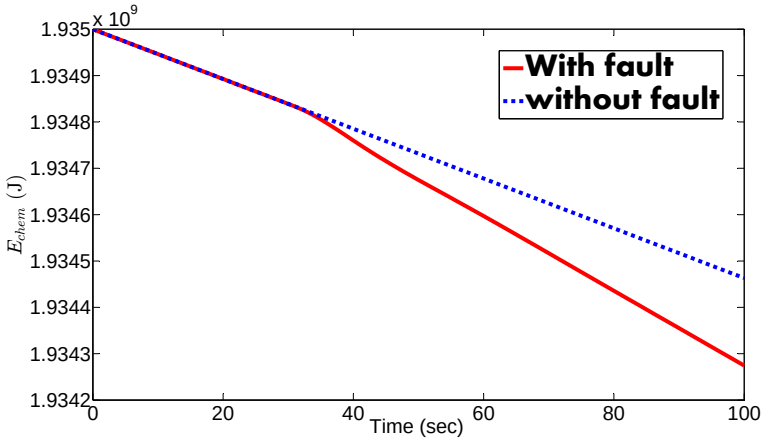

Figure 7.10: Time response of E_{chem}

Also, Fig. 7.12 presents time responses of u with respect to systems of different ω within the same range as defined for Fig. 7.11, which verifies robustness of the proposed controller.

7.3 Concluding remarks

This chapter has given an overview of the energy management strategies in HEVs, where the related problem description, as well as the general structure of an EMS controller are presented. Then, the classification and comparison of available energy management strategies in literature are given.

The main contribution of this chapter is the exploratory study on the influence of battery fault on the EMS controller. The fault here is supposed to result from battery

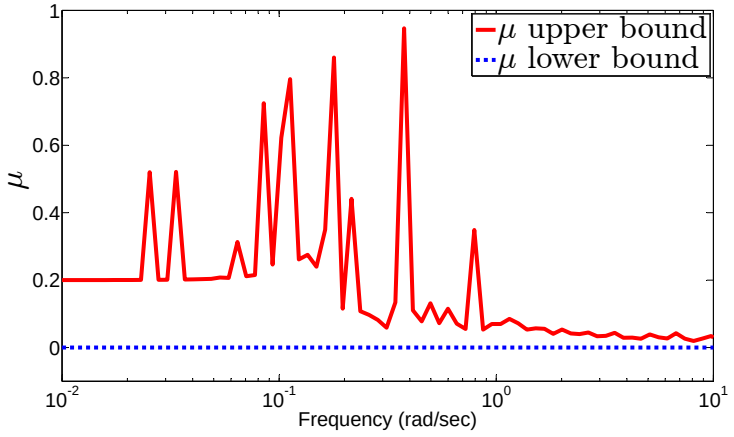

Figure 7.11: μ plot for robust stability analysis

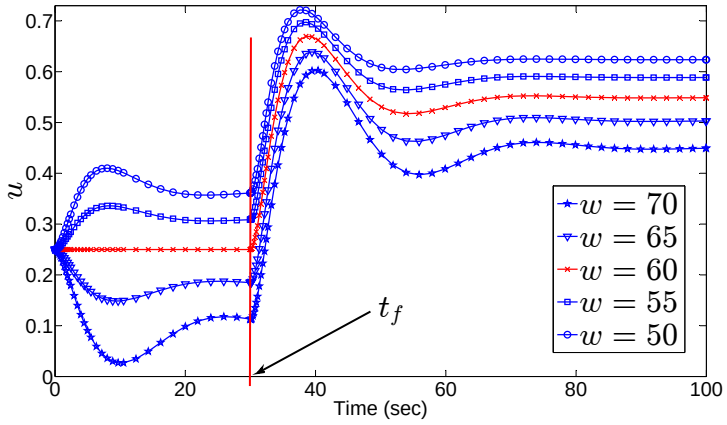

Figure 7.12: Time responses of u with respect to different ω

ageing, and be simply modeled as a voltage drop with respect to the nominal voltage of the battery without fault.

Based on the system model including the description of battery fault, the H_∞ based control structure is proposed. Then the EMS controller is achieved with a specific ω and T_r, simulation results have proved the effectiveness of the proposed controller that gives a regulated control signal in the presence of battery fault.

Unfortunately, as seen, since the achieved system matrices are dependent of ω and T_r, and the H_∞ control can just be used for linear system with constant system matrices, different EMS controllers should be designed for related specific ω and T_r.

Meanwhile, the controller obtained in this chapter is only suitable for fault accommodation. The objective of fuel consumption minimization will need further modifications of the control system structure.

In the last chapter, the combination of Linear Parameter Varying (LPV) method and H_∞ control will be adopted to deal with the varying parameters, as well as the problem of fuel consumption minimization.

Chapter 8

LPV/H_∞ Based Energy Management Strategy Design

In chapter 7, the H_∞ approach is adopted for the development of Energy Management Strategy (EMS) in a Parallel Hybrid Electric Vehicle (PHEV) accounting for the influence of battery ageing, and an output feedback controller which minimizes some cost functions is derived. Unfortunately, the state space matrices of the plant model are fixed at some operating conditions. This approach is often overly conservative when the physical parameters undergo large variations during system operation. One way of reducing conservatism is to design robust controllers around each operating point and to switch between controllers according to some interpolation policy, but stability and performances can not be guaranteed.

Recently, Linear Parameter Varying (LPV) methods have been widely used to approximate non-linear and linear time-varying systems, and two main approaches are usually adopted for LPV controller design: the polytopic approach and the Linear Fractional Transformation (LFT) approach. The main drawback of the polytopic method is the large number of Linear Matrix Inequalities (LMIs) to be solved if the number of parameter increases, but this is not the case for the LFT one. Moreover, the latter allows to consider, in the same formulation, varying parameters and uncertainties (adaptation to the parameters and robustness with respect to uncertainties), see Scherer (2001*a*) and Apkarian & Gahinet (1995).

This chapter presents two applications of the LPV/H_∞ approach on EMS developments and improvement. The first application is a touch of the LPV approach for HEV modeling and control. The objective is to test the effectiveness of such an approach on accounting for the influence of varying system parameters on the control strategy. Con-

sequently, a gain-scheduled EMS controller is achieved aiming at minimizing the fuel consumption of a PHEV, where the system is modeled under LFT form with varying system parameters (vehicle velocity and battery capacity) represented as an uncertainty block, and the controller is scheduled by the varying parameters. Availability of the LPV/H_∞ approach for EMS development is proved by simulations in the frequency and time domains, see Wang et al. (2013*b*).

Based on the fact proved above that the LPV is a capable method with respect to HEV modeling and control, another (the second) application of the LPV/H_∞ approach is concerned with the design of an EMS regulator. Assuming that an optimal EMS has been in existence, the aim is to determine the regulating quantity of battery current and the power split ratio between the engine and the battery with respect to the achieved optimal ones by the existing EMS, according to the driving cycle variation and battery capacity degradation. Similarly with the first application, the system model is also on the LFT form, and the LPV EMS is synthesized using the approach proposed in Apkarian & Gahinet (1995).

As stated above, these two controllers are for different control objectives. Also, as what will be see later, different control structures are adopted with different control inputs and outputs for each application. More importantly, the required torque T_r is with a fixed value for the first controller, which is not realistic for the real vehicle. Meanwhile, the wheel rotational speed ω is not controlled. The performance of the first EMS controller is also limited by the propriety of the predefined State of Charge (SOC) target. On the contrary, the second controller is more reasonable, T_r is adapted to varying road conditions, and the vehicle driveability is be satisfied (by means of vehicle speed control), see Wang et al. (2013*a*).

8.1 LPV/H_∞ approach to minimized fuel consumption and extended battery life

This section presents a novel gain-scheduled output feedback controller for a PHEV with minimized fuel consumption and prolonged battery life in the presence of battery capacity degradation (battery ageing). In detail, the problem under studying is described firstly, followed by the LPV system description with varying parameters (velocity and battery capacity) represented as uncertainty blocks. Then the LPV/H_∞ controller is constructed, as well as simulations and discussion are derived finally.

8.1.1 Problem description and objectives

8.1.1.1 Description of the control problem

Regardless of the topology, energy management strategies in HEVs are usually intended to achieve several simultaneous objectives. The primary one is usually the minimization of the vehicle fuel consumption, while also attempting to minimize the emissions, as well as maintaining or enhancing the driveability. Furthermore, the control objectives are often subject to integral constraints, such as nominally maintaining the battery State of Charge (SOC) in charge-sustaining hybrids, see Paganelli et al. (2001).

If fuel consumption minimization is the only objective, the energy management problem can be formulated as: find the instantaneous power split ratio between the engine and the battery such that:

$$\int_0^{t_f} \dot{m}_f dt$$

is minimized, and the constraints

$$0 \prec SOC_{min} \leq SOC \leq SOC_{max}$$

is satisfied, where, $\dot{m}_f$ is the instantaneous fuel consumption (fuel mass flow rate), SOC_{min} and SOC_{max} are allowed lower and upper SOC bound respectively.

8.1.1.2 Control objectives

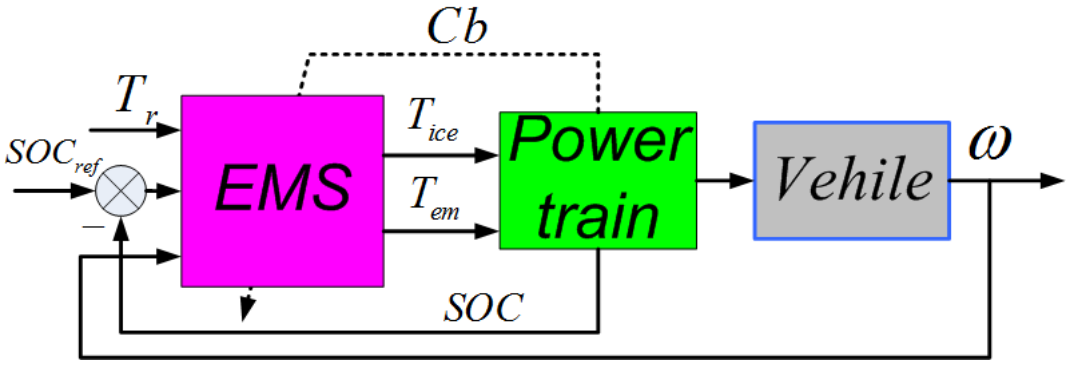

Figure 8.1: Block diagram of the proposed control system

In practice, the battery ages over time, and the rate of battery ageing is affected by operation profiles such as the C-rate, the temperature and the discharge depth, which are influenced directly by the control strategy. Therefore, it is meaningful that battery

ageing be taken into account in the development of gain-scheduled EMS controllers aiming at, on one hand prolonging the battery life, and on the other hand guaranteeing the system performance in spite of variant battery health state (ageing).

Generally, battery ageing can be described as capacity fade (battery capacity decreasing) or/and power fade (battery internal resistance increasing). Here, only the first fade case is taken into account.

In this application, a LPV/H_∞ controller which optimizes the fuel consumption, as well as prolongs the battery life is presented. The proposed controller is depicted by Fig. 8.1, where T_r is the required torque by the driver, T_{ice} is the torque of the engine, T_{em} is the torque of the electric motor, Cb is the battery's capacity that represents the battery ageing and is used to schedule the controller, and SOC_{ref} is the SOC target. The control objectives include:

- minimize fuel consumption by means of tracking to the predefined proper SOC_{ref}
- prolong the battery life by means of reasonable power split ratio based on the knowledge of the battery ageing (battery capacity)

Note that the engine control is not considered here, even if the achieved control strategy may have strong action on fuel consumption.

8.1.2 System description

The PHEV considered here adopts the architecture depicted by Fig. 6.1. In terms of system description, two main components are included: the driveline and the battery. All related component models are directly inherited from the results achieved in section 6.2.2, with the main equations given below. Detailed model explanations will not be recalled here (see section 6.2.2 for details).

$$\dot{\omega} = A_1 T_{ice} + A_2 T_{em} + A_3(A_4\omega^2 + A_5 cos(\theta) + A_6 sin(\theta) + A_7\dot{\omega}) \tag{8.1}$$

$$\dot{V}_1 = -\frac{1}{C_1 R_1} V_1 + \frac{1}{C_1} I \tag{8.2}$$

$$\dot{V}_2 = -\frac{1}{C_2 R_2} V_2 + \frac{1}{C_2} I \tag{8.3}$$

$$\dot{SOC} = -\frac{1}{Cb} I \tag{8.4}$$

$$V = k \cdot SOC + b - V_1 - V_2 - R_0 I \tag{8.5}$$

Here, we set the following ratio which belongs to [0,1]

$$\alpha = \frac{T_{ice}}{T_r} \tag{8.6}$$

Combinations of the notation above with (8.1) lead to:

$$\dot{\omega} = \Gamma_1 T_r \alpha + \Gamma_{\omega 1}(\omega) + A_2 T_r + \Gamma_6 cos(\theta) + \Gamma_7 sin(\theta) \tag{8.7}$$

where T_r is the required torque, $\Gamma_1 = A_1 - A_2$, $\Gamma_{\omega 1} = A_3 A_4 \omega^2$, $\Gamma_6 = A_3 A_5$, $\Gamma_7 = A_3 A_6$.

The dynamic equations (8.7) achieved above together with (8.2), (8.3) and (8.4) give the full system description.

8.1.3 LPV/LFT model formulation of the PHEV

As seen in section 8.1.2, the system model is non-linear with respect to the wheel rotational speed ω. Also, the model parameters, such as battery resistances and capacity, vary with environment changes and battery ageing evolution.

Based on the consideration that the LPV method could be used to approximate non-linear and linear time-varying systems, we define:

$$\omega = \bar{\omega} + P_\omega \delta_\omega \tag{8.8}$$

and

$$Cb = \bar{Cb} + P_{Cb} \delta_{Cb} \tag{8.9}$$

where $-1 \leq \delta_\omega \leq 1$, $-1 \leq \delta_{Cb} \leq 0$, $\bar{\omega}$ and $\bar{Cb}$ are so-called nominal value of ω and Cb, P_ω and P_{Cb} present the possible maximum variations of ω and Cb.

We also

- set $x_1 = \omega$, $x_2 = V_1$, $x_3 = V_2$, $x_4 = SOC$ as system state variables collected in the state vector x.
- set $u_1 = \alpha$, $u_2 = I$ as system input variables collected in the input vector u.
- set $y_1 = x_1 = \omega$, $y_2 = x_4 = SOC$, $y_3 = V$ as system output variables collected in the output vector y.
- treat $A_2 T_r$, $cos(\theta)$, $sin(\theta)$, b as disturbance variables collected in the disturbance vector d.

Remark: the slope of the road is here considered as a disturbance, but could be defined as varying-parameter if some measurement or estimation of the slope is available.

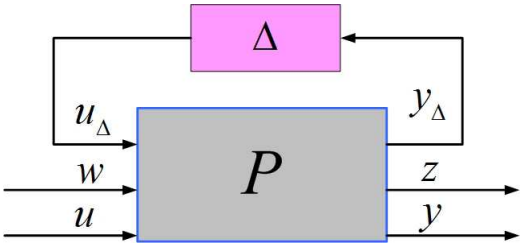

Figure 8.2: System in LPV/LFT form

Then, based on the definition presented above, the following LFT representation can be used to rewrite the PHEV model achieved in section 8.1.2, which owns the system interconnection as depicted in Fig. 8.2 (see section 2.4.2.2 for details).

$$\begin{cases} \dot{x} = Ax + Bu + B_\Delta u_\Delta + B_d d \\ y = Cx + Du + D_\Delta u_\Delta + D_d d \\ y_\Delta = Ex + Fu + F_\Delta u_\Delta + F_d d \\ u_\Delta = \Delta y_\Delta \end{cases} \tag{8.10}$$

where $x = [x_1; x_2; x_3; x_4]$, $u = [u_1; u_2]$, $u_\Delta = [u_{\Delta_1}; u_{\Delta_2}]$, $d = [d_1; d_2; d_3; d_4]$, $y = [y_1; y_2; y_3]$,

$$A = \begin{bmatrix} \Gamma_3 & 0 & 0 & 0 \\ 0 & -\Gamma_{19} & 0 & 0 \\ 0 & 0 & -\Gamma_{21} & 0 \\ 0 & 0 & 0 & 0 \end{bmatrix}, B = \begin{bmatrix} \Gamma_1 T_r & 0 \\ 0 & \Gamma_{20} \\ 0 & \Gamma_{22} \\ 0 & -\Gamma_{23} \end{bmatrix}, B_\Delta = \begin{bmatrix} 1 & 0 \\ 0 & 0 \\ 0 & 0 \\ 0 & -1 \end{bmatrix}, B_d = \begin{bmatrix} A_9 T_r & \Gamma_6 & \Gamma_7 & 0 \\ 0 & 0 & 0 & 0 \\ 0 & 0 & 0 & 0 \\ 0 & 0 & 0 & 0 \end{bmatrix},$$

$$C = \begin{bmatrix} 1 & 0 & 0 & 0 \\ 0 & 0 & 0 & 1 \\ 0 & -1 & -1 & k \end{bmatrix}, D = \begin{bmatrix} 0 & 0 \\ 0 & 0 \\ 0 & -R_0 \end{bmatrix}, D_\Delta = \begin{bmatrix} 0 & 0 \\ 0 & 0 \\ 0 & 0 \end{bmatrix}, D_d = \begin{bmatrix} 0 & 0 & 0 & 0 \\ 0 & 0 & 0 & 0 \\ 0 & 0 & 0 & \Gamma_{26} \end{bmatrix}, E = \begin{bmatrix} \Gamma_4 & 0 & 0 & 0 \\ 0 & 0 & 0 & 0 \end{bmatrix}, F = \begin{bmatrix} 0 & 0 \\ 0 & -\Gamma_{24} \end{bmatrix}, F_\Delta = \begin{bmatrix} 0 & 0 \\ 0 & -\Gamma_{25} \end{bmatrix}, F_d = \begin{bmatrix} 0 & 0 & 0 & 0 \\ 0 & 0 & 0 & 0 \end{bmatrix}, \Delta = \begin{bmatrix} \delta_\omega & 0 \\ 0 & \delta_{Cb} \end{bmatrix}.$$

with: $\Gamma_1 = A_8 - A_9$, $\Gamma_2 = A_3 A_4/(1 - A_3 A_7)$, $\Gamma_3 = \Gamma_2 \bar{\omega}$, $\Gamma_4 = \Gamma_2 P_\omega$, $\Gamma_6 = A_3 A_5/(1 - A_3 A_7)$, $\Gamma_7 = A_3 A_6/(1 - A_3 A_7)$, $\Gamma_8 = D_2 + D_3\bar{\omega} + D_4\bar{\omega}^2$, $\Gamma_9 = E_1 + E_2\bar{\omega}$, $\Gamma_{10} = D_1\bar{\omega}$, $\Gamma_{11} = \Gamma_9/\Gamma_8$, $\Gamma_{12} = \Gamma_{10}/\Gamma_8$, $\Gamma_{13} = (E_2 P_\omega - \Gamma_{11} D_3 P_\omega - 2\Gamma_{11} D_4 \bar{\omega} P_\omega)/\Gamma_8$, $\Gamma_{14} = (D_1 P_\omega - \Gamma_{12} D_3 P_\omega - 2\Gamma_{12} D_4 \bar{\omega} P_\omega)/\Gamma_8$, $\Gamma_{15} = (D_3 P_\omega + 2D_4 \bar{\omega} P_\omega)/\Gamma_8$, $\Gamma_{16} = (\Gamma_{11} D_4 P_\omega^2)/\Gamma_8$, $\Gamma_{17} = (\Gamma_{12} D_4 P_\omega^2)/\Gamma_8$, $\Gamma_{18} = (D_4 P_\omega^2)/\Gamma_8$, $\Gamma_{19} = 1/(C_1 R_1)$, $\Gamma_{20} = 1/C_1$, $\Gamma_{21} = 1/(C_2 R_2)$, $\Gamma_{22} = 1/C_2$, $\Gamma_{23} = 1/\bar{C}b$, $\Gamma_{24} = (\Gamma_{23} P_{Cb})/\bar{C}b$, $\Gamma_{25} = P_{Cb}/\bar{C}b$, $\Gamma_{26} = b$.

8.1.4 LPV/H_∞ Controller

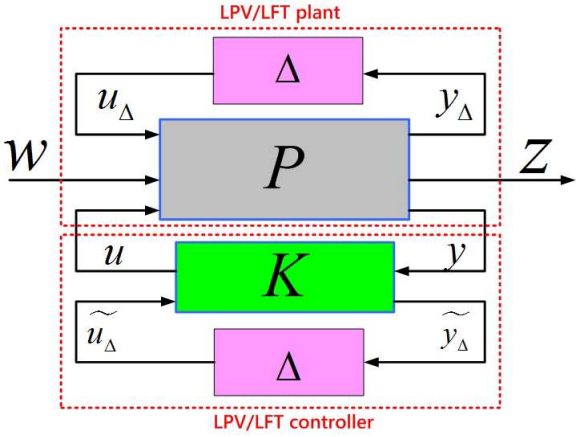

Figure 8.3: LPV/LFT control problem

Let us recall the LPV/LFT control scheme as depicted in Fig. 8.3, where the closed-loop operator from w to z is:

$$T_{zw} = F_l(F_u(P, \Delta), F_l(K, \Delta)) \tag{8.11}$$

The objective of a LPV/H_∞ controller is to guarantee some closed-loop performance $\gamma > 0$ from w to z for all admissible parameter Δ. Assuming Δ is bounded, the LPV/H_∞ control of a LPV/LFT system boils down to find a control structure K such that the following conditions are satisfied (see section 2.4.2.2 for details)

- the closed-loop system (8.11) is internally stable for all possible parameter Δ
- and, $\|T_{zw}\|_\infty < \gamma$

Here, the development of the EMS controller is considered as a LPV/LFT control problem, and the suggested control structure is illustrated in Fig. 8.4, where Σ is described by (8.10), P is referred to as the interconnected system that contains the weights (performance weighting functions), the uncertain part Δ specifies how varying parameters enters the plant dynamics, y_Δ and u_Δ can be interpreted as the inputs and outputs of the time-varying operator Δ. Furthermore d_1 to d_4 are disturbances defined in section 8.1.3, α and I are the control inputs, SOC_{ref} is the desired SOC, ω, SOC and V are measured outputs, z_1 and z_2 are controlled outputs to be minimized, W_{SOC} and W_u are weighting functions.

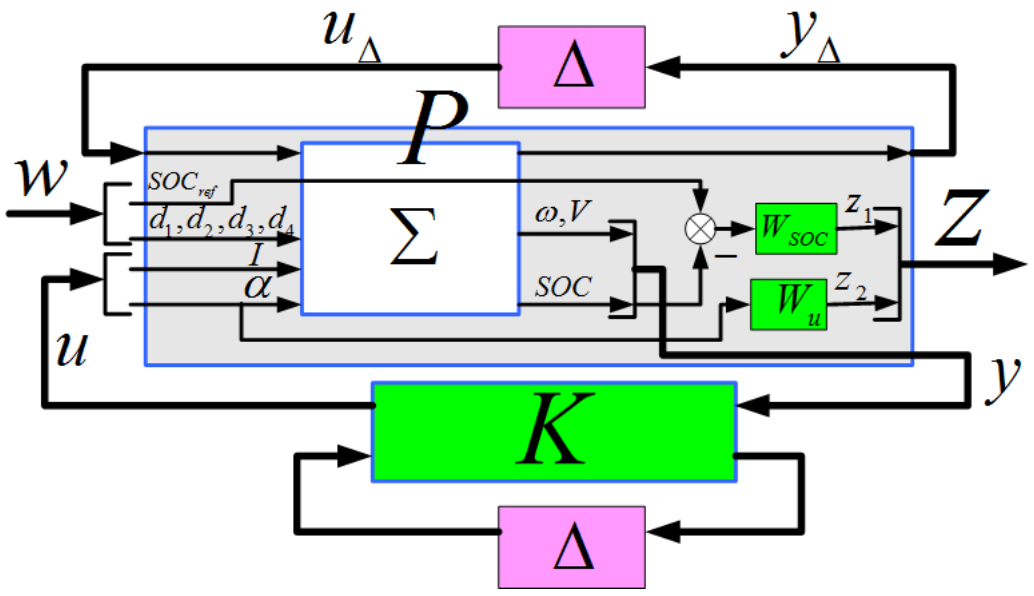

Figure 8.4: Diagram for PHEV control

The control problem could be described as seeking a LPV controller of the form:

$$u = F_l(K, \Delta)y \tag{8.12}$$

where the time-invariant K specifies the LFT dependency of the LPV controller on the measurements of Δ with (8.12) giving the rule for updating the controller, such that the following objectives are satisfied

- minimized fuel consumption by means of $min \left\| \frac{SOC_{ref} - SOC}{SOC_{ref}} \right\|_\infty$
- limited control active α by means of $min \left\| \frac{\alpha}{SOC_{ref}} \right\|_\infty$

To achieve the objectives specified above, the following weighting functions are chosen

- $W_{SOC} = \frac{s+1}{s+0.1}$ is used to achieve good reference tracking
- $W_u = \frac{s+10}{0.5s+10}$ is used to keep α less than 1

Then, the control problem can be solved using the LMI-based solution stated in section 2.4.2.2.

8.1.4.1 Controller synthesis

Recalling the definitions of varying parameters by (8.8) and (8.9), where $-1 \leq \delta_\omega \leq 1$, $-1 \leq \delta_{Cb} \leq 0$, $\bar{\omega}$ and $\bar{Cb}$ are so called nominal value of ω and Cb, P_ω and P_{Cb} present

the possible maximum variations of ω and Cb.

If we set $T_r = 28$, $\bar{\omega} = 60$, $\bar{Cb} = 138$, $P_\omega = 10$ and $P_{Cb} = 27.6$ for (8.10), which represents up to $\pm 17\%$ variations of ω ($50 \leq \omega \leq 70$), and 20% degradation of Cb ($110.4 \leq Cb \leq 138$), the LPV controller based on the structure of Fig. 8.4 is achieved with $\gamma = 1.303$.

8.1.5 Frequency domain analysis of the synthesis results

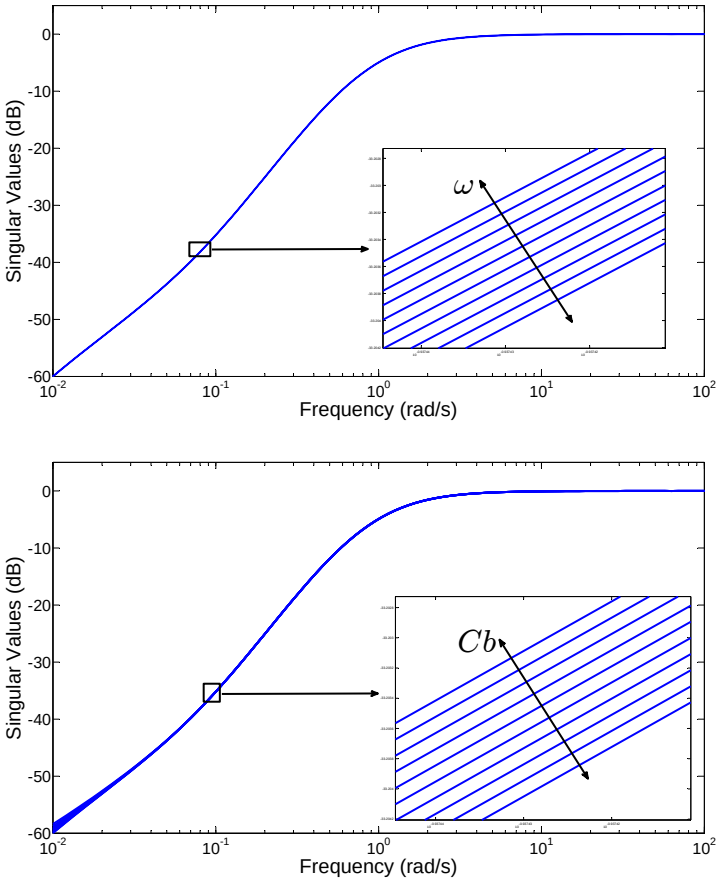

Figure 8.5: Frequency response of $(SOC_{ref} - SOC)/SOC_{ref}$

Fig. 8.5 shows the sensitivity functions from the reference SOC_{ref} to the reference error $SOC_{ref} - SOC$ of the closed-loop LPV system, which is based on the specified system and the achieved controller in section 8.1.4.1, with respect to 10 different ω (upper part) and 10 different Cb (bottom part) respectively.

Fig. 8.6 shows the sensitivity functions from the reference SOC_{ref} to the measured output SOC of the closed-loop LPV system with respect to 10 different ω (upper part) and 10 different Cb (bottom part) respectively.

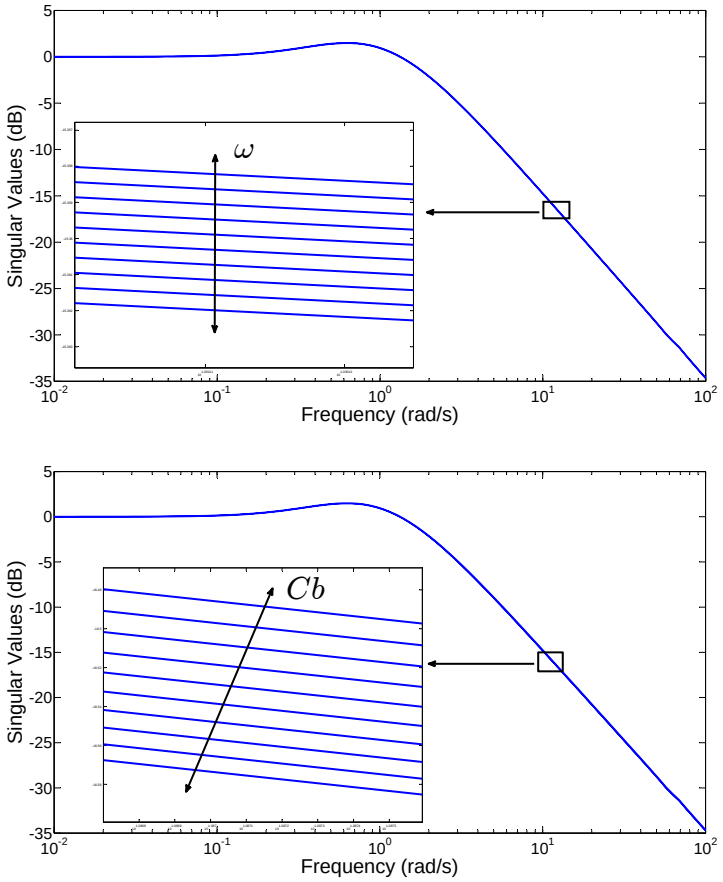

Figure 8.6: Frequency response of SOC/SOC_{ref}

It can be seen, almost similar performances are satisfied for all parameter variations within the same bandwidth, which means the closed-loop system with achieved LPV controller owns good reference tracking performance in spite of varying parameters (the time simulation given in the following section also verifies this point).

Fig. 8.7 shows the sensitivity functions from the reference SOC_{ref} to the controlled output α of the closed-loop LPV system according to 10 different ω (upper part) and 10 different Cb (bottom part) respectively. It can be seen, the closed-loop system with achieved LPV controller owns very limited control action α as required in spite of varying parameters, which is also proved by the time domain simulation presented below.

8.1.6 Time domain simulation

For system (8.10) specified with $T_r = 28$, $\bar{\omega} = 60$, $\bar{Cb} = 138$, $P_\omega = 10$ and $P_{Cb} = 27.6$, the time domain simulation is concerned with checking the effectiveness of the achieved

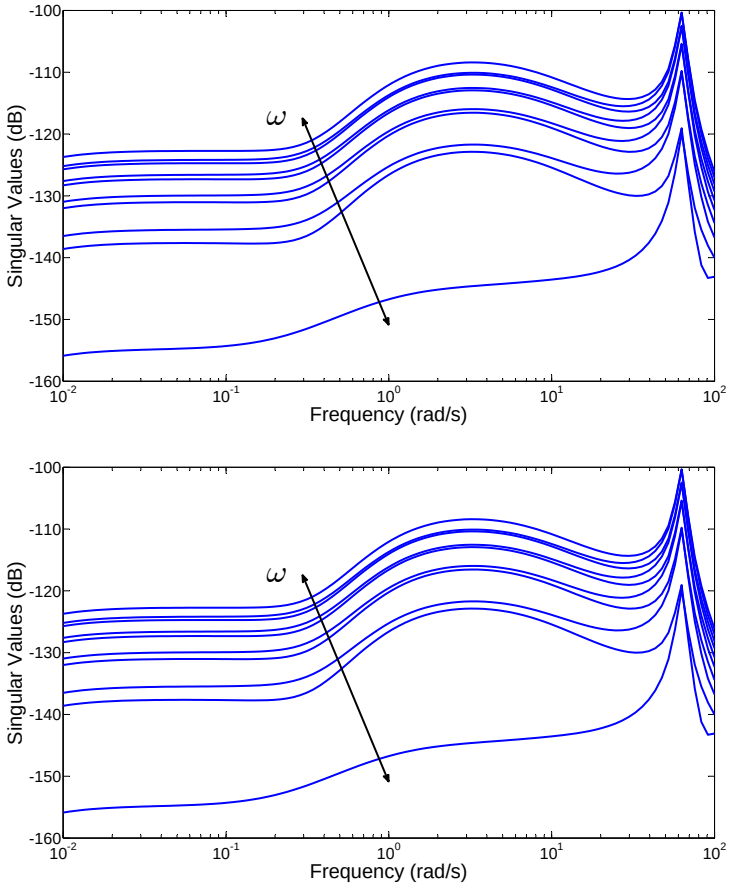

Figure 8.7: Frequency response of α / SOC_{ref}

controller in section 8.1.4.1 with respect to fuel consumption minimization (reflected via the tracking accuracy for the reference) and battery life extension (influenced directly by the control action α). Then, the time simulation is implemented under the condition of monotonically decreased SOC_{ref} as depicted by the red dotted line of Fig. 8.8. Meanwhile, the wheel rotational speed ω (vehicle velocity) is free of control (open loop).

Fig. 8.8 presents the reference tracking performance of the achieved gain-scheduled controller with respect to 5 different ω. As seen, the closed-loop LPV system (see the blue sold line) could always follow the trend of the reference (the red dotted line) in spite of varying parameters. It means that the minimized fuel consumption can be always satisfied.

Fig. 8.9 presents the control input α resulted from the gain-scheduled controller with respect to 3 different Cb. It can be seen, α increases slightly with the degradation of Cb, which means less battery energy is used when the battery ageing occurs (Cb decreases) to prevent further battery damage. Note that monotonous increase of the control signal

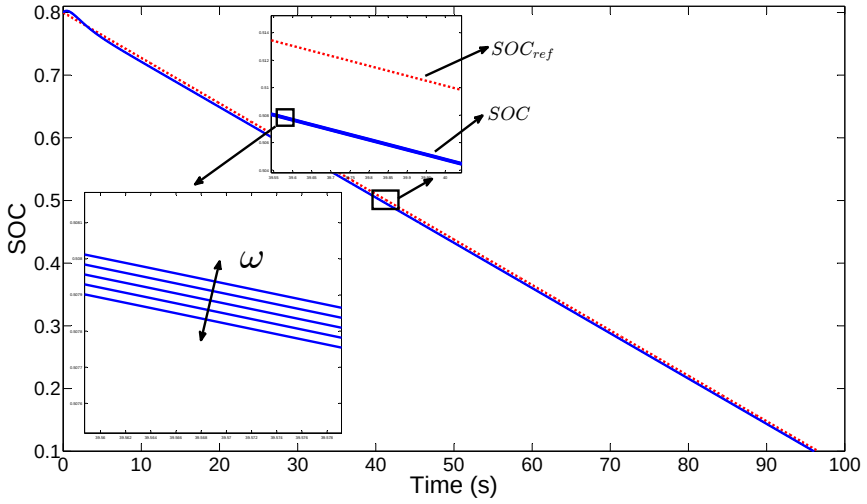

Figure 8.8: Reference tracking of the LPV controller

α is caused by the uncontrolled ω (open loop), and this trend is expected to be avoided by applying a more reasonable control structure.

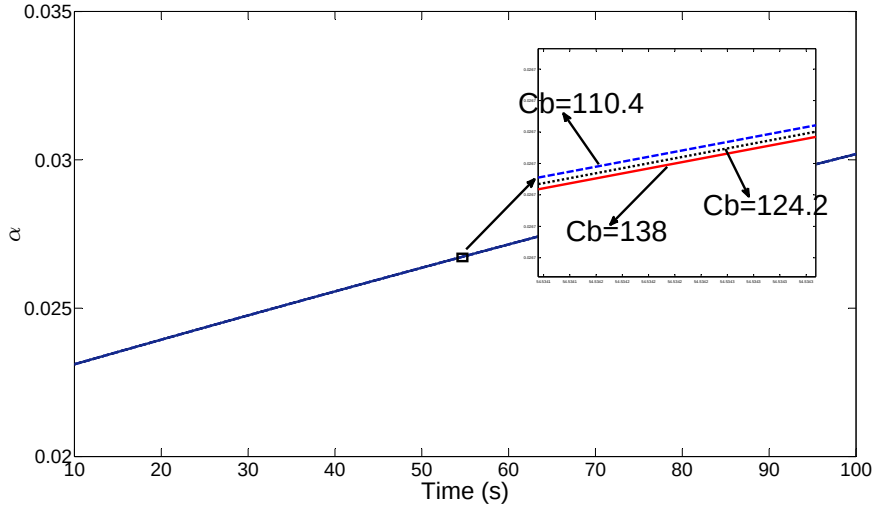

Figure 8.9: Varying α according to the degradation of Cb

8.2 LPV EMS regulator with battery life prolongation

In section 8.1, a gain-scheduled EMS strategy has been developed aiming at minimizing the fuel consumption, where the controller is scheduled by the varying parameters. However, performance of the achieved controller strongly depends on the propriety of

the SOC target that is not easy to be defined. Moreover, the value of T_r is fixed, and ω is not controlled, which is not realistic for the real vehicle.

In this part, a LPV/H_∞ EMS regulator is proposed, assuming that an optimal PHEV control strategy in terms of fuel consumption has been achieved in advance. The goal of such a regulator is to adapt the control strategy to the variation of battery state and vehicle driving cycle. Compared with the controller achieved in section 8.1, the EMS regulator is more reasonable, where T_r is adapted to varying road conditions, and the vehicle driveability is be satisfied (by means of vehicle speed control).

8.2.1 Problem description and control objectives of the EMS regulator

As stated in chapter 7, numerous optimal energy management strategies have been proposed in literature. In fact, optimality of the achieved EMS controller is also influenced by other factors, which change over time, such as the battery health state. Therefore, some critical corrections, which will guarantee the achieved optimality, to the achieved optimal EMS controller are required.

The EMS regulator developed here is used to determine the regulating quantity of battery current, which implicitly influences the power split ratio between engine and battery, with respect to present battery current indicated by the already existed optimal EMS controller, according to the driving cycle variation and battery capacity degradation. Then, such a regulator will on one hand prolong the battery life, and on the other hand guarantee the system performance and the achieved optimality in spite of variant system behaviors.

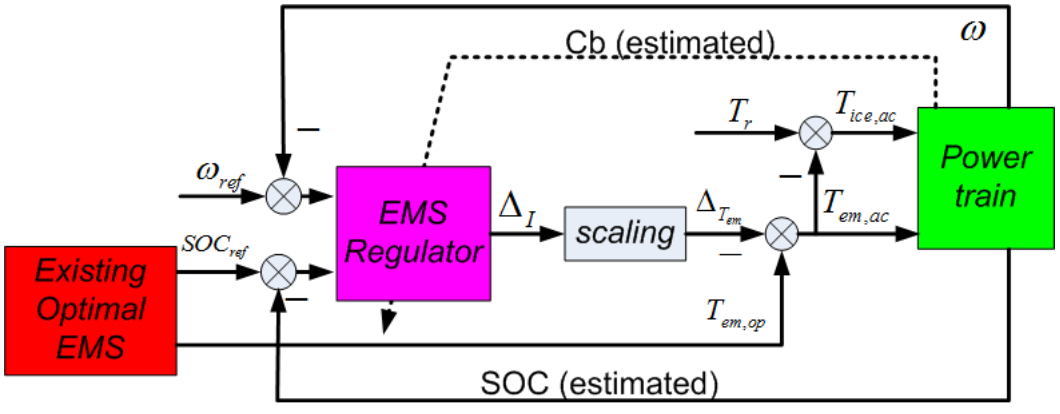

Figure 8.10: Block diagram of the proposed EMS regulator

The proposed regulator is depicted in Fig. 8.10, where T_r is the required torque by the driver, $T_{em,op}$ is the desired motor torque indicated by the unregulated EMS controller,

Δ_I is the regulating quantity of the battery current by the LPV regulator according to the varying battery capacity and the varying velocity, $\Delta_{T_{em}}$ is the regulating quantity of the motor torque with respect to Δ_I, $T_{ice,ac}$ is the revised engine torque requirement, $T_{em,ac}$ is the revised motor torque requirement, ω is the wheel rotational speed, Cb is the estimated battery capacity (see chapter 4) associated with the battery ageing, SOC_{ref} is the speed target, and SOC_{ref} is the SOC target (indicated by the existing optimal controller). The objectives of the EMS regulator are then to:

- guarantee the system performance in spite of the variation of system parameters
- ensure battery life prolongation by means of reasonable power split ratio based on the knowledge of the battery capacity

In details, on one hand, with the evolution of the battery ageing (Cb decreases), less battery current will be drawn (minus Δ_I), which results in the decrease of $T_{em,ac}$ with respect to a specific battery voltage, and on the other hand, if the velocity ω is increasing, which means more T_r is required, the battery current will increase accordingly (plus Δ_I) to meet the driving cycle requirement.

The development of EMS regulator then include the following steps: (1) construction of the system model taking into account of both the vehicle dynamics and the battery behaviors, (2) linear approximation of the non-linear system model based on the LPV/LFT method, (3) model transformation into the LFT form with varying parameters represented as an uncertainty block, (4) development of the gain-scheduled EMS regulator with prolonged battery life in the presence of battery capacity degradation (battery ageing).

8.2.2 Vehicle modeling

The vehicle considered here is a PHEV adopting the architecture depicted by Fig. 6.1. In terms of system modeling, two main components are included: the drive line and the battery, whose models are directly inherited from the results achieved in section 6.2.2, with the main equations given below. Detailed model explanations will not be recalled here (see section 6.2.2 for details).

$$\dot{\omega} = A_1 T_{ice} + A_2 T_{em} + A_3(A_4\omega^2 + A_5 cos(\theta) + A_6 sin(\theta) + A_7\dot{\omega}) \tag{8.13}$$

$$\dot{SOC} = -\frac{1}{Cb} I \tag{8.14}$$

For the specific powertrain architecture (as shown by Fig. 6.1) concerned in this study, the following equation holds

$$T_r = T_{ice} + \lambda_b T_{em} \tag{8.15}$$

where λ_b is the gear ratio between the engine and the motor.

Combination of the notation above with (8.13) leads to

$$\dot{\omega} = \Gamma_2 \omega^2 + A_8 T_r + \Gamma_6 cos(\theta) + \Gamma_7 sin(\theta) \tag{8.16}$$

where $\Gamma_2 = A_3 A_4/(1 - A_3 A_7)$, $A_8 = A_1/(1 - A_3 A_7)$, $\Gamma_6 = A_3 A_5/(1 - A_3 A_7)$, $\Gamma_7 = A_3 A_6/(1 - A_3 A_7)$.

The dynamic equations (8.16) achieved above together with (8.14) give the full system description.

8.2.3 LFT model of the PHEV

As seen in section 8.2.2, the vehicle model is non-linear with respect to the vehicle rotational speed ω. Also, model parameters, such as ω, the road slope θ, the required torque T_r and the battery capacity Cb, vary with the change of the driving cycle and the battery ageing evolution. Based on the consideration that the LPV method could be used to approximate non-linear and linear time-varying systems, we define:

$$\omega = \bar{\omega} + P_\omega \delta_\omega \tag{8.17}$$

$$T_r = \bar{T_r} + P_{T_r} \delta_{T_r} \tag{8.18}$$

$$cos(\theta) = \bar{cos} + P_{cos} \delta_{cos} \tag{8.19}$$

$$sin(\theta) = \bar{sin} + P_{sin} \delta_{sin} \tag{8.20}$$

$$Cb = \bar{Cb} + P_{Cb} \delta_{Cb} \tag{8.21}$$

$$I = \bar{I} + P_I \delta_I \tag{8.22}$$

where $-1 \leq \delta_\omega, \delta_{T_r}, \delta_{cos}, \delta_{sin}, \delta_I \leq 1$, $-1 \leq \delta_{Cb} \leq 0$, the instantaneous power split ratio between engine and battery, which is indicated by the unregulated optimal EMS, is based on $\bar{\omega}$, $\bar{T}_r$, $\bar{cos}$, $\bar{sin}$ and $\bar{Cb}$, P_ω together with P_{T_r}, P_{cos}, P_{sin}, P_{Cb} and P_I present the possible maximum variations of ω, T_r, $cos(\theta)$, $sin(\theta)$ and Cb with respect to $\bar{\omega}$, $\bar{T}_r$, $\bar{cos}$, $\bar{sin}$, $\bar{Cb}$ and $\bar{I}$ respectively, $\bar{I}$ is the battery current associated with the power split ratio indicated by the unregulated optimal EMS.

We also

- set $x_1 = \omega$, $x_2 = SOC$ as system states x.
- set δ_I, which is the regulating quantity of the battery current with respect to $\bar{I}$, $\bar{T}_r$, $\bar{cos}$, $\bar{sin}$ and $\bar{Cb}$, as system inputs u.
- set $y_1 = x_1 = \omega$, $y_2 = x_2 = SOC$ as system outputs y.
- treat δ_{T_r}, δ_{cos}, δ_{sin} as disturbances d.

Remark: δ_{T_r}, δ_{cos} and δ_{sin} are here treated as disturbances for simplicity, but could also be treated as the varying parameters (elements of Δ).

Based on the definition presented above, the following LFT representation can be used to rewrite the PHEV model achieved in section 8.2.2, which owns the system interconnection as depicted in Fig. 8.2 (see section 2.4.2.2 for details).

$$\begin{cases} \dot{x} = Ax + Bu + B_\Delta u_\Delta + B_d d \\ y = Cx + Du + D_\Delta u_\Delta + D_d d \\ y_\Delta = Ex + Fu + F_\Delta u_\Delta + F_d d \\ u_\Delta = \Delta y_\Delta \end{cases} \tag{8.23}$$

where $x = [\omega; SOC]$, $u = \delta_I$, $u_\Delta = [u_{\Delta_1}; u_{\Delta_2}]$, $y_\Delta = [y_{\Delta_1}; y_{\Delta_2}]$, $d = [1; \delta_{T_r}; \delta_{cos}; \delta_{cos}]$, $y = [\omega; SOC]$, and $\Delta = \begin{bmatrix} \delta_\omega & 0 \\ 0 & \delta_{Cb} \end{bmatrix}$.

Then, the LPV model (8.23) is adopted for the development of the LPV EMS regulator.

8.2.4 Development of the LPV/H_∞ EMS regulator

As stated previously, the EMS regulator developed here is used to determine the battery current regulation according to the driving cycle variation and battery capacity degradation, aiming at: (1) guaranteeing the system performance in spite of the variation of system parameters, and (2) prolonging the battery life by means of reasonable power split ratio based on the knowledge of the battery capacity.

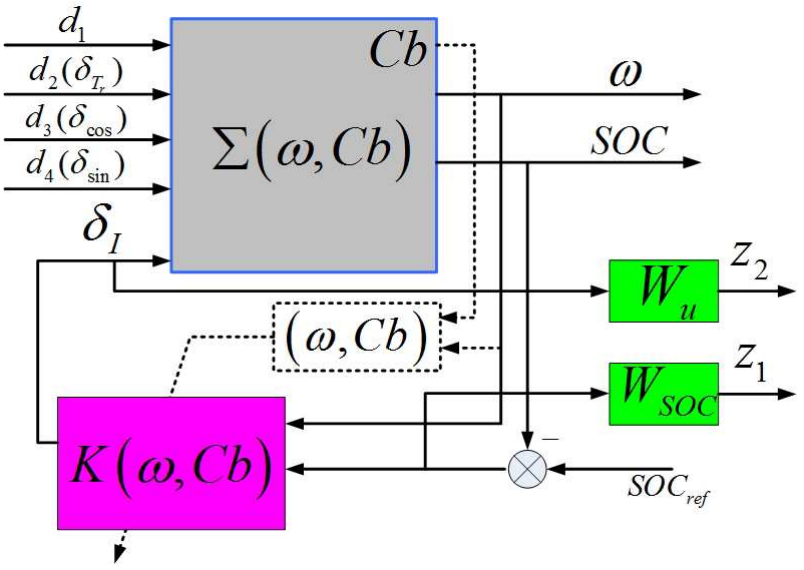

Figure 8.11: Diagram for the LPV EMS Regulator

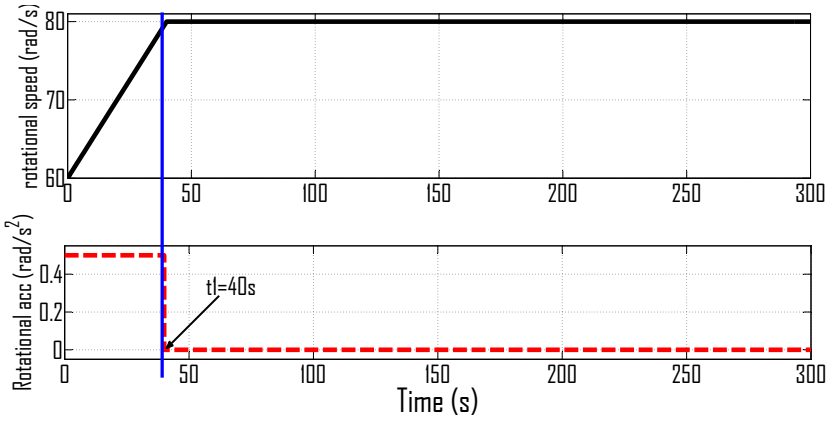

Figure 8.12: Driving cycle profile

Therefore, the regulator is suggested with the structure as illustrated in Fig. 8.11, where $\Sigma(\omega, Cb)$ is the LPV plant depending on the varying ω and Cb, $K(\omega, Cb)$ is therefore the LPV controller scheduled by measured ω and estimated Cb (see chapter 4). Furthermore, d_1 to d_4 are disturbances defined in section 8.2.3, δ_I is the control input, SOC_{ref} is the SOC target, ω and SOC are the measured output and estimated value (see chapter 4) respectively, z_1 and z_2 are the controlled outputs to be minimized, W_{SOC} and W_u are the weighting functions.

Then, the regulator design problem could be described as seeking $K(\omega, Cb)$ such that the following objectives are satisfied

- slower battery ageing evolution by means of $min \left\| \frac{SOC_{ref} - SOC}{SOC_{ref}} \right\|_\infty$

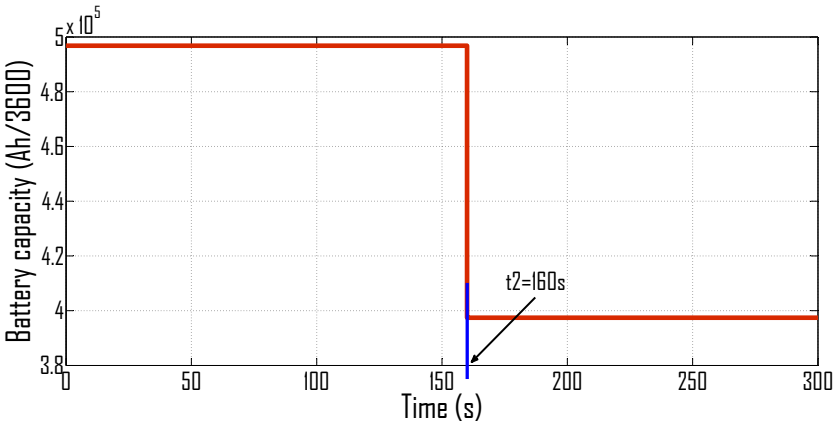

Figure 8.13: Battery capacity evolution

- limited control active δ_I by means of $min \left\| \frac{\delta_I}{SOC_{ref}} \right\|_\infty$

To achieve the objectives specified above, following weighting functions are chosen

- $W_{SOC} = \frac{s+1}{s+0.01}$ is used to achieve good reference tracking
- $W_u = \frac{s+0.06}{450s+30}$ is used to keep δ_I less than 1

Then, the regulator development problem can be solved using the LMI-based solution stated in section 2.4.2.2.

8.2.4.1 Controller (regulator) synthesis

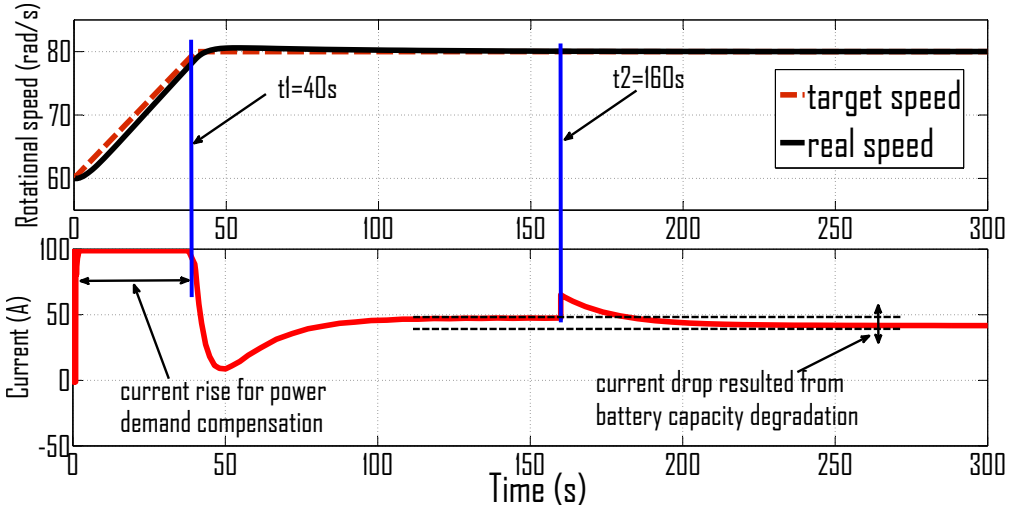

Figure 8.14: Battery current regulating

Recalling the definitions of the varying parameters in section 8.2.3, where the instantaneous power split ratio between the engine and the battery, which is indicated by the

unregulated optimal EMS, is based on $\bar{\omega}$, $\bar{T}_r$, $\bar{cos}$, $\bar{sin}$ and $\bar{Cb}$, P_ω together with P_{T_r}, P_{cos}, P_{sin}, P_{Cb} and P_I present the possible maximum variations of ω, T_r, $cos(\theta)$, $sin(\theta)$ and Cb, $\bar{I}$ is the battery current associated with the power split ratio indicated by the unregulated optimal EMS.

If we set $\bar{\omega} = 60$, $\bar{T}_r = 85$, $\bar{cos} = 1$, $\bar{sin} = 0$, $\bar{I} = 49$, $\bar{Cb} = 138$, $P_\omega = 10$, $P_{T_r} = 80$, $P_{cos} = 0.5$, $P_{sin} = 0.9$, $P_{Cb} = 27$, $P_I = 50$. The LPV regulator based on the structure of Fig. 8.11 can be derived with $\gamma = 1.6247$.

8.2.5 Simulation and discussion

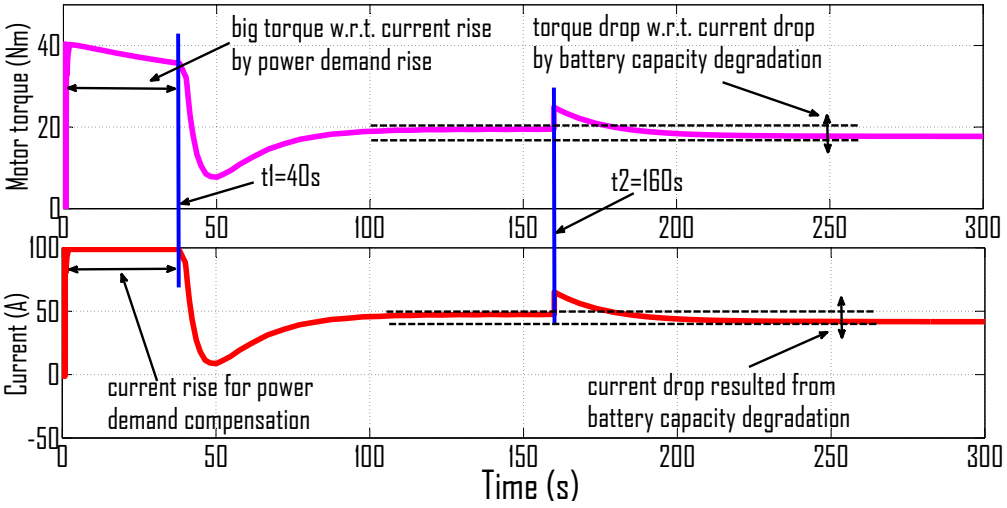

Figure 8.15: Motor torque regulating

The simulation is concerned with testing the effectiveness of the achieved EMS regulator in section 8.2.4.1 for battery current and power split ratio regulation with respect to driving cycle variation and battery capacity degradation.

Fig. 8.12 defines the rotational speed and acceleration profile for the test. As seen, during the first 40 seconds of the test, there is a acceleration requirement of about 0.5 rad/s^2 (refer to the bottom part of the figure) based on the initial speed of 40 rad/s, then the rotational speed remains at 80 rad/s from time $t1$ to the end of the test.

Fig. 8.13 shows the battery capacity scenario for the test. It can be seen, just a sudden jump is given at time $t2$ with the final value of 80% of the initial one.

As seen from the bottom part of Fig. 8.14, before time $t1$, peak battery current, and huge motor torque accordingly (refer to the top part of Fig. 8.15) is applied to meet the power demand resulted from the continuous acceleration. After that, smaller and steady current is applied to maintain the speed of 80 rad/s until time $t2$ when the sudden

battery capacity jump happens. After time $t2$, the regulation of current drop of about 10 A and motor torque decrease of about 5 Nm (refer to the top part of figure Fig. 8.15), which means regulated power split ratio is given to ensure battery life prolongation.

Also can be seen from the top part of Fig. 8.14, the actual speed is satisfactorily close to the required one, which means the system performance is guaranteed, based on well power split ratio regulation, in spite of the battery ageing (capacity degradation).

8.3 Concluding remarks

In this chapter, the LPV/H_∞ approach is used for: (1) the development of a gain-scheduled EMS controller in a PHEV with minimized fuel consumption and prolonged battery life in the presence of battery capacity degradation (battery ageing), and (2) an EMS regulator that is used to determine the regulating quantity of battery current, which implicitly influences the power split ratio between the engine and the battery, with respect to present battery current indicated by an already existed optimal EMS controller, according to the driving cycle variation and battery capacity degradation.

The EMS development in section 8.1 presents a test with respect to the effectiveness of the LPV approach on HEV modeling and control accounting for the influence of varying system parameters. While the regulator achieved in section 8.2 can be used to guarantee the achieved optimality by an existing optimal EMS controller in spite of the changing environmental factors and variant system parameters.

For both cases, the vehicle is modeled in LPV/LFT form, where the varying parameters are represented as an uncertainty block, and the controller/regulator development problem is solved using the LMI-based solution. More importantly, both the controller and the regulator own the function of prolonging the battery life.

Further works should be put on the test of the proposed LPV/H_∞ control strategy on an actual vehicle. Also, associated regenerative braking control strategy should be developed to ensure a complete energy management system.

Chapter 9

Conclusion and Perspective

General conclusion

This thesis is concerned with the development of robust control strategies in HEV. The main objective is to account for battery SOC and SOH indicated by battery capacity, in the EMS developments leading to extended battery life. The whole content is organized with nine chapters.

- The first chapter presents a general introduction on the HEV and its related classification and structure. The dissertation structure is also given in this chapter.
- In the second chapter, some key notions associated with the robust control are given in relatively basic level, problem formulation and LMI-based solutions of H_∞ controller synthesis and H_∞/LPV controller synthesis are presented in details.
- The third chapter aims at achieving the mathematical descriptions with respect to the behaviors of the Lithium-ion battery. In this chapter, the operation principle and classification of the Lithium-ion battery is given followed by some basic battery notions, the EEC battery model is constructed, all related battery parameters are included.
- Chapter four contributes to the estimation of battery SOC and parameters. The method considered for battery SOC estimation is the Kalman filter. This chapter also propose a novel method for battery capacity estimation, which is based on the LMS algorithm that is more simple than the KF.
- Chapter five is devoted to the development of a novel battery ageing estimation method based on the H_∞ observer accounting for the environment variations. In

this chapter, the influence of temperature changes and battery ageing on battery resistance and capacity are considered and modeled as additive variations from the nominal values of battery parameters. The proposed fault estimation method can detect continuously the ageing evolution while minimizing the influence of other factors, such as the temperature and battery current.

- Chapter six is dedicated to the model development of a PHEV that is capable of identifying the longitudinal dynamic behaviors of the vehicle that affects the fuel consumption and vehicle performance. In addition, battery dynamics are creatively incorporated into the system description aiming at taking battery age item into EMS developments.

- The main aim of chapter seven is to do some preliminary study on the influence of battery fault on the EMS, where the H_∞ approach is used to determine the power split ratio between the engine and the battery, which maintains the energy state of the battery within a reasonable range to prevent the battery from undesirable breakdown. This chapter also presents an overview of the EMS, where the motivation and general structure of the EMS controller including all input and control output signals.

- In chapter eight, the H_∞/LPV approach is used for: (1) the development of a gain-scheduled EMS controller with minimized fuel consumption and prolonged battery life in the presence of battery ageing, and (2) an EMS regulator that is used to determine the regulating quantity of battery current, which implicitly influences the power split ratio, with respect to the present battery current indicated by an already existed EMS controller, according to the driving cycle variation and battery capacity degradation.

Main contributions of this dissertation mainly concern:

- The design of battery capacity estimation based on the LMS algorithm that is more simple and less time-consuming than the KF approach in terms of parameter estimation.

- The development of H_∞ battery fault observer, where the extended battery model is used treating the temperature change as a disturbance and battery ageing as a fault, minimizing the influence of the temperature and battery current on the estimation accuracy.

- The development of EMS taking into account both vehicle dynamics and battery behaviors.
- The development of system models with LPV ones of LFT form representing variant velocity and battery capacity as an uncertainty block.
- The design of a gain-scheduled EMS controller aiming at minimizing the fuel consumption and prolonging the battery life in the presence of battery ageing.
- The development of a LPV EMS regulator that determines the regulating quantity of battery current and the power split ratio between the engine and the battery with respect to the so-called optimal ones by the existing EMS, according to the driving cycle variation and battery capacity degradation.

Perspectives

As a perspective of the method adopted, as well as the main results achieved in this work, the following seem to be of great interest to the author in the mid term:

- **Battery modeling**: Development of a more complex battery model that takes into account the influences of the battery temperature and other factors, such as the hysteresis effect, current direction and C-rate, which can model the real battery behaviors and operation environment more accurately.
- **Vehicle modeling**: Development of a HEV model that contains more dynamic descriptions with respect to driveline components, such as the gear box and the final differential, which will lead to more accurate system description and energy control strategy.
- **Model identification and validation**: Determination of model parameters, as well validation of the battery model and HEV model proposed in this work, based on intensive tests with the real system.
- **Regenerative braking control**: Development of the regenerative braking control strategy which ensure a complete energy management system.

while, the following over a long term:

- **Battery fault observer**: Design of a LPV battery fault observer that is more suitable for the real non-linear battery systems.

- **Energy control strategy**: (1) Combination of the proposed fault observer with the conventional control scheme of an HEV, which ensures the energy control strategy adapting to the battery ageing evolution, (2) Test of the proposed H_∞ and H_∞/LPV control strategies on a actual vehicle.

Bibliography

Alzieu, J., Smimite, H. & Glaize, C. (1997), 'Improvement of intelligent battery controller: state-of-charge indicator and associated functions', *Journal of power sources* **67**(1), 157–161.

Amrhein, M. & Krein, P. T. (2005), 'Dynamic simulation for analysis of hybrid electric vehicle system and subsystem interactions, including power electronics', *IEEE Transactions on Vehicular Technology* **54**(3), 825–836.

Antoniou, A. & Emadi, A. (2009), Adaptive control strategy for hybrid electric vehicles, *in* 'IEEE Vehicle Power and Propulsion Conference', IEEE, pp. 242–246.

Apkarian, P. & Gahinet, P. (1995), 'A convex characterization of gain-scheduled $\mathcal{H}_\infty$ controllers', *IEEE Transactions on Automatic Control* **40**(5), 853–864.

Apkarian, P., Gahinet, P. & Becker, G. (1995), 'Self-scheduled $\mathcal{H}_\infty$ control of linear parameter-varying systems: a design example', *Automatica* **31**(9), 1251–1261.

Aylor, J. H., Thieme, A. & Johnso, B. (1992), 'A battery state-of-charge indicator for electric wheelchairs', *IEEE Transactions on Industrial Electronics* **39**(5), 398–409.

Barbarisi, O., Westervelt, E. R., Vasca, F. & Rizzoni, G. (2005), Power management decoupling control for a hybrid electric vehicle, *in* '44th IEEE Conference on Decision and Control', IEEE, pp. 2012–2017.

Barlak, C. & Ozkazan, Y. (2009), A classification based methodology for estimation of state-of-health of rechargeable batteries, *in* 'International Conference on Electrical and Electronics Engineering', IEEE, pp. II–101.

Battery University, n. (2013), 'Types of lithium-ion', `http://batteryuniversity.com/learn/article/types_of_lithium_ion`. Accessed May 17, 2013.

Bedir, A. & Alouani, A. (2009), A simple power based control strategy for hybrid electric vehicles, *in* 'IEEE Vehicle Power and Propulsion Conference', IEEE, pp. 803–807.

Bernard, J., Delprat, S., Guerra, T. & Büchi, F. (2010), 'Fuel efficient power management strategy for fuel cell hybrid powertrains', *Control Engineering Practice* **18**(4), 408–417.

Bhangu, B., Bentley, P., Stone, D. & Bingham, C. (2005), 'Nonlinear observers for predicting state-of-charge and state-of-health of lead-acid batteries for hybrid-electric vehicles', *IEEE Transactions on Vehicular Technology* **54**(3), 783–794.

Bishop, G. & Welch, G. (2001), 'An introduction to the kalman filter', *Proc of SIGGRAPH, Course* **8**, 27599–3175.

Blanke, M. (2003), *Diagnosis and fault-tolerant control*, Springer.

Bo, C., Zhifeng, B. & Binggang, C. (2008), 'State of charge estimation based on evolutionary neural network', *Energy conversion and management* **49**(10), 2788–2794.

Borhan, H. A., Vahidi, A., Phillips, A. M., Kuang, M. L. & Kolmanovsky, I. V. (2009), Predictive energy management of a power-split hybrid electric vehicle, *in* '2009 American Control Conference', IEEE, pp. 3970–3976.

Bowen, L., Zarr, R. & Denton, S. (1994), 'A microcontroller-based intelligent battery system', *IEEE Aerospace and Electronic Systems Magazine* **9**(5), 16–19.

Boyd, S., El Ghaoul, L., Feron, E. & Balakrishnan, V. (1987), *Linear matrix inequalities in system and control theory*, Vol. 15, Society for Industrial and Applied Mathematics.

Brahma, A., Guezennec, Y. & Rizzoni, G. (2000), Optimal energy management in series hybrid electric vehicles, *in* 'Proceedings of the 2000 American Control Conference', Vol. 1, IEEE, pp. 60–64.

Brandwein, R. & Gupta, M. L. (1974), 'Nickel-cadmium battery monitor'. US Patent 3,940,679.

Briat, C., Sename, O., Lafay, J. et al. (2009), '$\mathcal{H}_\infty$ delay-scheduled control of linear systems with time-varying delays', *IEEE Transactions on Automatic Control* **54**(9), 2255–2260.

Bruzelius, F. (2004), Linear Parameter Varying Systems, PhD thesis, PhD Dissertation, Departement of Signal and Systems, Chalmers University of Technology, Goteborg, Sweden.

Buller, S., Thele, M., Karden, E. & De Doncker, R. W. (2003), 'Impedance-based nonlinear dynamic battery modeling for automotive applications', *Journal of Power Sources* **113**(2), 422–430.

Çağatay Bayindir, K., Gözüküçük, M. A. & Teke, A. (2011), 'A comprehensive overview of hybrid electric vehicle: Powertrain configurations, powertrain control techniques and electronic control units', *Energy Conversion and Management* **52**(2), 1305–1313.

Chan, C. (2007), 'The state of the art of electric, hybrid, and fuel cell vehicles', *Proceedings of the IEEE* **95**(4), 704–718.

Chan, C., Bouscayrol, A. & Chen, K. (2010), 'Electric, hybrid, and fuel-cell vehicles: architectures and modeling', *IEEE Transactions on Vehicular Technology* **59**(2), 589–598.

Chaturvedi, N., Klein, R., Christensen, J., Ahmed, J. & Kojic, A. (2010), 'Algorithms for advanced battery-management systems', *IEEE Control Systems Magazine* **30**(3), 49–68.

Chen, J. & Patton, R. (1999), 'Robust model-based fault diagnosis for dynamic systems'.

Chen, M. & Rincon-Mora, G. A. (2006), 'Accurate electrical battery model capable of predicting runtime and iv performance', *IEEE transactions on Energy conversion* **21**(2), 504–511.

Chiang, Y.-H. & Sean, W.-Y. (2009), Dynamical estimation of state-of-health of batteries by using adaptive observer, *in* '2nd International Conference on Power Electronics and Intelligent Transportation System', Vol. 1, IEEE, pp. 110–115.

Chilali, M. & Gahinet, P. (1996), '$\mathcal{H}_\infty$ design with pole placement constraints: an lmi approach', *IEEE Transactions on Automatic Control* **41**(3), 358–367.

Chilali, M., Gahinet, P. & Apkarian, P. (1999), 'Robust pole placement in lmi regions', *IEEE Transactions on Automatic Control* **44**(12), 2257–2270.

Choi, T. G. (2008), Modeling, Sizing and Control of Plug-in Light Duty Fuel Cell Hybrid Electric Vehicle, PhD thesis, Ohio State University.

Christianson, C. C. & Bourke, R. F. (1975), 'Battery state of charge gauge'. US Patent 3,946,299.

Codecà, F. (2008), Analysis and Development of Electric Vehicles: Modeling of Li-ion Batteries and Control of Vehicle Dynamics, PhD thesis, POLITECNICO DI MILANO.

Codecà, F., Savaresi, S. & Rizzoni, G. (2008), On battery state of charge estimation: A new mixed algorithm, *in* 'International Conference on Control Applications', IEEE, pp. 102–107.

de Lucena, S. E. (2013), 'A survey on electric and hybrid electric vehicle technology', `http://cdn.intechweb.org/pdfs/18661.pdf`. Accessed July 1, 2013.

Dees, D. W., Battaglia, V. S. & Bélanger, A. (2002), 'Electrochemical modeling of lithium polymer batteries', *Journal of power sources* **110**(2), 310–320.

Delprat, S., Lauber, J., Guerra, T. M. & Rimaux, J. (2004), 'Control of a parallel hybrid powertrain: optimal control', *IEEE Transactions on Vehicular Technology* **53**(3), 872–881.

Desai, C. & Williamson, S. (2009), Comparative study of hybrid electric vehicle control strategies for improved drivetrain efficiency analysis, *in* 'IEEE Electrical Power & Energy Conference', IEEE, pp. 1–6.

Di Domenico, D., Prada, E. & Creff, Y. (2011), An adaptive strategy for li-ion battery soc estimation, *in* 'Proceedings of 2011 IFAC World Congress'.

Do, D., Forgez, C., El Kadri Benkara, K. & Friedrich, G. (2009), 'Impedance observer for a li-ion battery using kalman filter', *IEEE Transactions on Vehicular Technology* **58**(8), 3930–3937.

Doerffel, D. & Sharkh, S. A. (2006), 'A critical review of using the peukert equation for determining the remaining capacity of lead-acid and lithium-ion batteries', *Journal of Power Sources* **155**(2), 395–400.

Dong, T., Kirchev, A., Mattera, F., Kowal, J. & Bultel, Y. (2011), 'Dynamic modeling of li-ion batteries using an equivalent electrical circuit', *Journal of the Electrochemical Society* **158**, 326.

Dowgiallo, E. J. J. (1975), 'Method for determining battery state of charge by measuring ac electrical phase angle change'. US Patent 3,984,762.

Doyle, J. C., Francis, B. A. & Tannenbaum, A. (1992), *Feedback control theory*, Vol. 1, Macmillan Publishing Company New York.

Doyle, J. C., Glover, K., Khargonekar, P. P. & Francis, B. A. (1989), 'State-space solutions to standard $\mathcal{H}_\in$ and $\mathcal{H}_\infty$ control problems', *IEEE Transactions on Automatic Control* **34**(8), 831–847.

Doyle, M., Fuller, T. F. & Newman, J. (1993), 'Modeling of galvanostatic charge and discharge of the lithium/polymer/insertion cell', *Journal of the Electrochemical Society* **140**(6), 1526–1533.

Dreer, H. (1984), Curtis wheelchair battery fuel gauge, Technical report, Marketing Services Dept., Curtis Instruments.

Durr, M., Cruden, A., Gair, S. & McDonald, J. (2006), 'Dynamic model of a lead acid battery for use in a domestic fuel cell system', *Journal of Power Sources* **161**(2), 1400–1411.

Duttweiler, D. L. (2000), 'Proportionate normalized least-mean-squares adaptation in echo cancelers', *IEEE Transactions on Speech and Audio Processing* **8**(5), 508–518.

Fang, W., Kwon, O. J. & Wang, C.-Y. (2010), 'Electrochemical-thermal modeling of automotive li-ion batteries and experimental validation using a three-electrode cell', *International journal of energy research* **34**(2), 107–115.

Feng, D.-Z., Bao, Z. & Jiao, L.-C. (1998), 'Total least mean squares algorithm', *IEEE Transactions on Signal Processing* **46**(8), 2122–2130.

Gahinet, P. & Apkarian, P. (1994), 'A linear matrix inequality approach to $\mathcal{H}_\infty$ control', *International journal of robust and nonlinear control* **4**(4), 421–448.

Gao, D. W., Mi, C. & Emadi, A. (2007), 'Modeling and simulation of electric and hybrid vehicles', *Proceedings of the IEEE* **95**(4), 729–745.

Gao, L., Liu, S. & Dougal, R. A. (2002), 'Dynamic lithium-ion battery model for system simulation', *IEEE Transactions on Components and Packaging Technologies* **25**(3), 495–505.

Garche, J. & Jossen, A. (2000), Battery management systems (bms) for increasing battery life time, *in* 'The Third International Telecommunications Energy Special Conference', IEEE, pp. 81–88.

Gérard, O., Patillon, J.-N. & d'Alché Buc, F. (1997), Neural network adaptive modeling of battery discharge behavior, *in* 'Artificial Neural Networks-ICANN'97', Springer, pp. 1095–1100.

Gielniak, M. & Shen, Z. (2004), Power management strategy based on game theory for fuel cell hybrid electric vehicles, *in* 'IEEE 60th Vehicular Technology Conference', Vol. 6, IEEE, pp. 4422–4426.

Gomez, J., Nelson, R., Kalu, E., Weatherspoon, M. & Zheng, J. (2011), 'Equivalent circuit model parameters of a high-power li-ion battery: Thermal and state of charge effects', *Journal of Power Sources* **196**, 4826–4831.

Gong, Q., Li, Y. & Peng, Z.-R. (2008), 'Trip-based optimal power management of plug-in hybrid electric vehicles', *IEEE Transactions on Vehicular Technology* **57**(6), 3393–3401.

Greg, W. & Gary, B. (2006), 'An introduction to the kalman filter', *Department of Computer Science, University of North Carolina at Chapel Hill, NC* .

Gu, D., Petkov, P. & Konstantinov, M. (2005), *Robust control design with MATLAB*, Vol. 1, Springer Verlag.

Gu, W. & Wang, C. (2000), 'Thermal-electrochemical modeling of battery systems', *Journal of The Electrochemical Society* **147**(8), 2910–2922.

Guerra, T. M. & Vermeiren, L. (2004), 'Lmi-based relaxed nonquadratic stabilization conditions for nonlinear systems in the takagi–sugeno's form', *Automatica* **40**(5), 823–829.

Gurkaynak, Y., Khaligh, A. & Emadi, A. (2009), State of the art power management algorithms for hybrid electric vehicles, *in* 'IEEE Vehicle Power and Propulsion Conference', IEEE, pp. 388–394.

Guzzella, L. & Amstutz, A. (2005), 'The qss toolbox manual', *Measurement and Control Laboratory in Swiss Federal Institute of Technology Zurich* .

Guzzella, L. & Sciarretta, A. (2007), *Vehicle propulsion systems: introduction to modeling and optimization*, Springer Verlag.

Haifeng, D., Xuezhe, W. & Zechang, S. (2009), A new soh prediction concept for the power lithium-ion battery used on hevs, *in* 'IEEE Vehicle Power and Propulsion Conference', IEEE, pp. 1649–1653.

Hansen, T. & Wang, C.-J. (2005), 'Support vector based battery state of charge estimator', *Journal of Power Sources* **141**(2), 351–358.

He, H., Xiong, R. & Fan, J. (2011), 'Evaluation of lithium-ion battery equivalent circuit models for state of charge estimation by an experimental approach', *Energies* **4**(4), 582–598.

Hochgraf, C. G., Ryan, M. J. & Wiegman, H. L. (1996), 'Engine control strategy for a series hybrid electric vehicle incorporating load-leveling and computer controlled energy management', *SAE* **960230**, 11–24.

Hu, Y., Yurkovich, S., Guezennec, Y. & Yurkovich, B. (2011), 'Electro-thermal battery model identification for automotive applications', *Journal of Power Sources* **196**(1), 449–457.

Huet, F. (1998), 'A review of impedance measurements for determination of the state-of-charge or state-of-health of secondary batteries', *Journal of power sources* **70**(1), 59–69.

Isermann, R. (2006), *Fault-diagnosis systems: an introduction from fault detection to fault tolerance*, Springer.

Jalil, N., Kheir, N. A. & Salman, M. (1997), A rule-based energy management strategy for a series hybrid vehicle, *in* 'Proceedings of the 1997 American Control Conference', Vol. 1, IEEE, pp. 689–693.

Jana, K. (2000), 'Genesis application manual'.

Johnson, V. H., Wipke, K. B. & Rausen, D. J. (2000), 'Hev control strategy for real-time optimization of fuel economy and emissions', *SAE transactions* **109**(3), 1677–1690.

Johnson, V., Pesaran, A., Sack, T., (US), N. R. E. L. & America, S. (2001), *Temperature-dependent battery models for high-power lithium-ion batteries*, National Renewable Energy Laboratory.

Kalman, R. E. et al. (1960), 'A new approach to linear filtering and prediction problems', *Journal of basic Engineering* **82**(1), 35–45.

Khargonekar, P. P. & Rotea, M. A. (1991), 'Mixed $\mathcal{H}_\in/\mathcal{H}_\infty$ control: a convex optimization approach', *IEEE Transactions on Automatic Control* **36**(7), 824–837.

Kikuoka, T., Yamamoto, H., Sasaki, N., Wakui, K., Murakami, K., Ohnishi, K., Kawamura, G., Noguchi, H., Ukigaya, F. et al. (1980), 'System for measuring state of charge of storage battery'. US Patent 4,377,787.

Koprubasi, K. (2008), Modeling and control of a hybrid-electric vehicle for drivability and fuel economy improvements, PhD thesis, Ohio State University.

Lam, L. (2011), A practical circuit-based model for state of health estimation of li-ion battery cells in electric vehicles, Master's thesis, University of Technology Delft.

Larsson, V., Johannesson, L. & Egardt, B. (2011), Influence of state of charge estimation uncertainty on energy management strategies for hybrid electric vehicles, *in* '18th IFAC World Congress', Vol. 18, pp. 9703–9708.

Lee, H.-D., Koo, E.-S., Sul, S.-K., Kim, J.-S., Kamiya, M., Ikeda, H., Shinohara, S. & Yoshida, H. (2000), 'Torque control strategy for a parallel-hybrid vehicle using fuzzy logic', *IEEE Industry Applications Magazine* **6**(6), 33–38.

Lee, H. & Sul, S. (1998), 'Fuzzy-logic-based torque control strategy for parallel-type hybrid electric vehicle', *IEEE Transactions on Industrial Electronics* **45**(4), 625–632.

Lee, S., Kim, J., Lee, J. & Cho, B. (2008), 'State-of-charge and capacity estimation of lithium-ion battery using a new open-circuit voltage versus state-of-charge', *Journal of Power Sources* **185**(2), 1367–1373.

Lerner, S., Lennon, H. & Seiger, H. (1970), 'Development of an alkaline battery state of charge indicator', *Power Sources* **3**, 135–7.

Liaw, B. Y., Jungst, R. G., Nagasubramanian, G., Case, H. L. & Doughty, D. H. (2005), 'Modeling capacity fade in lithium-ion cells', *Journal of power sources* **140**(1), 157–161.

Lin, C.-C., Peng, H. & Grizzle, J. (2004), A stochastic control strategy for hybrid electric vehicles, *in* 'Proceedings of the 2004 American Control Conference', Vol. 5, IEEE, pp. 4710–4715.

Lin, C.-C., Peng, H., Grizzle, J. W. & Kang, J.-M. (2003), 'Power management strategy for a parallel hybrid electric truck', *IEEE Transactions on Control Systems Technology* **11**(6), 839–849.

Lin, C., Chen, Q., Wang, J., HUANG, W. & WANG, Y. (2006), 'Improved ah counting method for state of charge estimation of electric vehicle batteries', *JOURNAL-TSINGHUA UNIVERSITY* **46**(2), 247.

Liu, J. & Peng, H. (2006), Control optimization for a power-split hybrid vehicle, *in* 'American Control Conference', IEEE, pp. 6–pp.

Lo, E. (2009), Review on the configurations of hybrid electric vehicles, *in* '3rd International Conference on Power Electronics Systems and Applications', IEEE, pp. 1–4.

Mohammadpour, J. & Scherer, C. W. (2012), *Control of linear parameter varying systems with applications*, Springer.

Momoh, O. & Omoigui, M. (2009), An overview of hybrid electric vehicle technology, *in* 'IEEE Vehicle Power and Propulsion Conference', IEEE, pp. 1286–1292.

Moura, S. J., Fathy, H. K., Callaway, D. S. & Stein, J. L. (2011), 'A stochastic optimal control approach for power management in plug-in hybrid electric vehicles', *IEEE Transactions on Control Systems Technology* **19**(3), 545–555.

Musardo, C., Rizzoni, G., Guezennec, Y. & Staccia, B. (2005), 'A-ecms: An adaptive algorithm for hybrid electric vehicle energy management', *European Journal of Control* **11**(4), 509–524.

Ng, K. S., Moo, C.-S., Chen, Y.-P. & Hsieh, Y.-C. (2009), 'Enhanced coulomb counting method for estimating state-of-charge and state-of-health of lithium-ion batteries', *Applied energy* **86**(9), 1506–1511.

Packard, A. (1994), 'Gain scheduling via linear fractional transformations', *Systems & Control Letters* **22**(2), 79–92.

Paganelli, G., Tateno, M., Brahma, A., Rizzoni, G. & Guezennec, Y. (2001), Control development for a hybrid-electric sport-utility vehicle: strategy, implementation and field test results, *in* 'Proceedings of the 2001 American Control Conference', Vol. 6, IEEE, pp. 5064–5069.

Pang, S., Farrell, J., Du, J. & Barth, M. (2001), Battery state-of-charge estimation, *in* 'American Control Conference', Vol. 2, IEEE, pp. 1644–1649.

Pattipati, B., Pattipati, K., Christopherson, J. P., Namburu, S. M., Prokhorov, D. V. & Qiao, L. (2008), *Automotive battery management systems*, IEEE.

Pattipati, B., Sankavaram, C. & Pattipati, K. (2011), 'System identification and estimation framework for pivotal automotive battery management system characteristics', *IEEE Transactions on Systems Man and Cybernetics* **41**(6), 869–884.

Peled, E., Yamin, H., Reshef, I., Kelrich, D. & Rozen, S. (1984), 'Method and apparatus for determining the state-of-charge of batteries particularly lithium batteries'. US Patent 4,725,784.

Penina, N., Turygin, Y. & Racek, V. (2010), Comparative analysis of different types of hybrid electric vehicles, *in* '13th International Symposium MECHATRONIKA', IEEE, pp. 102–104.

Pérez, L. V., Bossio, G. R., Moitre, D. & García, G. O. (2006), 'Optimization of power management in an hybrid electric vehicle using dynamic programming', *Mathematics and Computers in Simulation* **73**(1), 244–254.

Phillips, A. M., Jankovic, M. & Bailey, K. E. (2000), Vehicle system controller design for a hybrid electric vehicle, *in* 'Proceedings of the 2000 IEEE International Conference on Control Applications', IEEE, pp. 297–302.

Picciano, N. (2007), 'Battery aging and characterization of nickel metal hydride and lead-acid batteries'.

Piccolo, A., Ippolito, L. & Vaccaro, A. (2001), Optimisation of energy flow management in hybrid electric vehicles via genetic algorithms, *in* 'IEEE/ASME International Conference on Advanced Intelligent Mechatronics', Vol. 1, IEEE, pp. 434–439.

Piller, S., Perrin, M. & Jossen, A. (2001), 'Methods for state-of-charge determination and their applications', *Journal of power sources* **96**(1), 113–120.

Pisu, P. & Rizzoni, G. (2004), $\mathcal{H}_\infty$ control for hybrid electric vehicles, *in* '43rd IEEE Conference on Decision and Control', Vol. 4, IEEE, pp. 3497–3502.

Pisu, P. & Rizzoni, G. (2007), 'A comparative study of supervisory control strategies for hybrid electric vehicles', *IEEE Transactions on Control Systems Technology* **15**(3), 506–518.

Pisu, P., Silani, E., Rizzoni, G. & Savaresi, S. M. (2003), A lmi-based supervisory robust control for hybrid vehicles, *in* 'Proceedings of the 2003 American Control Conference', Vol. 6, IEEE, pp. 4681–4686.

Plett, G. (2004*a*), 'Extended kalman filtering for battery management systems of lipb-based hev battery packs:: Part 1. background', *Journal of Power sources* **134**(2), 252–261.

Plett, G. L. (2004*b*), 'Extended kalman filtering for battery management systems of lipb-based hev battery packs: Part 2. modeling and identification', *Journal of power sources* **134**(2), 262–276.

Plett, G. L. (2004*c*), 'Extended kalman filtering for battery management systems of lipb-based hev battery packs: Part 3. state and parameter estimation', *Journal of power sources* **134**(2), 277–292.

Pop, V., Bergveld, H. J., Notten, P. & Regtien, P. P. (2005), 'State-of-the-art of battery state-of-charge determination', *Measurement Science and Technology* **16**(12), R93.

Poussot-Vassal, C. (2008), Commande robuste LPV multivariable de chassis automobile, PhD thesis, Grenoble INP.

Powell, B., Bailey, K. & Cikanek, S. (1998), 'Dynamic modeling and control of hybrid electric vehicle powertrain systems', *IEEE Control Systems* **18**(5), 17–33.

Pradhan, A., Routray, A. & Basak, A. (2005), 'Power system frequency estimation using least mean square technique', *IEEE Transactions on Power Delivery* **20**(3), 1812–1816.

Radio-Electronics, n. (2013), 'Lithium ion battery types', `http://www.radio-electronics.com/info/power-management/battery-technology/lithium-ion-battery-types.php`. Accessed May 17, 2013.

Rajagopalan, A., Washington, G., Rizzoni, G. & Guezennec, Y. (2003), *Development of fuzzy logic and neural network control and advanced emissions modeling for parallel hybrid vehicles*, National Renewable Energy Laboratory.

Ramadass, P., Haran, B., White, R. & Popov, B. N. (2003), 'Mathematical modeling of the capacity fade of li-ion cells', *Journal of power sources* **123**(2), 230–240.

Richter, G. & Meissner, E. (2000), 'Method for determining the state of charge of storage batteries'. US Patent 6,388,450.

Rizzoni, G., Guzzella, L. & Baumann, B. (1999), 'Unified modeling of hybrid electric vehicle drivetrains', *IEEE/ASME Transactions on Mechatronics* **4**(3), 246–257.

Rizzoni, G. & Onori, S. (2012), Optimal energy management of hybrid electric vehicles: 15 years of development at the ohio state university, *in* 'Proceeding of IFAC E-COSM'12'.

Roche, E. (2011), Commande lineaire a parametres variants discrete a echantillonnage variable: application a un sous-marin autonome, PhD thesis, Grenoble INP.

Rodrigues, S., Munichandraiah, N. & Shukla, A. (2000), 'A review of state-of-charge indication of batteries by means of ac impedance measurements', *Journal of Power Sources* **87**(1), 12–20.

Roscher, M. A., Bohlen, O. & Vetter, J. (2011), 'Ocv hysteresis in li-ion batteries including two-phase transition materials', *International Journal of Electrochemistry* **2011**.

Rotea, M. A. (1993), 'The generalized $\mathcal{H}_\in$ control problem', *Automatica* **29**(2), 373–385.

Rousseau, A., Sharer, P., Pagerit, S. & Duoba, M. (2006), 'Integrating data, performing quality assurance, and validating the vehicle model for the 2004 prius using psat', *SAE paper* **1**, 0667.

Salameh, Z. M., Casacca, M. A. & Lynch, W. A. (1992), 'A mathematical model for lead-acid batteries', *IEEE Transactions on Energy Conversion* **7**(1), 93–98.

Salkind, A. J., Fennie, C., Singh, P., Atwater, T. & Reisner, D. E. (1999), 'Determination of state-of-charge and state-of-health of batteries by fuzzy logic methodology', *Journal of Power Sources* **80**(1), 293–300.

Salmasi, F. R. (2007), 'Control strategies for hybrid electric vehicles: Evolution, classification, comparison, and future trends', *IEEE Transactions on Vehicular Technology* **56**(5), 2393–2404.

Sánchez, E. V. (2003), Robust and fault tolerant control of CD-players, PhD thesis, Department of Control Engineering, Aalborg University, Aalborg, Denmark.

Santhanagopalan, S. & White, R. E. (2006), 'Online estimation of the state of charge of a lithium ion cell', *Journal of power sources* **161**(2), 1346–1355.

Scherer, C. (2001*a*), 'Lpv control and full block multipliers', *Automatica* **37**(3), 361–375.

Scherer, C. (2001*b*), 'Theory of robust control', *Delft University of Technology* .

Scherer, C., Gahinet, P. & Chilali, M. (1997), 'Multiobjective output-feedback control via lmi optimization', *IEEE Transactions on Automatic Control* **42**(7), 896–911.

Scherer, C. W. (1996), 'Mixed $\mathcal{H}_{\in}/\mathcal{H}_{\infty}$ control for time-varying and linear parametrically-varying systems', *International Journal of Robust and Nonlinear Control* **6**(910), 929–952.

Scherer, C. & Weiland, S. (2000), 'Linear matrix inequalities in control', *Lecture Notes, Dutch Institute for Systems and Control, Delft, The Netherlands* .

Schmidt, A. P., Bitzer, M., Imre, Á. W. & Guzzella, L. (2010), 'Model-based distinction and quantification of capacity loss and rate capability fade in li-ion batteries', *Journal of Power Sources* **195**(22), 7634–7638.

Schwunk, S., Armbruster, N., Straub, S., Kehl, J. & Vetter, M. (2012), 'Particle filter for state of charge and state of health estimation for lithium-iron phosphate batteries', *Journal of Power Sources* .

Sename, O., Gaspar, P., Bokor, J. et al. (2013), *Robust Control and Linear Parameter Varying approaches: Application to Vehicle Dynamics*, Springer.

Serrao, L. (2009), A comparative analysis of energy management strategies for hybrid electric vehicles, PhD thesis, The Ohio State University.

Seyfang, G. R. (1988), 'Battery state of charge indicator'. US Patent 4,949,046.

Shen, W. (2007), 'State of available capacity estimation for lead-acid batteries in electric vehicles using neural network', *Energy conversion and management* **48**(2), 433–442.

Shen, W., Chan, C., Lo, E. & Chau, K. (2002), 'A new battery available capacity indicator for electric vehicles using neural network', *Energy Conversion and Management* **43**(6), 817–826.

Shepherd, C. (1965), 'Design of primary and secondary cells', *Journal of the Electrochemical Society* **112**, 252.

Singh, P., Fennie, C., Reisner, D. & Salkind, A. (1998), A fuzzy logic approach to state-of-charge determination in high performance batteries with applications to electric vehicles, *in* 'Electric Vehicle Symp', Vol. 15, pp. 30–3.

Skogestad, S. & Postlethwaite, I. (2007), *Multivariable feedback control: analysis and design*, Vol. 2, Wiley.

Slock, D. T. (1993), 'On the convergence behavior of the lms and the normalized lms algorithms', *IEEE Transactions on Signal Processing* **41**(9), 2811–2825.

Spotnitz, R. (2005), Advanced ev and hev batteries, *in* 'IEEE Vehicle Power and Propulsion Conference', IEEE, pp. 334–337.

Srinivasan, V., Weidner, J. W. & Newman, J. (2001), 'Hysteresis during cycling of nickel hydroxide active material', *Journal of The Electrochemical Society* **148**(9), A969–A980.

Sun, Y.-H., Jou, H.-L. & Wu, J.-C. (2007), Novel auxiliary diagnosis method for state-of-health of lead-acid battery, *in* '7th International Conference on Power Electronics and Drive Systems', IEEE, pp. 262–266.

Syed, F., Kuang, M., Czubay, J. & Ying, H. (2006), 'Derivation and experimental validation of a power-split hybrid electric vehicle model', *IEEE Transactions on Vehicular Technology* **55**(6), 1731–1747.

Tóth, R. (2010), *Modeling and identification of linear parameter-varying systems*, Vol. 403, Springer Verlag.

Tulpule, P., Marano, V. & Rizzoni, G. (2010), 'Energy management for plug-in hybrid electric vehicles using equivalent consumption minimisation strategy', *International Journal of Electric and Hybrid Vehicles* **2**(4), 329–350.

Van den Bossche, P., Vergels, F., Van Mierlo, J., Matheys, J. & Van Autenboer, W. (2006), 'Subat: An assessment of sustainable battery technology', *Journal of power sources* **162**(2), 913–919.

Vasebi, A., Bathaee, S. & Partovibakhsh, M. (2008), 'Predicting state of charge of lead-acid batteries for hybrid electric vehicles by extended kalman filter', *Energy Conversion and Management* **49**(1), 75–82.

Verbrugge, M. & Tate, E. (2004), 'Adaptive state of charge algorithm for nickel metal hydride batteries including hysteresis phenomena', *Journal of Power Sources* **126**(1), 236–249.

Verbrugge, M. W., Tate Jr, E. D., Sarbacker, S. D. & Koch, B. J. (2000), 'Quasi-adaptive method for determining a battery's state of charge'. US Patent 6,359,419.

Vinot, E., Trigui, R., Jeanneret, B., Scordia, J. & Badin, F. (2007), Hevs comparison and components sizing using dynamic programming, *in* 'IEEE Vehicle Power and Propulsion Conference', IEEE, pp. 314–321.

Waltermann, P. (1996), Modelling and control of the longitudinal and lateral dynamics of a series hybrid vehicle, *in* 'Proceedings of the 1996 IEEE International Conference on Control Applications', IEEE, pp. 191–198.

Wang, T.-H., Sename, O. & Martinez-Molona, J. (2013*a*), A lpv ems regulator for the parallel hev with battery life prolongation, *in* '21st Mediterranean Conference on Control and Automation'.

Wang, T.-H., Sename, O. & Martinez-Molona, J. (2013*b*), A lpv/$\mathcal{H}_\infty$ approach for fuel consumption minimization of the phev with battery life prolongation, *in* '7th IFAC International Symposium on Advances in Automotive Control (IFAC-AAC)'.

Wei, X. (2004), Modeling and control of a hybrid electric drivetrain for optimum fuel economy, performance and driveability, PhD thesis, Ohio State University.

Wei, Z., Chan, C. & Shumei, C. (2006), Optimization of switching rule and operating modes of hybrid electric vehicles, *in* 'International Joint Conference SICE-ICASE', IEEE, pp. 2412–2415.

Widrow, B. (1971), 'Adaptive filters', *Aspects of network and system theory* pp. 563–587.

Widrow, B. & Stearns, S. D. (1985), *Adaptive signal processing*, Vol. 15, IET.

Wipke, K. B., Cuddy, M. R. & Burch, S. D. (1999), 'Advisor 2.1: a user-friendly advanced powertrain simulation using a combined backward/forward approach', *IEEE Transactions on Vehicular Technology* **48**(6), 1751–1761.

Wirasingha, S. G. & Emadi, A. (2011), 'Classification and review of control strategies for plug-in hybrid electric vehicles', *IEEE Transactions on Vehicular Technology* **60**(1), 111–122.

Xuyun, F. & Zechang, S. (2008), A battery model including hysteresis for state of charge estimation in nimh battery, *in* 'IEEE Vehicle Power and Propulsion Conference', IEEE, pp. 1–5.

Yann Liaw, B., Nagasubramanian, G., Jungst, R. G. & Doughty, D. H. (2004), 'Modeling of lithium ion cells a simple equivalent circuit model approach', *Solid state ionics* **175**(1), 835–839.

Zames, G. (1981), 'Feedback and optimal sensitivity: Model reference transformations, multiplicative seminorms, and approximate inverses', *IEEE Transactions on Automatic Control* **26**(2), 301–320.

Zames, G. & Francis, B. (1983), 'Feedback, minimax sensitivity, and optimal robustness', *IEEE Transactions on Automatic Control* **28**(5), 585–601.

Zaugg, E. (1982), 'Process and apparatus for determining the state of charge of a battery'. US Patent 4,433,295.

Zhang, J. & Lee, J. (2011), 'A review on prognostics and health monitoring of li-ion battery', *Journal of Power Sources* **196**, 6007–6014.

Zhang, L. & Huang, A. Q. (2011), 'Model-based fault detection of hybrid fuel cell and photovoltaic direct current power sources', *Journal of Power Sources* **196**, 5197–5204.

Zhou, K. & Doyle, J. C. (1998), *Essentials of robust control*, Vol. 104, Prentice Hall Upper Saddle River, NJ.

Zhou, K., Doyle, J. C., Glover, K. et al. (1996), *Robust and optimal control*, Vol. 40, Prentice Hall New Jersey.

Zhu, Y., Chen, Y., Tian, G., Wu, H. & Chen, Q. (2004), A four-step method to design an energy management strategy for hybrid vehicles, *in* 'Proceedings of the 2004 American Control Conference', Vol. 1, IEEE, pp. 156–161.